# Non-equilibrium dynamics of a trapped one-dimensional Bose gas

Andrii Gudyma

NNT : 2015SACLS064

# THÈSE DE DOCTORATE DE L'UNIVERSITÉ PARIS-SACLAY, préparée à l'Université Paris-Sud

ÉCOLE DOCTORALE No 564
Physique en Île-de-France (EDPIF)

Spécialité de doctorat: Physique

Par
**M. Andrii Gudyma**

# Non-equilibrium dynamics of a trapped one-dimensional Bose gas

**Thèse présentée et soutenue à Orsay, le 28 Octobre 2015:**

**Composition du Jury :**

M. Chris Westbrook, Directrice de Recherche, Université Paris-Sud, Président du jury
M. Jean-Sebastien Caux, Professeur, Universiteit van Amsterdam, Rapporteur
M. Vadim Cheianov, Professeur, Leiden University, Rapporteur
Mme Anna Minguzzi, Chargée de Recherche, CNRS, Examinatrice
M. Gora Shlypnikov, Université Paris-Sud, Directeur de thèse
M. Mikhail Zvonarev, Université Paris-Sud, Invité

ÉCOLE DOCTORALE
Physique en île-de-France (EDPIF)

**Titre:** Dynamique hors d'équilibre de gaz de Bose unidimensionnel piégé

**Mots clés:** mode de respiration, atomes froids, Condensat de Bose-Einstein;

**Résumé:**

Une étude des modes d'oscillations d'une gaz de Bose unidimensionnel dans la piège est présentée. Les oscillations sont initiées par une changement instantanée de la fréquence de piégeage. Dans la thèse il est considéré d'un gaz de Bose quantique 1D dans un piège parabolique à la température nulle, et il est expliqué, analytiquement et numériquement, comment la fréquence d'oscillation dépend du nombre de particules, leur interaction répulsive, et les paramètres de piège. Nous sommes concentres sur la description spectrale, en utilisant les règles de somme. La fréquence d'oscillation est identifiée comme la différence d'énergie entre l'état fondamental et un état excité donne. L'existence de trois régimes est démontrée, à savoir le régime de Tonks, le régime de Thomas-Fermi et le régime de Gauss. La transition entre les régime de Tonks et de Thomas-Fermi est décrite dans l'approximation de la densité locale (LDA). Pour la transition entre le régime de Thomas-Fermi et le régime de Gauss l'approximation de Hartree est utilisée. Dans les deux cas, nous avons calculé les paramP"PΊtres pour quelles les transitions se produisent. Les simulations extensif de Monte Carlo de diffusion pour un gaz contenant jusqu'à N = 25 particules ont été effectuées. Lorsque le nombre de particules augmente, les prédictions des simulations convergent vers celles d'Hartree et LDA dans ces régimes. Cela rend les résultats des modes d'oscillation applicables pour des valeurs arbitraires du nombre de particule et de l'interaction. L'analyse est complétée par les résultats perturbatifs dans les cas limites avec N finis. La théorie prédit le comportement réentrant de la fréquence de mode d'oscillation lors de la transition du régime de Tonks au régime de Gauss et explique bien les données de l'expérience récente du groupe d'Innsbruck.

université PARIS-SACLAY | ÉCOLE DOCTORALE Physique en île-de-France (EDPIF)

**Title:** Non-equilibrium dynamics of a trapped one-dimensional Bose gas

**Keywords:** breathing mode, cold atoms, Bose-Einstein Condensate

**Abstract:**

A study of breathing oscillations of a one-dimensional trapped interacting Bose gas is presented. Oscillations are initiated by an instantaneous change of the trapping frequency. In the thesis a 1D quantum Bose gas in a parabolic trap at zero temperature is considered, and it is explained, analytically and numerically, how the oscillation frequency depends on the number of particles, their repulsive interaction, and the trap parameters. We have focused on the many-body spectral description, using the sum rules approximation. The oscillation frequency is identified as the energy difference between the ground state and a particular excited state. The existence of three regimes is demonstrated, namely the Tonks regime, the Thomas-Fermi regime and the Gaussian regime. The transition from the Tonks to the Thomas-Fermi regime is described in the terms of the local density approximation (LDA). For the description of the transition from the Thomas-Fermi to the Gaussian regime the Hartree approximation is used. In both cases the parameters where the transitions happen are found. The extensive diffusion Monte Carlo simulations for a gas containing up to N = 25 particles is performed. As the number of particles increases, predictions from the simulations converge to the ones from the Hartree and LDA in the corresponding regimes. This makes the results for the breathing mode frequency applicable for arbitrary values of the particle number and interaction. The analysis is completed with the finite N perturbative results in the limiting cases. The theory predicts the reentrant behavior of the breathing mode frequency when moving from the Tonks to the Gaussian regime and fully explains the recent experiment of the Innsbruck group.

# Contents

# Acknowledgements

The work presented in this Thesis was carried out from November 2012 to October 2015 at the Laboratory of Theoretical Physics and Statistical Models (LPTMS). Herein I would like to give thanks to several people who have made it a pleasure to work here as well as to those people who have supported me in my studies.

I would like to thank my scientific advisor Gora Shlyapnikov for his patience and for his kind and unwavering support over the last three years, guiding me to the end point while allowing me to explore interesting topics along the way. His broad view on science and his advises made my work much easier. I would like to express my special appreciation and thanks to my co-advisor Mikhail Zvonarev, who has been a tremendous mentor for me. I would like to thank him for encouraging my research and for allowing me to grow as a research scientist. His advices on my research and career have been priceless. In addition I am very grateful to Vadim Cheianov, Jean-Sébastien Caux, Anna Minguzzi and Christoph Westbrook for agreeing to be part of my examination committee.

Without the help of a number of people this Thesis would not have been possible. In the organization and defence of my Thesis at LPTMS I would like to especially thank Mme. Claudine Le Vaou. I would like to acknowledge the following people (in no particular order): Dmitry Petrov, Kabir Ramola, Vincent Michal, Bess Fang, Thomas Bartel and Gregory Astrakharchik. Finally, I would like to thank my parents for their unceasing encouragement and belief in me. They inspired me to always look for the best in life and all that I have and that I am is due to them.

Special thanks should be given to the Palaiseau group for providing access to their experimental data, and to the Innsbruck group for numerous enlightening discussions. The Barcelona Supercomputing Center (The Spanish National Supercomputing Center – Centro Nacional de Supercomputación) is acknowledged for the provided computational facilities. The Thesis was supported by the grant from Region Ile-de-France DIM NANO-K.

# Introduction

*"Good tests kill flawed theories; we remain alive to guess again."*

*Karl Popper*

All existing ultracold-gas experiments are carried out with systems which are spatially inhomogeneous due to the presence of an external confining potential [1, 2]. Exciting temporal oscillations of the gas density distribution in such a confined geometry is a basic tool for investigating the spectrum of collective excitations and phase diagrams [3–9].

One-dimensional (1D) gases have unique properties: enhanced quantum correlations affect their collective excitation spectrum drastically, masking out signatures of the Bose/Fermi statistics of the constituent particles [10, 11]. Increasing the interaction strength suppresses spatial overlap between any two bosons. In the limiting case of an infinite repulsion, known as the Tonks-Girardeau (TG) gas, this leads to the many-body excitation spectrum identical to that of a free Fermi gas [12]. The presence of an external parabolic potential causes the low-lying part of excitation spectrum to be discrete. The first excited state of the gas, the dipole mode, is interaction-independent. It is associated with the center-of-mass oscillations at the trap frequency $\omega_z$. The second excited state of center-of-mass oscillations has the frequency $2\omega_z$. Another mode (with frequency $2\omega_z$ in the non-interacting case) is called the breathing (or the lowest compressional) mode. Being excited by a small instantaneous change of the trapping frequency $\omega_z$, this mode has the frequency $\omega$ which depends on the interaction strength, the number of particles $N$ in the trap, and the gas temperature $T$.

Experimental investigations of the breathing mode oscillations in 1D ultracold-gas experiments have been reported by several groups [13–15]. It was found that the frequency ratio $\omega/\omega_z$ goes through two crossovers with increasing the interaction strength. First, it decreases from the value 2 down to $\sqrt{3}$, which corresponds to the crossover from the from non- to weakly interacting regime. Further increase of the interaction transforms the weakly interacting to strongly interacting regime (see Ref. [14]) and the ratio $\omega/\omega_z$ returns to 2 (see, e.g., Fig. 29). The latter crossover has been described theoretically for $N$ going to infinity by using the local density approximation (LDA) [16]. A description of the former crossover has been done only numerically for a few particles: $N \leq 5$ by using the multilayer multiconfiguration time-dependent Hartree method [17] and $N \leq 7$ by using numerical di-

agonalization [18]. Experiments [13, 15] were performed in the regime of weak coupling, for which $\omega/\omega_z = \sqrt{3}$ is expected as $N$ goes to infinity at zero temperature. It is presently an open question to which extent the observed deviations from the value $\sqrt{3}$ are related to finite values of $N$ and $T$. Resolving this question paves a way towards understanding interaction effects in the dynamics and thermalisation of 1D quantum gases.

In this Thesis we present analytical and numerical results for the breathing mode frequency $\omega$ in the repulsive Lieb-Liniger gas in a parabolic trap of frequency $\omega_z$. Using the Hartree approximation we explain how the decrease of $\omega/\omega_z$ from the 2 to $\sqrt{3}$ with increasing the repulsion is linked to a crossover from the Gaussian Bose–Einstein condensate (BEC) to the Thomas–Fermi (TF) BEC regime. A parameter which controls this crossover is introduced. For any number of particles, the perturbation expansion of the breathing frequency in the interaction parameter is demonstrated.

With further increasing the repulsion strength, the ratio $\omega/\omega_z$ increases from $\sqrt{3}$ to 2. This is associated with a crossover from the TF BEC to the Tonks-Girardeau regime, which is described within the local density approximation (LDA). A single dimensionless interaction parameter of the LDA is introduced and an analytical perturbative analysis for finite N is made. We then perform extensive diffusion Monte Carlo simulations for a gas containing up to $N = 25$ particles. As the number of particles increases, predictions from the simulations converge to the values obtained from the Hartree and LDA in their respective regimes. This makes our results for $\omega$ applicable for an arbitrary number of particles and for any value of the repulsion strength. We find an excellent quantitative agreement with the data from the Innsbruck experiment [14]. We also estimate relevant temperature scales for the Palaiseau experiment [15].

# 1. Trapped quantum gases

*"If I have seen further, it is by standing on the shoulders of giants."*

*Sir Isaac Newton*

Chapter I reviews the history of cold atom research, recent achievements and progress. Experimental techniques which give a possibility to create one-dimensional systems and to control parameters are described. The model Hamiltonian is introduced and the definition of the breathing mode is given. Remarks on the measurement procedure are also given, and the connection with the spectrum is established. A significant part of the chapter is dedicated to the discussion of theoretical tools for the breathing mode calculation. Several different methods resulting in the same formula for the lowest compressional mode frequency are described.

Only about two decades ago experimental techniques for cold-atom physics became accessible. A wide spectrum of different experiments was made. For example, particles in a perfect lattice potential perform Bloch oscillations (BO) when subject to a constant force leading to localization and preventing conductivity [19].

The earlier discussion of low-dimensional Bose gases was mostly academic as there was no realization of such a system. Fast progress in evaporative and optical cooling of trapped atoms and the observation of Bose-Einstein condensation (BEC) in trapped clouds of alkali atoms stimulated a search for non-trivial trapping geometries. Present facilities allow one to tightly confine the motion of trapped particles in two directions to zero point oscillations. Then, statical and kinematic properties of the gas are one-dimensional. The difference from purely 1D gases is only related to the value of the effective interparticle interaction which now depends on the tight confinement.

One of the questions under discussion in the cold-atom community is the question of the dependence of the lowest compressional mode in 1D on such parameters of the system as interparticle interaction, trapping potential, number of particles and temperature of the system. This problem has a history starting from first attempts to deal with it using one-dimensional hydrodynamical approach [16, 20, 21]. After that there was a break until the first measurement [13] of the lowest compressional mode in 2003 performed for $^{87}Rb$ atoms. These experiments confirmed the existence of different regimes in which the ratio of the

lowest compressional mode to the trapping potential frequency takes values $\sqrt{3}$ or 2. One of the most significant experimental results on this problem was obtained in 2005 in Innsbruck [14, 22], where the frequency of the breathing mode was measured for both repulsive and attractive regimes. The Innsbruck group used $^{133}Cs$ atoms in a two-dimensional optical lattice. These atoms have a fairly wide Feshbach resonance and the interaction can be tuned easily. The data show a good agreement with the existing theory for the Tonks-Girardeau regime, and for the weak coupling they demonstrated a mismatch with calculations. Moreover, in the attractive regime experimental data show a mismatch with the theory in all regimes. There was an attempt to explain this mismatch by using mixed (anionic) statistics [23].

## 1.1. Interaction potential

Ultracold gases are dilute at low temperatures and thus certain details of two-body interactions are not important. Atom-atom interaction $U$ can be described with only the scattering amplitude, which for cold atoms in three dimensions is given by the combination (see Ref. [24]):

$$F(k) = \frac{1}{a_{3D}^{-1} - \frac{1}{2}R^*k^2 + ik}. \tag{1.1}$$

Here $a_{3D}$ is the scattering length, $R^*$ is the effective radius of interactions, and $k$ is the relative momentum. Typically for cold atoms $kR^* \ll 1$ and

$$F(k) = \frac{1}{a_{3D}^{-1} + ik}, \tag{1.2}$$

which corresponds to a 3-dimensional pseudo-potential

$$U(r) = g_{3D}\delta(r)\frac{\partial}{\partial r}r, \tag{1.3}$$

where $g_{3D}$ is the interaction strength related to the scattering length as

$$g_{3D} = \frac{4\pi\hbar^2 a_{3D}}{m}. \tag{1.4}$$

This potential is often called "the contact potential" or "contact interaction". The operator $\frac{\partial}{\partial r}r$ in Eq. (1.3) eliminates the singular $1/r$ short-range behavior in the wave-function. The use of the potential (1.3) is equivalent to imposing the boundary condition on the wave-function [25]

$$\frac{1}{r\psi}\left.\frac{\delta(r\psi)}{\delta r}\right|_{r=0} = -\frac{1}{a_{3D}}. \tag{1.5}$$

Under the conditions of diluteness and low temperature the potential (1.3) is equivalent to using the potential

$$U(r) = g_{3D}\delta(r) \tag{1.6}$$

in the many body interaction Hamiltonian [24]. The scattering length $a_{3D}$ can be both positive an negative.

## 1.2. Experimental realizations of quasi-one-dimensional quantum gas

*"Orbis non sufficit"*

*Latin phrase*

There are several different techniques to realize a quantum gas in reduced dimensionality. The most popular ones are the optical lattice [14, 22] and atom chip [15] techniques.

The optical lattice technique uses a few lasers shining from opposite directions in the $x$–$y$ plane. The interference of the sinusoidal waves forms a two-dimensional optical lattice. The axis perpendicular to the plane of laser beams we will call the z-axis. The frequency and intensity of the trapping potential are usually chosen such that the distance between two neighbouring minima is much larger then the characteristic radius of interaction. Thus, we have a system of tubes (weakly interacting in the $z$-direction) and each tube can be considered independently. In the vicinity of a minimum an intensity can be approximated by the harmonic potential of frequency $\omega_x = \omega_y = \omega_\perp$. This approximation is valid only for low-energy states. Along the $z$-axis a harmonic trapping with frequency $\omega_z$ is modulated by the intensity gradient of the laser beams.

Thus, the trapping potential has the form:

$$V(x, y, z) = \frac{m}{2}\left(\omega_\perp^2 x^2 + \omega_\perp^2 y^2 + \omega_z^2 z^2\right). \tag{1.7}$$

Such a system can be used for realization of different geometries such as $3D$ condensate, cigar-shaped, and quasi-$1D$ systems.

In experiments atoms are loaded into the optical trap. After evaporative cooling a typical temperature of the system is from dozens to hundreds of nano-Kelvins ($nK$). Using the

Feshbach (FR) and confinement induced resonances (CIR) one can change the strength of the inter-particle interaction $g$.

### 1.2.1. Quasi-onedimensional potential

The quasi-1D geometry can be reached if the confinement in the $x$–$y$ plane is so strong that no excitations along this direction are present. For this the condition $\hbar\omega_\perp \ll \hbar\omega_z, \mu, k_B T$ should hold. This allows one to take a Gaussian shape of the particle wave-function:

$$\psi(x, y, z) = \psi_0^{HO}(x)\psi_0^{HO}(y)\psi(z), \qquad (1.8)$$

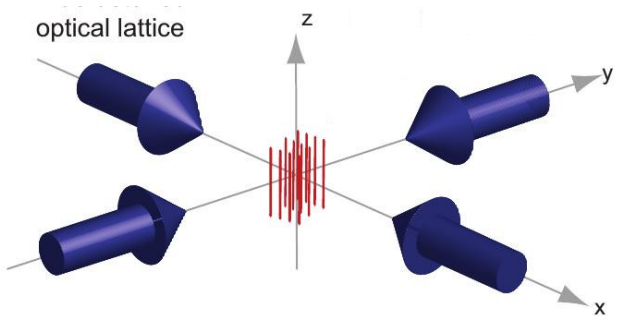


Figure 1: Optical trap geometry

where $\psi_0^{HO}$ is the ground-state wave-function of a harmonic oscillator. It is then possible to integrate out the system over $x$ and $y$ coordinates. After the integration we have an effective one-dimensional interaction potential

$$U(z) = g\delta(z), \qquad (1.9)$$

with a rescaled interaction strength

$$g = \frac{g_{3D}}{2\pi a_\perp^2}. \qquad (1.10)$$

### 1.2.2. CIR and Olshanii formula

The confinement induced resonance is a phenomenon which makes it possible to tune the quasi-1$D$ interparticle interaction strength by changing the parameters of the tight confinement. The so-called one-dimensional scattering length is connected with the strength of the interaction as [26]

$$a_{1D} = -\frac{2\hbar^2}{mg}, \qquad (1.11)$$

and is related to the 3$D$-scattering length by the Olshanii formula [26, 27]

$$\frac{1}{a_{1D}} = -\frac{a_{3D}}{a_\perp^2}\frac{1}{1 - A\frac{a_{3D}}{a_\perp}}, \qquad (1.12)$$

where $A = \zeta(\frac{1}{2})\sqrt{2} \approx 1.0326$ is a constant, and $\zeta(x)$ is the Riemann's zeta-function.

The scattering length $a_{1D}$ can be positive as will as negative or infinite. When $a_{1D}$ is negative atoms experience repulsive interaction. When $a_{1D}$ is positive atoms experience attractive interaction. When $a_{1D}$ goes to infinity the interaction strength $g$ goes to 0. This corresponds to the non-interacting limit. Finally, small negative and positive values of the scattering length $a_{1D}$ correspond to the so-called Tonks and super-Tonks regimes, respectively.

## 1.3. Trapped Lieb-Liniger gas

A quantum one-dimensional system of $N$ particles is described by an $N$-body wave function $\Psi$. Its time evolution is governed by the time-dependent Schrödinger equation (TDSE)

$$i\hbar\frac{\partial}{\partial t}\Psi = \hat{H}\Psi. \tag{1.13}$$

In the terms of quantum fields the corresponding Hamiltonian has the general form:

$$\hat{H} = \int \left(\frac{\hbar^2}{2m}\partial_z\hat{\Psi}^\dagger(z)\partial_z\hat{\Psi}(z) + \hat{\Psi}^\dagger(z)V_{ext}(z)\hat{\Psi}(z)\right)dz + \iint \hat{\Psi}^\dagger(z)\hat{\Psi}^\dagger(z')U(z-z')\hat{\Psi}(z')\hat{\Psi}(z)dzdz', \tag{1.14}$$

where $m$ is the mass of a particle, and

$$V_{ext}(z) = \frac{m\omega_z^2 z^2}{2}, \tag{1.15}$$

is the external harmonic potential.

The bosonic field operators $\hat{\Psi}$ and $\hat{\Psi}^\dagger$ satisfy canonical equal-time commutation relations

$$\left[\hat{\Psi}(z), \hat{\Psi}(z')\right] = \hat{\Psi}(z)\hat{\Psi}(z') - \hat{\Psi}(z')\hat{\Psi}(z) = 0, \tag{1.16a}$$

$$\left[\hat{\Psi}^\dagger(z), \hat{\Psi}^\dagger(z')\right] = 0, \tag{1.16b}$$

$$\left[\hat{\Psi}(z), \hat{\Psi}^\dagger(z')\right] = \delta(z-z'). \tag{1.16c}$$

In the first quantization the Hamiltonian reads

$$\hat{H} = -\frac{\hbar^2}{2m}\sum_{n=1}^{N}\frac{\partial^2}{\partial z_n^2} + g\sum_{n>k=1}^{N}\delta(z_n - z_k) + \frac{m\omega_z^2}{2}\sum_{n=1}^{N} z_n^2. \tag{1.17}$$

We will call the system described by the Hamiltonian (1.17) the Lieb-Liniger gas in analogy with the uniform system [28, 29] described by the first two terms in the right hand side of (1.17).

The external potential introduces a characteristic length $a_z = (m\omega_z/\hbar)^{\frac{1}{2}}$. Now we introduce dimensionless variables $x = z/a_z$, and the dimensionless coupling constant $\alpha = -2a_z/a_{1D}$. In the dimensionless variables we have the following Hamiltonian:

$$\hat{H} = -\frac{1}{2}\sum_{n=1}^{N}\frac{\partial^2}{\partial x_n^2} + \frac{1}{2}\sum_{n=1}^{N}x_n^2 + \alpha\sum_{n>k=1}^{N}\delta(x_n - x_k), \tag{1.18}$$

where the energy is measured in units of $\hbar\omega_z$. We can see that $\alpha$ is the only parameter which tunes our system if the number of particles $N$ is fixed. As particles are identical bosons, for any interaction strength the wave-function of the system has the symmetry:

$$\psi(x_1, x_2, \ldots, x_i, \ldots, x_j, \ldots, x_N) = \psi(x_1, x_2, \ldots, x_j, \ldots, x_i, \ldots, x_N), \tag{1.19}$$

for any $1 \leq i, j \leq N$.

## 1.4. Breathing oscillations

The procedure of exciting breathing oscillations is the following. At first, the system is brought to the ground state. Then, one instantaneously changes the frequency of the confining potential by a small amount. This procedure implies that the amount of energy transferred to the system is small and only low-energy modes are excited. After such a quench the system undergoes the time-evolution in which oscillations of the center-of-mass are not excited.

Formally speaking, in the beginning we consider the system in the ground state with the trapping frequency $\omega_z$. Then the trapping frequency instantaneously changes to the frequency to $\omega_z + \delta\omega_z$. Due to a small time of quench, after the quench the system will still be in the same state as before. We need to consider a time evolution of the system with the Hamiltonian

$$\hat{H}(t) = \hat{H} + \delta V(t), \tag{1.20}$$

where

$$\delta\hat{V}(t) = \begin{cases} 0 & \text{if } t < 0, \\ m\omega_z\delta\omega_z\hat{Q}_0 & \text{if } t > 0, \end{cases} \tag{1.21}$$

The small parameter $\delta\omega_z/\omega_z$ guarantees a weak perturbation.

So the breathing mode is defined as a collective oscillation which is induced by the perturbation operator

$$Q_0 \equiv \sum_{i=1}^{N} z_i^2, \tag{1.22}$$

or more precisely, by the operator

$$Q = Q_c \equiv \sum_{i=1}^{N} (z_i - Z_{\rm cm})^2, \tag{1.23}$$

where $Z_{cm} = \frac{1}{N}\sum_{i=1}^{N} z_i$ is center-of-mass coordinate. These two operators coincide in the thermodynamic limit, but for finite systems the choice between them can be important. The difference comes from the fact that the operator $Q_0$ excites the center-of-mass motion while the operator $Q_c$ does not. Later we will discuss the difference between these two operators for few-particle systems.

### 1.4.1. Connection with the spectrum

For sufficiently small $\delta\omega_z$ one can use perturbation theory to establish connection with the spectrum of the Hamiltonian (1.17). Let us consider the system at ground state at the time $t = 0$. After the quench (1.20) will lo longer be in the ground state. We can think in terms of the first-order perturbation theory for connecting the ground state wave-function before the quench and many-body wave-functions after the quench (see Ref. [30]):

$$\psi_0^{old}(t=0) = \psi_0^{new} + 2\frac{\delta\omega}{\omega}\sum_{l\neq 0}^{\infty} \frac{V_{pot\,0,l}}{E_0 - E_l}\psi_l^{new}, \tag{1.24}$$

where $\psi_0^{old}$ is the ground state wave-function before the quench, $\psi_l^{new}$ are eigenfunctions of the Hamiltonian after the quench, and $V_{pot\,l,k} = \int_{-\infty}^{\infty} \psi_l(x)\frac{m\omega^2 x^2}{2}\psi_k(x)dx$. Analytically $V_{pot\,l,k}$ can be calculated in a few limiting cases. For two particles exact functions are known for any interaction. Also occupation numbers can be calculated for a free boson gas and Tonks gas following the procedure described in Sec. 5.2. The time evolution of the state after the quench is described by the equation [30]:

$$\psi = \psi_0^{new}\exp\left(i\frac{E_0}{\hbar}t\right) + 2\frac{\delta\omega}{\omega}\sum_{l\neq 0}^{\infty}\frac{V_{pot\,0,l}}{E_0 - E_l}\psi_l^{new}\exp\left(i\frac{E_l}{\hbar}t\right). \tag{1.25}$$

In experiments the breathing mode frequency is obtained by measuring the average radius of the cloud. We write

$$\left\langle z^2 \right\rangle (t) = \left\langle z^2 \right\rangle (0) + 2\frac{\delta\omega}{\omega} \sum_{l\neq 0}^{\infty} \frac{V_{pot\,0,l}}{E_0 - E_l} z_{l,0}^2 \cos\left(\frac{E_l - E_0}{\hbar} t\right). \tag{1.26}$$

In Eq. (1.26) we ignore phases as they are not important for the physics and it is clear that they always come with $E_j - E_k$ as $\phi_j - \phi_k$ in the argument of cosine and can be restored at any moment. The amplitude of oscillations is proportional to the quench strength $\delta\omega/\omega$. In the limiting cases $g \to \infty$ and $g \to 0$ we have $V_{pot\,0,l} \neq 0$ only for $l = 2$. However, for a finite interaction one has $V_{pot\,0,l} \neq 0$ for any $l$. One can expect that $V_{pot\,0,l}$ would decay with increasing $l$. Moreover, $E_l - E_0 \approx l\hbar\omega_z$, so that the first term in the sum (1.26) will be the dominant one. Thus, measuring the frequency of the oscillations by the method used in most experiments [14, 15] we measure the frequency of the second excited state

$$\omega_{2,0} = \left|\frac{E_2 - E_0}{\hbar}\right|. \tag{1.27}$$

It is clear that in the case of zero-interactions (free bosons) the breathing mode frequency is equal to $2\omega_z$ as the spectrum is equidistant. For the case of infinite repulsion, $g \to \infty$, the spectrum of the system is the same as in the case of free fermions. Thus, the breathing mode frequency will be also equal to $2\omega_z$.

## 1.5. Quasi-classical equation of motion and virial theorem

In this section we write a virial theorem and a formula for the calculation of the breathing mode frequency, which wee will use extensively. Our presentation follows Ref. [2]. Let us assume that during the motion of the cloud the density profile maintains its shape, but its spatial size depends on time.

$$\psi(r) = AN^{\frac{1}{2}} R^{-\frac{1}{2}} f(z/R) e^{i\phi(z)}, \tag{1.28}$$

where $f$ is an arbitrary real function, and A is a normalization constant. The total energy of the cloud may be written as

$$E = E_{flow} + U(R). \tag{1.29}$$

Here the first term is the kinetic energy associated with particle currents, and is given by

$$E_{flow} = \frac{\hbar^2}{2m} \int_{-\infty}^{\infty} |\psi(z)|^2 (\nabla\phi)^2 dz. \tag{1.30}$$

The second term is an effective potential energy, and it is equal to the energy of the cloud when the phase does not vary in space. It is made up of the kinetic energy, energy of interaction with the trapping potential, and the energy of interparticle interaction:

$$U(R) = E_{kin} + E_{pot} + E_{int}, \tag{1.31}$$

where

$$E_{pot} = N\frac{m\omega_z^2}{2} \int_{-\infty}^{\infty} z^2 \psi(z)^2 dz, \tag{1.32a}$$

$$E_{kin} = N\frac{\hbar^2}{2m} \int_{-\infty}^{\infty} \left(\frac{\partial\psi(z)}{\partial z}\right)^2 dz, \tag{1.32b}$$

$$E_{int} = \frac{N(N-1)}{2} g \int_{-\infty}^{\infty} \psi(z)^4 dz. \tag{1.32c}$$

The equilibrium radius of the cloud $R_0$ is determined by minimizing the total energy:

$$\left.\frac{\partial U}{\partial R}\right|_{R=R_0} = 0, \tag{1.33}$$

or, since the contributions to the energy behave as powers of $R$:

$$R\left.\frac{\partial U}{\partial R}\right|_{R=R_0} = -2E_{kin} + 2E_{pot} - E_{int} = 0. \tag{1.34}$$

When $R$ differs from its equilibrium value there is a force tending to change $R$. To derive an equation describing the dynamics of the cloud, we need to find the kinetic energy associated with a time dependence of $R(t)$. Changing $R$ from its initial value to a new value $\tilde{R}$ amounts to a uniform dilation of the cloud, since the new density distribution may be obtained from the old one by changing the radial coordinate of each atom by a factor of $\tilde{R}/R$. The velocity of a particle is therefore equal to

$$v(r) = r\frac{\dot{R}}{R}, \tag{1.35}$$

where $\dot{R}$ is the time derivative of $R$. The energy of the flow of the gas is given by

$$E_{flow} = \frac{m\dot{R}^2}{2R^2} \int_{-\infty}^{\infty} z^2 n(z) dz = \frac{\dot{R}^2}{\omega_z^2 R^2} E_{pot}. \tag{1.36}$$

The total energy of the cloud may thus be written as a sum of the energy of the static cloud and the flow energy term:

$$E = \frac{1}{2} m_{eff} \dot{R}^2 + U(R), \tag{1.37}$$

where $m_{eff} = \frac{2}{\omega_z^2 R^2} E_{pot}$. From the condition of energy conservation $dE/dt = 0$, it follows that the equation of motion is

$$m_{eff} \ddot{R} = -\frac{\partial U}{\partial R}. \tag{1.38}$$

We investigate the frequency of small oscillations about the equilibrium state. Expanding the effective potential to second order in $R - R_0$, one finds

$$U(R) = U(R_0) + \frac{\partial^2 U}{\partial R^2}(R - R_0)^2, \tag{1.39}$$

From Eq. (1.32) one sees that

$$R^2 \frac{\partial^2 U}{\partial R^2} = 6E_{kin} + 2E_{pot} + 2E_{int}. \tag{1.40}$$

Thus the frequency is given by [2]

$$\omega^2 = \omega_z^2 \left(4 - \frac{E_{int}}{2E_{pot}}\right) = \omega_z^2 \left(3 + \frac{E_{kin}}{E_{pot}}\right). \tag{1.41}$$

When interactions may be neglected one finds $\omega = 2\omega_z$, in agreement with the exact result, corresponding quantum-mechanically to two oscillator quanta. In the limit of strong interactions, the term $E_{kin}$ can be neglected to first approximation, and therefore $\omega^2 = 3\omega_z^2$. This agrees with the exact result in this limit (see Sec. 3.8.2). Equation (1.41) is very useful as it connects the frequency of the oscillations with kinetic, potential and exchange energies averaged over the steady state. This is the link between dynamical and static properties. In the next sections we will obtain the same result in other approximations.

## 1.6. Hierarchy of sum rules

*"Numquam ponenda est pluralitas sine necessitate."*

*William of Ockham*

Sum rule approximation connects the frequency of collective oscillations with statical properties of the system in the steady state. For any excitation operator $\hat{Q}$ and integer $n$

the moment $m_n$ is introduced as follows [20, 31, 32]:

$$m_n = \sum_{i=1}^{\infty} (E_i - E_0)^n \left| \left\langle i \left| \hat{Q} \right| 0 \right\rangle \right|^2 . \tag{1.42}$$

Sum rule approximation can be treated by taking ratios of different moments $m_n$ and $m_{n-2}$ [20, 32]

$$\omega^2 = \frac{m_n}{m_{n-2}}. \tag{1.43}$$

If the operator $\hat{Q}$ excites the mode with energy $E_k$ and does not excite any modes with lower energy then in the limit $n \to -\infty$ frequency $\omega$ converges to the $\frac{E_k - E_0}{\hbar}$. Hence, the best choice of operator is the following. If we want to find the frequency of a certain state we should take the projector of the ground state on this state. However, in the general case there is no method of constructing such an operator. Thus, for any finite $n$ the frequency $\omega$ is only an approximation. In this section we make the analysis of two moment ratios with close indices.

### 1.6.1. Sum rule $m_3/m_1$

Taking the operator $\hat{Q} = x^2$ we have

$$\hat{Q}_1 = i \left[ \hat{H}, \hat{Q} \right] = \frac{2\hbar}{m} \left( \hat{x}\hat{p} - \frac{i\hbar}{2} \right), \tag{1.44}$$

$$\hat{Q}_2 = i \left[ \hat{H}, \hat{Q}_1 \right] = \frac{2h^2}{m} \left( 2\hat{H}_{kin} - 2\hat{H}_{pot} + \hat{H}_{int} \right), \tag{1.45}$$

where $\hat{p}$ is the momentum operator, $\hat{H}_{kin}$, $\hat{H}_{pot}$ and $\hat{H}_{int}$ are operators of the kinetic energy, energy of the interaction with the trapping potential and energy of the interparticle interaction.

The first and third moments are:

$$m_1 = \frac{i}{2} \left[ \hat{Q}_1, \hat{Q} \right] = \frac{2\hbar^2}{m} \langle 0 \left| x^2 \right| 0 \rangle. \tag{1.46}$$

$$m_3 = \frac{i}{2} \left[ \hat{Q}_2, \hat{Q}_1 \right] = \frac{2\hbar^4}{m^2} \left( 4E_{kin} + 4E_{pot} + E_{int} \right). \tag{1.47}$$

Thus we have

$$\hbar^2\omega^2 = \frac{m_3}{m_1} = \hbar^2\omega_z^2 \frac{4E_{kin} + 4E_{pot} + E_{int}}{2E_{pot}}. \tag{1.48}$$

Equation (1.48) together with the virial theorem (1.34) gives the following formula for the frequency of breathing oscillations

$$\omega^2 = \omega_z^2 \left(4 - \frac{E_{int}}{2E_{pot}}\right) = \omega_z^2 \left(3 + \frac{E_{kin}}{E_{pot}}\right). \tag{1.49}$$

We focus attention on the fact that Eqs. (1.49) and (1.41) are identical.

### 1.6.2. Sum rule $m_1/m_{-1}$

As we saw in section 1.6.1, the moment $m_1$ is proportional to the potential energy:

$$m_1 = 4E_{pot}/a_z^2. \tag{1.50}$$

The moment with index $-1$ is related to the static polarizability $\alpha$:

$$m_{-1} = \frac{1}{2}\alpha. \tag{1.51}$$

This is equivalent to adding an infinitesimal perturbation $\epsilon Q$ to the Hamiltonian and calculating the corresponding change of the cloud size:

$$\alpha = \frac{\delta \langle z^2 \rangle}{\epsilon}. \tag{1.52}$$

Up to second order, adding the perturbation $\epsilon Q$ is equivalent to changing the frequency by $\delta\omega_z = \epsilon/m$. Thus, we arrive at the compact formula for the frequency of breathing oscillations:

$$\omega^2 = -2\frac{\langle Q \rangle}{\frac{\partial \langle Q \rangle}{\partial \omega_z^2}}. \tag{1.53}$$

# 2. Two interacting particles in a parabolic trap

A system of two particles is interesting for us as it is always integrable and keeps main characteristics of collective phenomena. The study of this system is important because it gives us an intuitive understanding of many-body phenomena. Later we will use the results obtained for two-particle systems as a test for other theories in some particular regimes.

The case of two ultracold atoms interacting via a contact potential in a $3D$ parabolic trap is analysed, for example, in Ref. [33]. Let us consider a 1D system with two particles described by the first-quantized Hamiltonian

$$\hat{H} = -\frac{\hbar^2}{2m}\frac{\partial^2}{\partial z_1^2} - \frac{\hbar^2}{2m}\frac{\partial^2}{\partial z_2^2} + \frac{m\omega_z^2 z_1^2}{2} + \frac{m\omega_z^2 z_2^2}{2} + g\delta(z_1 - z_2). \tag{2.1}$$

The case $g > 0$ corresponds to the repulsive interaction and $g < 0$ to the attractive interaction. Making a substitution $\eta = z_1 - z_2$, $\xi = (z_1 + z_2)/2$, and introducing effective masses $m^{(\eta)} = m/2$, $m^{(\xi)} = 2m$ we obtain the Hamiltonian with separable variables:

$$\hat{H} = \hat{H}^{(1)}(\xi) + \hat{H}^{(2)}(\eta) = -\frac{\hbar^2}{2m^{(\xi)}}\frac{\partial^2}{\partial \xi^2} + \frac{m^{(\xi)}\omega_z^2\xi^2}{2} - \frac{\hbar^2}{2m^{(\eta)}}\frac{\partial^2}{\partial \eta^2} + \frac{m^{(\eta)}\omega_z^2\eta^2}{2} + g\delta(\eta). \tag{2.2}$$

This means that

$$\psi_{n_1,n_2}(\xi,\eta) = \psi_{\xi,n_1}(\xi)\psi_{\eta,n_2}(\eta), \tag{2.3a}$$

$$E_{n_1,n_2} = E_{\xi,n_1} + E_{\eta,n_2}. \tag{2.3b}$$

We see that the Hamiltonian $\hat{H}^{(1)}(\xi)$ has the form of a one-dimensional harmonic oscillator and it has the same spectrum.

Considering two bosons implies restrictions on the symmetry of the wave-function. More precisely, we are looking only for solutions which do not change after the transformation $z_1 \leftrightarrow z_2$. This means that only even wave-functions $\psi_\eta(\eta)$ should be considered. We can find an analytical solution for the spectrum of $\hat{H}^2(\eta)$ from the corresponding Schrödinger equation:

$$-\frac{\hbar^2}{2m^{(\eta)}}\frac{\partial^2}{\partial \eta^2}\psi_\eta(\eta) + \frac{m^{(\eta)}\omega_z^2\eta^2}{2}\psi_\eta(\eta) + g\delta(\eta)\psi_\eta(\eta) = E\psi_\eta(\eta). \tag{2.4}$$

Introducing the one-dimensional scattering length $a_{1D} = -2\hbar^2/(mg)$, harmonic length $a_z = (\hbar/m\omega_z)^{\frac{1}{2}}$, dimensionless interaction $\alpha = -2a_z/a_{1D}$, and the dimensionless variable $x = \eta/\left(\sqrt{2}a_z\right)$ we obtain the following equation

$$-\frac{1}{2}\frac{\partial^2}{\partial x^2}\psi_\eta(x) + \frac{x^2}{2}\psi_\eta(x) + \frac{\alpha}{\sqrt{2}}\delta(x)\psi_\eta(x) = E\psi_\eta(x). \tag{2.5}$$

In this equation and further in this chapter the energy $E$ is measured in units of $\hbar\omega_z$. The solution of Eq. (2.5) has a jump in the first derivative at $x = 0$. This can be seen by the integration of equation (2.5) in the vicinity of $x = 0$:

$$\left.\frac{\partial\psi_\eta(x)}{\partial x}\right|_{+0} - \left.\frac{\partial\psi_\eta(x)}{\partial x}\right|_{-0} = \frac{\alpha}{\sqrt{2}}\psi_\eta(0). \tag{2.6}$$

Eq. (2.5) under the condition (2.6) has the solution

$$\psi_\eta(x) = A\left(F\left(\frac{1}{4} - \frac{E}{2}, \frac{1}{2}, x^2\right) + B|x|F\left(\frac{3}{4} - \frac{E}{2}, \frac{3}{2}, x^2\right)\right)\exp\left(-\frac{1}{2}x^2\right), \tag{2.7}$$

where the constants $A$, $B$ and energy $E$ should be determined from the asymptotic behavior at $\eta \to \infty$, the normalization condition, and equation (2.6). The confluent hypergeometric function $F(a, b, u)$ has the asymptotic behaviour:

$$F(a, b, u) = \frac{\Gamma(b)}{\Gamma(a)}u^{a-b}\exp(u), u \to \infty, \tag{2.8}$$

and hence

$$\psi_\eta(x) \to A\left(\frac{\Gamma(\frac{1}{2})}{\Gamma\left(\frac{1}{4} - \frac{E}{2}\right)} - B\frac{\Gamma\left(\frac{3}{2}\right)}{\Gamma\left(\frac{3}{4} - \frac{E}{2}\right)}\right)x^{-\frac{1}{2}-E}\exp\left(\frac{1}{2}x^2\right), \qquad x \to \infty. \tag{2.9}$$

The wave-function has to be normalized, which means that it has to vanish as $x \to \infty$. This leads to an expression for the coefficient $B$:

$$B = -\frac{\Gamma\left(\frac{1}{2}\right)\Gamma\left(\frac{3}{4} - \frac{E}{2}\right)}{\Gamma\left(\frac{3}{2}\right)\Gamma\left(\frac{1}{4} - \frac{E}{2}\right)} = -\frac{2\Gamma\left(\frac{3}{4} - \frac{E}{2}\right)}{\Gamma\left(\frac{1}{4} - \frac{E}{2}\right)}. \tag{2.10}$$

Thus, we can rewrite equation (2.6) as

$$\frac{2\sqrt{2}\Gamma\left(\frac{3}{4} - \frac{E}{2}\right)}{\Gamma\left(\frac{1}{4} - \frac{E}{2}\right)} = -\alpha, \tag{2.11}$$

which gives the energy for $E/\hbar\omega_z < 1/2$. For the states with higher energy we can use the following equation:

$$\frac{2\sqrt{2}\Gamma\left(\frac{3}{4} + \frac{E}{2}\right)}{\Gamma\left(\frac{1}{4} + \frac{E}{2}\right)}\tan\left(\pi\left(\frac{1}{4} - \frac{E}{2}\right)\right) = -\alpha. \tag{2.12}$$

Solutions of this equation give us the spectrum of the Hamiltonian $\hat{H}^{(2)}(\eta)$. The dependence of the spectrum (lowest states) on the interaction parameter $\alpha = \sqrt{\frac{m}{\hbar^3\omega_z}}g$ is in full agreement with the results of Ref. [34] (see Fig. 2).

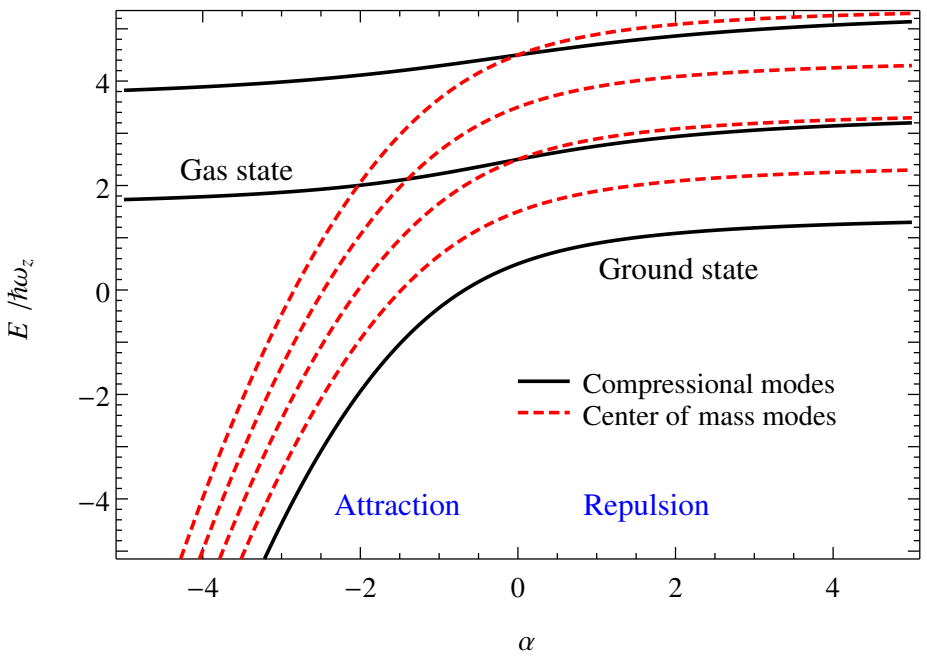


Figure 2: The dependence of the spectrum of two particles in a parabolic trap on the interaction parameter $\alpha$. The red dashed curves represent the energies of the modes related to the center-of-mass motion. The black solid curves represent the energies of the compressional modes.

One can see that when $\alpha$ is large and negative (the strong attraction regime) the energy of the ground state is also large and negative. Using Stirling's formula we find that

$$E = -\frac{1}{2}\alpha^2, \tag{2.13}$$

when $\alpha \to -\infty$. One sees from Eq. (2.13) that the energy gap between the ground state and the gas state becomes infinitely large for $\alpha \to -\infty$.

Combining Eqs. (2.7) and (2.10) we obtain

$$\psi_\eta(x) = A\left(F\left(\frac{1}{4}-\frac{E}{2},\frac{1}{2},x^2\right) - \frac{2\Gamma\left(\frac{3}{4}-\frac{E}{2}\right)}{\Gamma\left(\frac{1}{4}-\frac{E}{2}\right)}|x|F\left(\frac{3}{4}-\frac{E}{2},\frac{3}{2},x^2\right)\right)\exp\left(-\frac{1}{2}x^2\right), \tag{2.14}$$

where $A$ is the normalization constant, and the energy $E$ is given by Eq. (2.12). The energies are analytic functions of the interaction at the point $g = 0$.

The ground-state density profiles for different values of the parameter $\alpha$ are shown in Fig. 3.

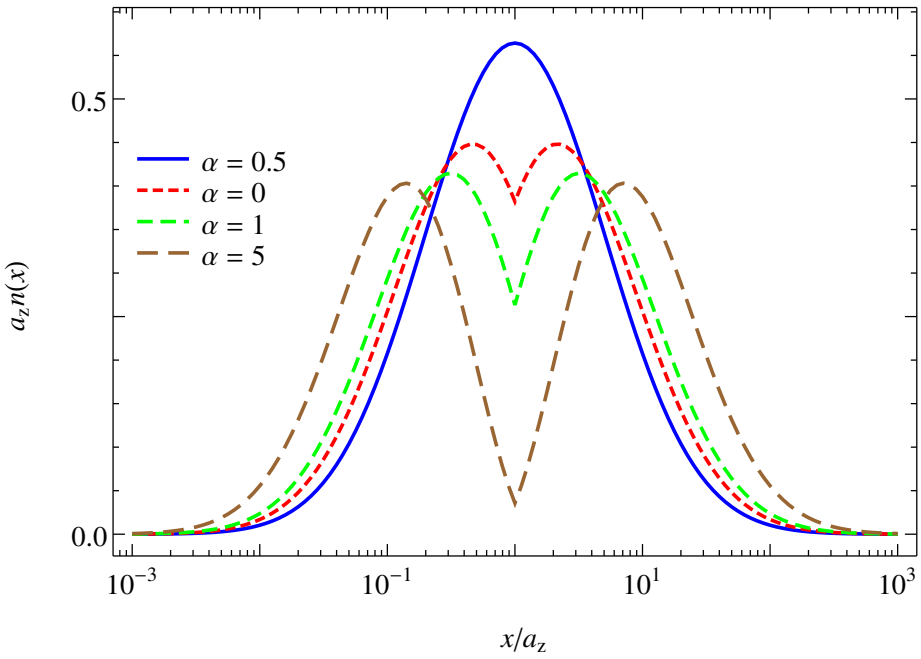


Figure 3: The density profiles for the relative motion ($|\psi|^2$ integrated over the center of mass motion) for the interaction parameter $\alpha = 0$, 0.5, 1.0, and 5.0.

## 2.1. Perturbative analysis for two particles in the trap

Now we find the ground state and the first exited state of the Hamiltonian $\hat{H}^{(2)}(\eta)$ using perturbation theory. We can use the Hamiltonian of the harmonic oscillator (HO) as an unperturbed Hamiltonian, and consider the interparticle interaction as perturbation. Thus we have:

$$\begin{aligned}\psi_{n,\eta}(x) = \psi_n^{HO}(x) &+ \frac{\alpha}{\sqrt{2}} \sum_{k\neq n}^{\infty} \frac{V_{n,k}}{E_n^{HO} - E_k^{HO}} \psi_k^{HO}(x) \\ &+ \frac{\alpha^2}{2} \sum_{k\neq n, l\neq n}^{\infty,\infty} \frac{V_{k,l} V_{l,n}}{\left(E_n^{HO} - E_k^{HO}\right)\left(E_n^{HO} - E_l^{HO}\right)} \psi_k^{HO}(x) \\ &- \frac{\alpha^2}{2} \sum_{k\neq n}^{\infty} \frac{V_{n,n} V_{k,n}}{\left(E_n^{HO} - E_k^{HO}\right)^2} \psi_k^{HO}(x) - \frac{\alpha^2}{4} \sum_{k\neq n}^{\infty} \frac{V_{n,k}^2}{\left(E_n^{HO} - E_k^{HO}\right)^2} \psi_n^{HO}(x),\end{aligned} \tag{2.15a}$$

$$E_n = E_n^{HO} + \frac{\alpha}{\sqrt{2}} V_{n,n} + \frac{\alpha^2}{2} \sum_{k\neq n}^{\infty} \frac{|V_{k,n}|^2}{E_n^{HO} - E_k^{HO}}, \tag{2.15b}$$

where $\psi_n^{HO}(x) = \frac{1}{\sqrt{\pi 2^n n!}} \exp(-x^2/2) H_n(x)$ are the eigenfunctions of the harmonic oscillator, the matrix elements $V_{2n,2k} = \frac{(-1)^{n+k}\sqrt{(2n)!(2k)!}}{\sqrt{\pi} 2^{n+k} n! k!}$, and the energies $E_n^{HO} = n + \frac{1}{2}$. The functions

$H_n$ are Hermite polynomials. The ground state wave-function of $\hat{H}^{(2)}(\eta)$ reads:

$$\begin{aligned}\psi_0(x) &= \psi_0^{HO}(x) + \frac{\alpha}{\sqrt{2}}\sum_{k\neq 0}\frac{(-1)^{k+1}\sqrt{(2k)!}}{\sqrt{\pi}2^{k+1}k!k}\psi_{2k}^{HO}(x) \\ &+ \frac{\alpha^2}{2}\sum_{k\neq 0}\frac{(-1)^k\sqrt{(2k)!}}{\pi 2^{k+2}kk!}\left(\ln 4 - \frac{1}{k}\right)\psi_{2k}^{HO}(x) - \frac{\alpha^2}{2}\frac{\pi^2 - 3\left(\ln 4\right)^2}{48\pi}\psi_0^{HO}(x),\end{aligned} \tag{2.16a}$$

$$E_0[\eta] = \frac{1}{2} + \frac{\alpha}{\sqrt{2}}\frac{1}{\sqrt{\pi}} - \alpha^2\frac{\ln 4}{4\pi}. \tag{2.16b}$$

Thus the wave-function of the ground state of the system is $\psi_{gs}(\xi,\eta) = \psi_0^{HO}(\xi)\psi_{0,\eta}(\eta)$, and the ground-state energy is

$$E_{gs}[\xi,\eta] = \frac{1}{2} + \frac{1}{2} + \alpha\frac{1}{\sqrt{2\pi}} - \alpha^2\frac{\ln 4}{4\pi} + \ldots. \tag{2.17}$$

The first exited state has the form

$$\psi_{1,0}(\xi,\eta) = \psi_{\xi,1}(\xi)\psi_{\eta,0}^{HO}(\eta), \tag{2.18a}$$

$$E_{1,0}[\xi,\eta] = E_1^{HO}[\xi] + E_0[\eta] = \frac{3}{2} + \frac{1}{2} + \alpha\frac{1}{\sqrt{2\pi}} - \alpha^2\frac{\ln 4}{4\pi}, \tag{2.18b}$$

and the difference in the energies of this excitation and the ground state is $\hbar\omega$. This excitation is related to the center-of-mass motion.

Let us calculate the first excited one-particle state of the Hamiltonian $\hat{H}^{(2)}(\eta)$. Since we have bosonic particles, the wave-function has to satisfy the condition $\psi(x_1,x_2) = \psi(x_2,x_1)$, which means that the wave-function has to be an even function of $\eta$. The first symmetric excited state has a non-perturbed wave-function $\psi_2^{HO}(\eta)$. The perturbed wave-function of this state is:

$$\begin{aligned}\psi_2(x) &= \psi_2^{HO}(x) + \frac{\alpha}{\sqrt{2}}\sum_{k\neq 1}\frac{(-1)^k\sqrt{(2k)!2}}{\sqrt{\pi}\,2^{k+2}\,k!\,(k-1)}\psi_{2k}^{HO}(x) \\ &+ \frac{\alpha^2}{2}\sum_{k\neq 1}\frac{(-1)^k\sqrt{(2k)!2}}{\pi(k-1)\,k!\,2^{k+4}}\left((\ln 4 - 1) - \frac{1}{k-1}\right)\psi_{2k}^{HO}(x) \\ &- \frac{\alpha^2}{4}\left(\frac{{}_3F_3\left(1,1,1,\frac{5}{2};2,3,3;1\right)}{64\,\pi} + \frac{1}{8\pi}\right)\psi_2^{HO}(x),\end{aligned} \tag{2.19a}$$

$$E_2[\eta] = \frac{5}{2} + \alpha\frac{1}{2\sqrt{2\pi}} + \alpha^2\frac{1-\ln 4}{16\pi}, \tag{2.19b}$$

$$E_4[\eta] = \frac{9}{2} + \alpha\frac{3}{8\sqrt{2\pi}} + \alpha^2\frac{21 - 3\ln 4096}{512\pi}. \tag{2.20}$$

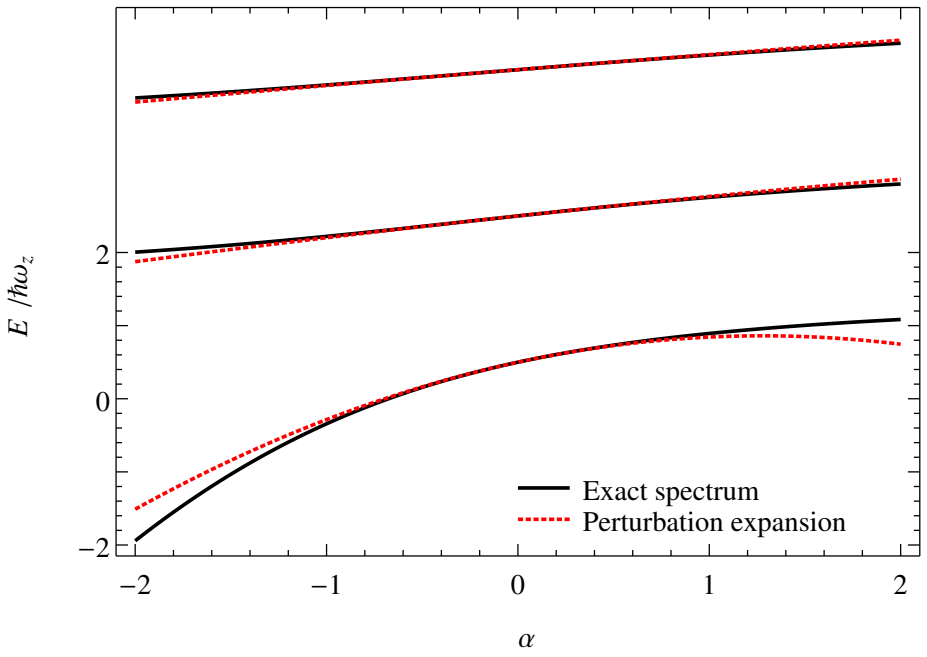


Figure 4: Comparison of the energies of the lowest states of the relative motion of the two-particle system in a parabolic trap (black) and their perturbative approximations (red dashed). The data are presented as functions of the interaction parameter $\alpha$.

Let us notice that the sum in (2.19a) includes only even functions. The total wave-function of the excited system is

$$\psi_{2,0}(\xi,\eta) = \psi_2(\xi)\psi_0^{HO}(\eta). \tag{2.21}$$

So, the difference in the energies of the first excited state of the Hamiltonian $\hat{H}^{(2)}(\eta)$ (second excited state in the full Hamiltonian (2.2)) and the ground state is

$$E_2 - E_0 = \hbar\omega\left(2 - \alpha\frac{1}{2\sqrt{2\pi}} + \alpha^2\frac{1+3\ln 4}{16\pi}\right) + \dots. \tag{2.22}$$

The energies of the first five levels and their perturbation approximation are shown in Fig. 4. The perturbation theory gives correct values for the expansion of the energy $E_{\eta,n}(\alpha)$ in powers of $\alpha$ near $\alpha = 0$ at least up to the third order.

The expressions for the energies (2.16b, 2.19b, 2.20) are in full correspondence with the expansions for the same energy levels from (2.12). This shows that the perturbation theory can be applied in this case.

## 2.2. Exact breathing mode for two particles

Now we calculate the exact breathing mode frequency based on the solution of Eq. (2.12). In the repulsive regime the breathing mode can be defined as the difference in the energies of the first exited state (yellow curve in Fig. 2) and the ground state (blue curve in Fig. 2). In this regime the breathing mode frequency is less then $2\omega_z$. In the attractive regime the

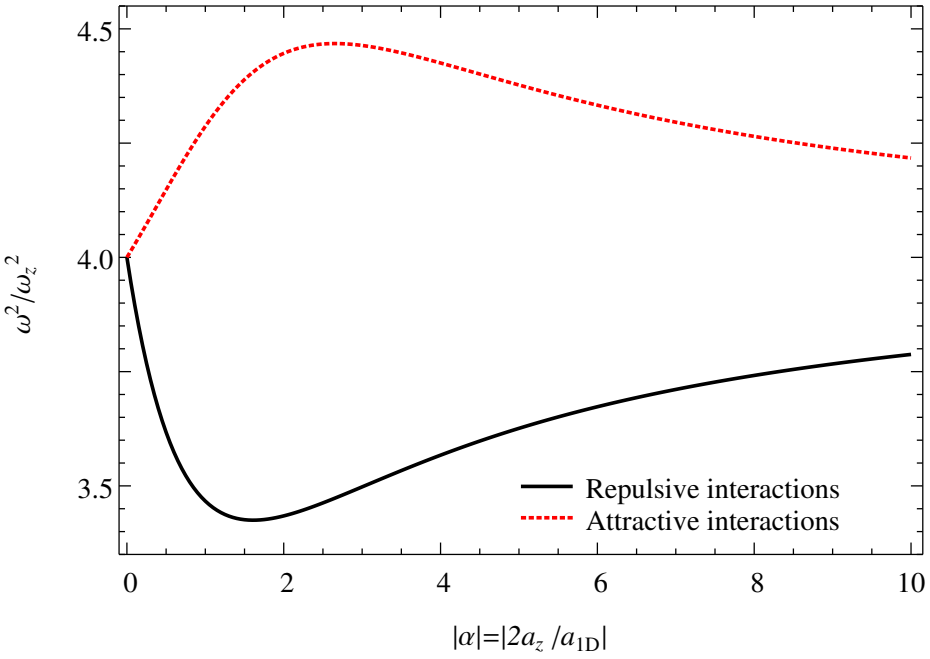


Figure 5: The dependence of the breathing mode frequency for two particles in a parabolic trap versus the interaction parameter $|\alpha| = |2a_z/a_{1D}|$. For attractive interactions $\omega/\omega_z \geq 2$ and for repulsive interactions $\omega/\omega_z \leq 2$. In both cases we have $\omega/\omega_z = 2$ for $\alpha \to 0$.

breathing mode frequency is defined in another way. The definition comes from the method of how the breathing mode was measured in the experiment [14]. In this experiment the system was in the strong repulsive regime using the confinement induced resonance (the repulsive Tonks-Girargeau regime corresponding to the right part of the blue curve in Fig. 2), and then the interaction adiabatically was switched to attractive. After this switch the system gets to the super-Tonks-Girargeau regime. In Fig. 2 this corresponds to the transition from the right part of the ground state curve to the left part of the gas state curve. The excitation above this state is called the breathing mode. In this regime (super-Tonks-Girargeau regime, as it was mentioned in Ref. [16]), we can see that the breathing mode frequency is higher

than $2\hbar\omega_z$. The dependence of the breathing mode frequency on the interaction parameter $\alpha$ is shown in Fig. 5. The breathing mode frequency and its perturbation approximation in the region of small interactions, $\alpha < 1$, are plotted in Fig. 6.

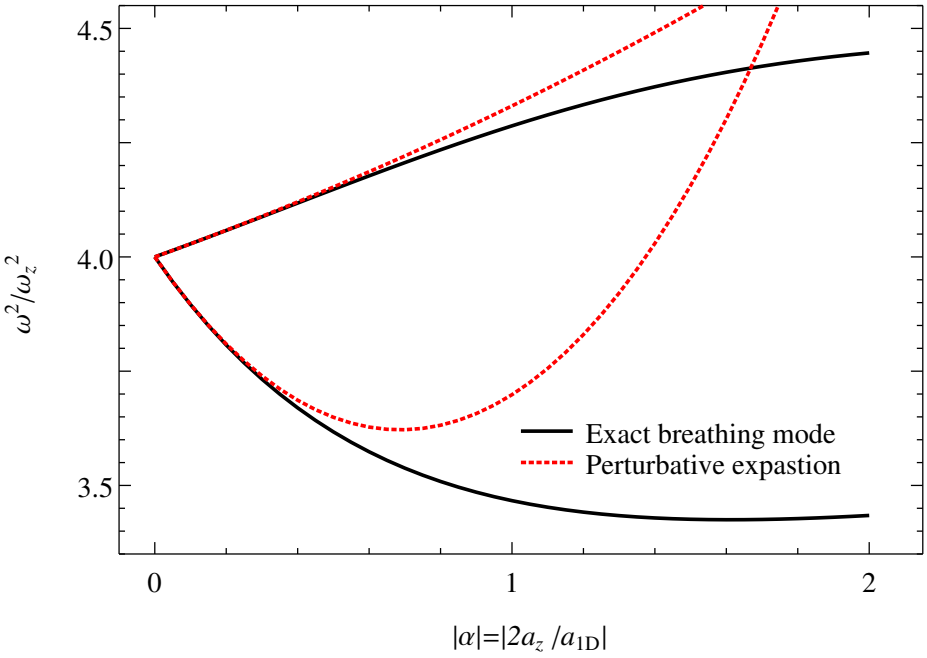


Figure 6: Comparison of the breathing mode frequency of the two-particle system in a parabolic trap (black) and perturbative approximation (red, dashed). The data are presented as functions of the interaction parameter $|\alpha|$.

## 2.3. Breathing mode frequency calculated using sum rules

Considering the operator $\hat{Q} = z^2 = x_1^2 + x_2^2$ as perturbation one can calculate the breathing mode frequency (1.53) using the relation [20, 32]:

$$\omega^2 = -2\frac{\langle z^2 \rangle}{\frac{\partial \langle z^2 \rangle}{\partial \omega_z^2}}, \tag{2.23}$$

where the average of the operator $\hat{Q}$ is taken over the ground state

$$\langle \hat{Q} \rangle = \iint_{-\infty,-\infty}^{\infty,\infty} \psi_{gs}(x_1, x_2)\hat{Q}(x_1, x_2)\psi_{gs}^*(x_1, x_2)dx_1dx_2. \tag{2.24}$$

We use the exact ground state wave-function (2.14) for the calculation of the breathing mode. Thus we use the property (2.3a):

$$\psi_{gs}(x_1, x_2) = \psi_{gs}^{HO}\left(\frac{x_1 + x_2}{2}\right)\psi_{gs}^{\eta}\left(x_1 - x_2\right). \tag{2.25}$$

This allows us to calculate the average value of the perturbation operator:

$$\begin{aligned}\left\langle x_1^2 + x_2^2\right\rangle &= \iint_{0,0}^{\infty,\infty} \left|\psi_{gs}^{HO}\left(R_{12}\right)\psi_{gs}^{\eta}(r_{12})\right|^2 \left(2R_{12}^2 + \frac{1}{2}r_{12}^2\right) dR_{12}dr_{12} \\ &= a_z^2\left(\frac{1}{2} + \int_0^{\infty} r_{12}^2\left|\psi_{gs}^{\eta}(r_{12})\right|^2 dr_{12}\right), \end{aligned} \tag{2.26}$$

where $R_{12} = \left(x_1 + x_2\right)/2$ and $r_{12} = x_1 - x_2$ are center of mass and relative coordinates, respectively.

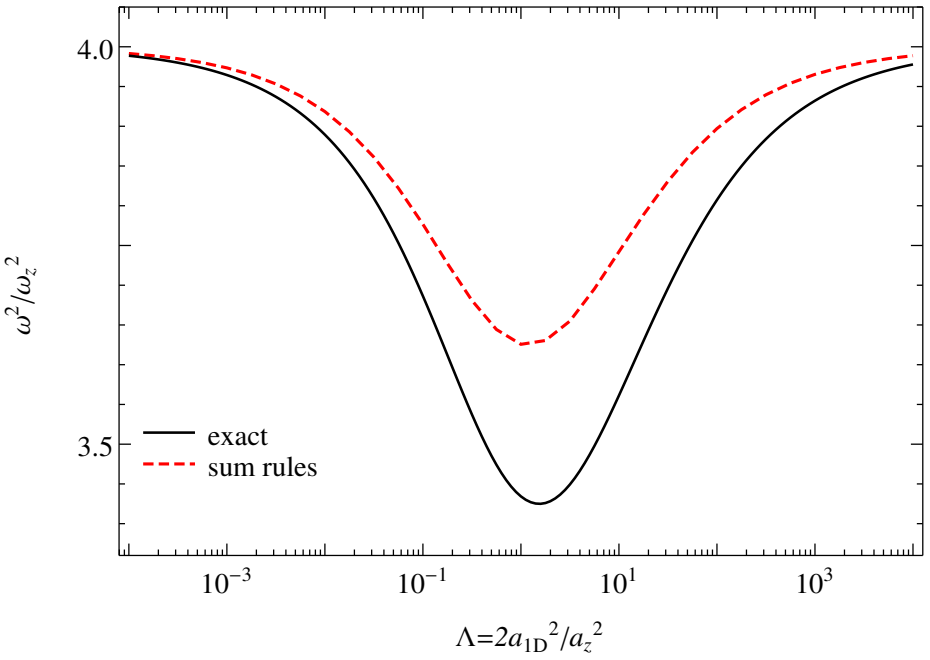


Figure 7: The dependence of the breathing mode frequency of two particles in a parabolic trap (solid black) versus the interaction parameter $\Lambda = 2\left(\frac{a_{1D}}{a_z}\right)^2$ and its approximation by the sum rule (1.53) (red dashed). The significance of the parameter $\Lambda$ will be clarified when considering the solution for N-particle systems.

The dependence of the exact breathing mode frequency and the breathing mode frequency calculated using the sum rules are shown in Fig. 7. The sum rule formula gives the result which is bigger than the exact one.

It is interesting to compare the first order correction to the breathing mode frequency calculated using the sum rules with the perturbative result (2.22). Thus, we use the wave-function expansion (2.16a). This leads to the following result:

$$\left\langle x_1^2 + x_2^2 \right\rangle = a_z^2 + a_z^2 \frac{\alpha}{2\sqrt{2\pi}}, \tag{2.27a}$$

$$\omega_z^2 \frac{\partial}{\partial \omega_z^2} \left\langle x_1^2 + x_2^2 \right\rangle = -\frac{1}{2} a_z^2 - \frac{3}{4} a_z^2 \frac{\alpha}{2\sqrt{2\pi}}. \tag{2.27b}$$

Finally, the breathing mode frequency expansion is

$$\left( \frac{\omega}{\omega_z} \right)^2 = 4 \left( 1 - \frac{\alpha}{4\sqrt{2\pi}} \right). \tag{2.28}$$

We now compare the asymptotic formula (2.22) obtained from the exact solution for two particles with the asymptotic formula (2.28) obtained from the sum rule approximation (1.53). We see that the first coefficient in the breathing mode frequency expansion is different from the result of the sum rule approximation. The ratio of the first coefficient in the exact breathing mode frequency to the one in the sum rule expansion is 2. The reason for this discrepancy is that the operator $x_1^2 + x_2^2$ excites not only the breathing mode but also the mode related to the center of mass motion. To avoid this we propose to analyse another operator. For instance, the operator $(x_1 - x_2)^2$ is more appropriate for sum rules, because it does not excite the center of mass oscillations.

The breathing mode frequency calculated using the sum rules and the exact wave-function (2.14) with the operator $(x_1 - x_2)^2$ is in excellent agreement with the exact breathing mode frequency (see Fig. 8). Now let us compare the first order correction to the breathing mode frequency calculated using the sum rules with the perturbative result (2.22). We write

$$\left\langle (x_1 - x_2)^2 \right\rangle = \frac{1}{2} a_z^2 + a_z^2 \frac{\alpha}{2\sqrt{2\pi}}, \tag{2.29a}$$

$$\omega_z^2 \frac{\partial}{\partial \omega_z^2} \left\langle (x_1 - x_2)^2 \right\rangle = -\frac{1}{4} a_z^2 - \frac{3}{4} a_z^2 \frac{\alpha}{2\sqrt{2\pi}}. \tag{2.29b}$$

The perturbative expansion for the breathing mode frequency is

$$\left( \frac{\omega}{\omega_z} \right)^2 = 4 \left( 1 - \frac{\alpha}{2\sqrt{2\pi}} \right). \tag{2.30}$$

Comparing formula (2.30) with equation (2.22) we see that the first coefficient in the breathing mode frequency expansion is the same for the exact result and for the modified sum rule approximation.

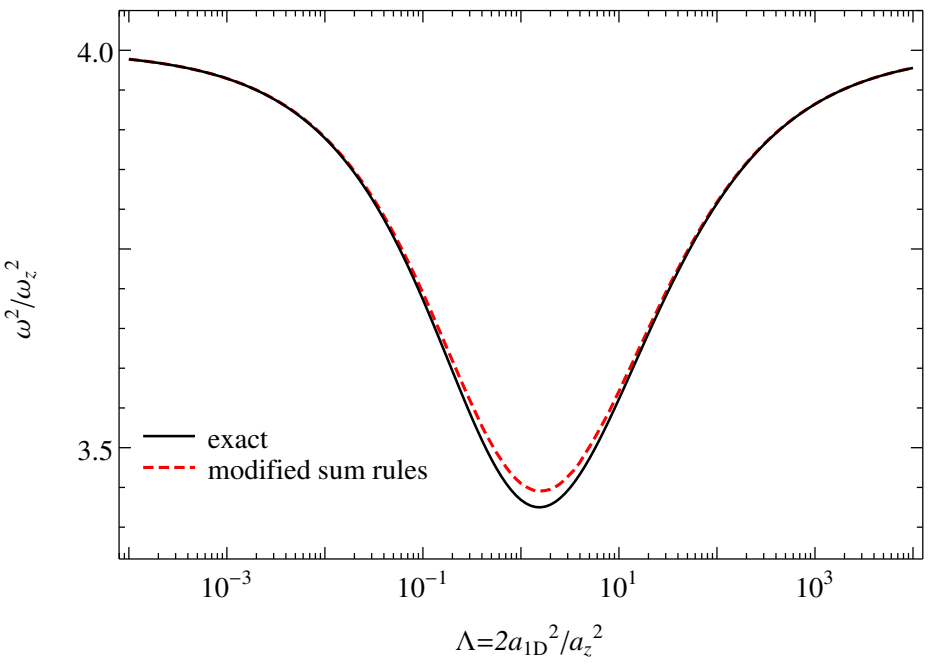


Figure 8: Comparison of the breathing mode frequency of the two particles in a parabolic trap (black) and its approximation by the sum rule (1.53) with the operator $Q_c = (x_1 - x_2)^2$ (red, dashed). The operator $Q_c$ does not excite states related to the center-of-mass motion. Thus it gives a better approximation than $Q$ (Fig. 7).

Concluding, we have to say that the sum rules give the upper bound for the breathing mode frequency in the repulsive regime, as they take into account all modes excited with the operator $Q$. So, a choice of the operator plays a dramatic role in this approach. The easiest way to improve the sum rules is to use the operator $\sum_{n=1}^{N} x_n^2 - \frac{1}{N}\left(\sum_{n=1}^{N} x_n\right)^2$ instead of $\sum_{n=1}^{N} x_n^2$. This choice plays a dramatic role for finite-$N$ many-body systems.

## 2.4. Variational Ansatz for two particles

In this section we discuss the Ansatz proposed in Ref. [35]. The ground state wave-function is constructed as follows:

$$\psi(x_1, x_2) = A(\sigma)\psi_0^{HO}\left(\frac{x_1 + x_2}{2}\right)\left(H_1\left(|x_1 - x_2|\right) + a_{1D}H_0\left(|x_1 - x_2|\right)\right)\exp\left(-\frac{1}{2\sigma^2}(x_1 - x_2)^2\right), \tag{2.31}$$

where $\sigma$ is the variational parameter, $A(\sigma)$ is the normalization constant, and $H_n$ are the Hermite polynomials. This Ansatz automatically satisfies the boundary conditions, namely

$$\frac{1}{\psi}\frac{\partial\psi}{\partial x_{12}}\bigg|_{x_{12}=0-} - \frac{1}{\psi}\frac{\partial\psi}{\partial x_{12}}\bigg|_{x_{12}=0+} = \frac{1}{a_{1D}}. \tag{2.32}$$

The other feature of this Ansatz is that in the limits of both strong and weak coupling it recovers the exact wave-functions (as we will see later in these limits $\sigma \to 1$). The parameter $\sigma$ has to be found from the minimisation of the energy functional:

$$\frac{\partial E[\sigma]}{\partial \sigma} = 0. \tag{2.33}$$

This Ansatz leads to the following expressions for the normalization constant and the energy

$$A^{-2} = \frac{1}{2}\sigma\left(2a_{1D}^2\sqrt{\pi} + 4a_{1D}\sigma + \sqrt{\pi}\sigma^2\right), \tag{2.34a}$$

$$E_{gs} = \frac{1+\sigma^4}{4\sigma^2}\frac{8a_{1D}\sigma + 2a_{1D}^2\sqrt{\pi} + 3\sqrt{\pi}\sigma^2}{2a_{1D}^2\sqrt{\pi} + 4a_{1D}\sigma + \sqrt{\pi}\sigma^2}. \tag{2.34b}$$

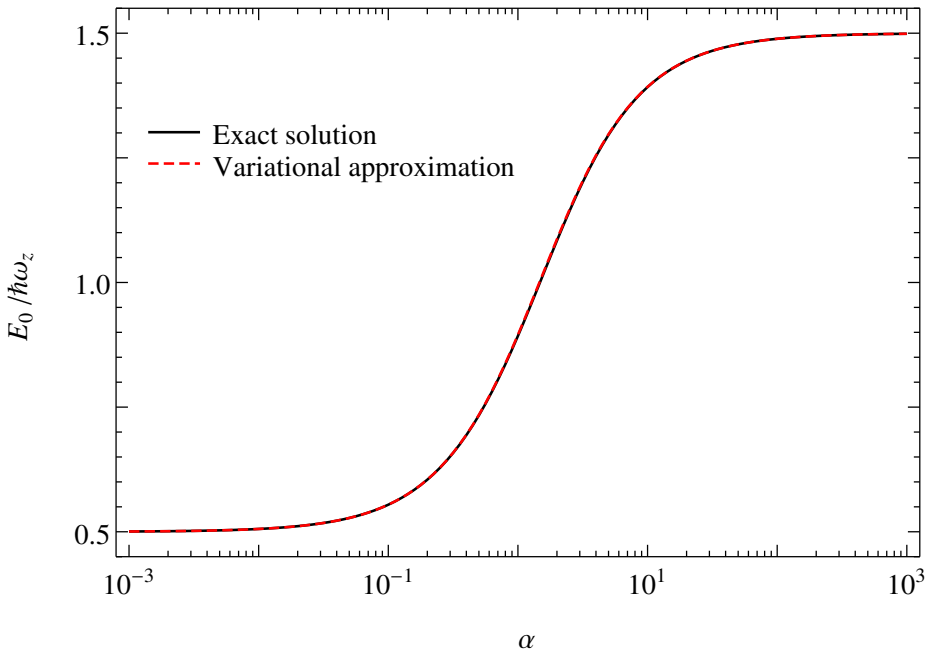


Figure 9: Comparison of the ground state energy of two particles in a parabolic trap (black) and its variational approximation (2.34b) (red, dashed). The agreement is good at any value of the interaction parameter $\alpha = -2a_z/a_{1D}$.

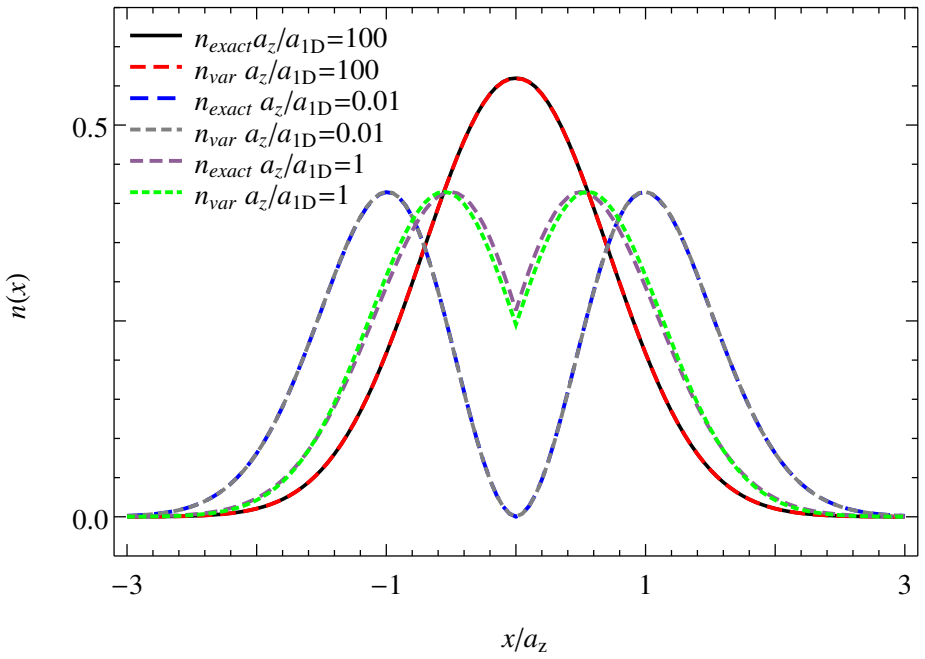


Figure 10: Comparison of the ground state densities for the two-particle system in a parabolic trap and their variational approximations for various values of the scattering length. The largest mismatch is at $a_z/a_{1D} \approx 1$.

It is clearly seen that the use of the variational wave-function reproduces well the exact spectrum for two particles in a parabolic trap (see Fig. 9) and gives a good approximation of the exact density for all values of the scattering length $a_{1D}$ (see Fig. 10).

Now we construct the variational wave-function for the second excited state in the form

$$\psi(x_1, x_2) = A(\sigma)\psi_0^{HO}\left(\frac{x_1+x_2}{2}\right)\left(H_3\left(|x_1-x_2|\right) + 3a_{1D}H_2\left(|x_1-x_2|\right)\right)\exp\left(-\frac{1}{2\sigma^2}(x_1-x_2)^2\right), \tag{2.35}$$

where $\sigma$, $A(\sigma)$ and $H_n$ have the same meaning as in Eq.(2.31). Thus we have

$$A^{-2} = 4\sigma(a_{1D}^2\sqrt{\pi}(1-2\sigma^2+3\sigma^4) + 6\sqrt{\pi}\sigma^2(3-6\sigma^2+5\sigma^4) + 4a_{1D}\sigma(3-8\sigma^2+8\sigma^4)), \tag{2.36a}$$

$$E_2 = A^{-2}\left(a_{1D}^2\sqrt{\pi}(1+2\sigma^2+8\sigma^4-6\sigma^6+15\sigma^8) + 8a_{1D}\sigma(3-4\sigma^2+11\sigma^4-16\sigma^6+24\sigma^8)\right.$$
$$\left.+6\sqrt{\pi}\sigma^2(9-6\sigma^2+20\sigma^4-30\sigma^6+35\sigma^8)\right) \tag{2.36b}$$

The parameter $\sigma$ is determined from the minimization condition irrespectively of the ground state.

We conclude that the variational function catches main physical features of the system because both the exact second exited state energy and the exact breathing mode frequency

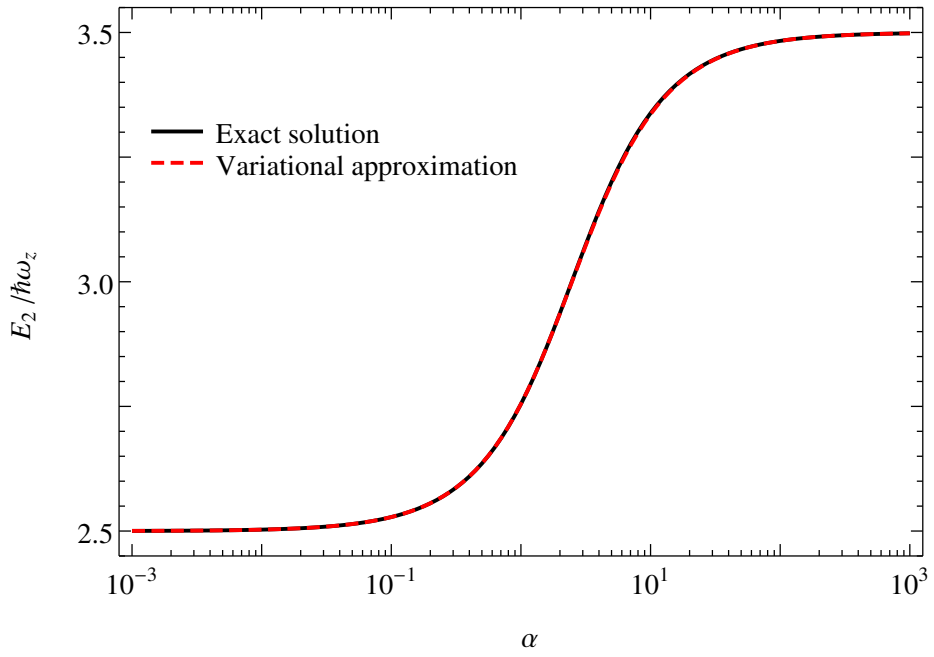


Figure 11: Comparison of the second excited state energy of the two-particle system in a parabolic trap (black) and its variational approximation (2.36b) (red, dashed). The data are presented as functions of the interaction parameter $\alpha = -2a_z/a_{1D}$.

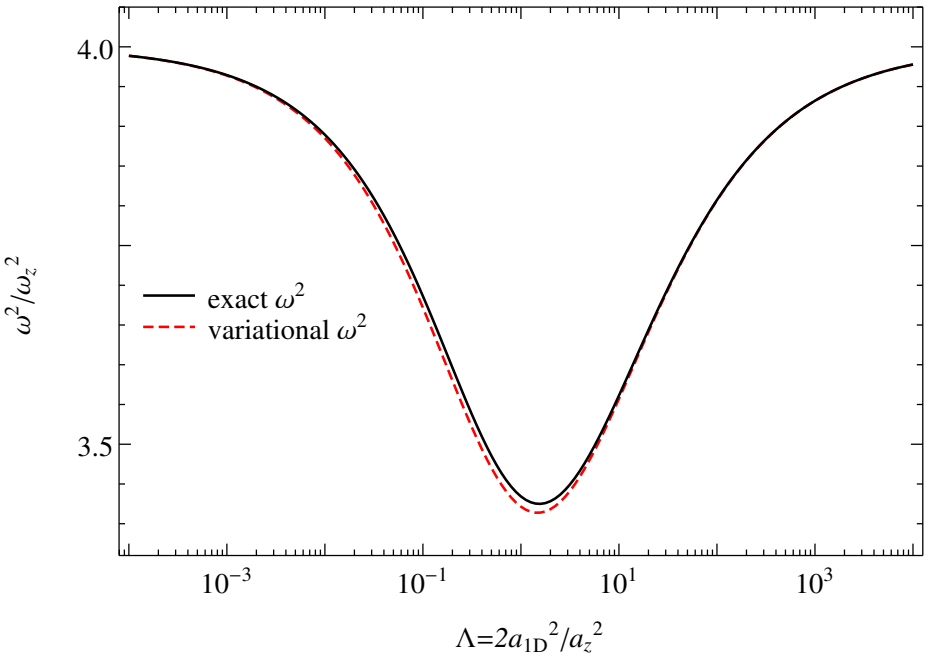


Figure 12: The dependence of the breathing mode frequency of two particles in a parabolic trap (black) on the interaction parameter $\Lambda = N\left(\frac{a_{1D}}{a_z}\right)^2$ and its variational approximation (red, dashed).

are in a good agreement with the results obtained using the variational function (see Fig. 11 and Fig. 12).

# 3. Crossover from the Tonks-Girargeau to Thomas-Fermi regime

In this Chapter we describe a crossover from the Thomas-Fermi to the Tonks-Girargeau regime. We use the hydrodynamic approach and imply the Local Density Approximation (LDA). We demonstrate that in the LDA all quantities depend only on a single dimensionless parameter which we call the LDA parameter. We calculate the breathing mode frequency using the sum rule approximation and make assymptotic expansions for both repulsive and attractive regimes. We complete our analysis with the exact perturbative calculations of the spectrum based on the Bose-Fermi mapping in the Tonks-Girargeau regime. It is shown that calculations at finite $N$ converge to the LDA result in the thermodynamic limit.

## 3.1. 1D Hydrodynamics

We start with a (3D) system described by the Hamiltonian (1.14). For such a system Gross and Pitaevskii independently derived an equation for the wave-function of the condensate [36, 37]. It was derived from the equation of motion for the field operator:

$$i\hbar\frac{\partial}{\partial t}\hat{\Psi}(\vec{r},t) = \left[\hat{\Psi}(\vec{r},t)\,, \hat{H} - \mu\hat{N}\right], \tag{3.1}$$

where $\mu$ is the Lagrange multiplier which corresponds to the chemical potential. Substituting the Hamiltonian (1.14) into Eq. (3.1) we get:

$$i\hbar\frac{\partial}{\partial t}\hat{\Psi}(\vec{r},t) = \left[-\frac{\hbar^2}{2m}\nabla^2 + V_{ext}(\vec{r}) - \mu + \int U(\vec{r}-\vec{r}')\hat{\Psi}^\dagger(\vec{r}',t)\hat{\Psi}(\vec{r},t)d\vec{r}'\right]\hat{\Psi}(\vec{r},t). \tag{3.2}$$

Representing the field operator $\hat{\Psi}(\vec{r},t)$ in (3.2) as a sum of the condensate wave-function $\Psi(\vec{r},t)$ and the non-condensed part $\hat{\Psi}'(\vec{r},t)$ we then omit $\hat{\Psi}'(\vec{r},t)$ and obtain the Gross-Pitaevskii equation for $\Psi(\vec{r},t)$ [1]:

$$i\hbar\frac{\partial}{\partial t}\Psi(\vec{r},t) = \left[-\frac{\hbar^2}{2m}\nabla^2 + V_{ext}(\vec{r}) - \mu + \int U(\vec{r}-\vec{r}')\Psi(\vec{r}',t)\Psi(\vec{r},t)d\vec{r}'\right]\Psi(\vec{r},t). \tag{3.3}$$

Another derivation of this equation will be introduced in Section 4.1. In the Gross-Pitaevskii (GPE) equation an assumption of a small BEC depletion is made. The GPE gives a good

description of the condensate when the temperature is low. Turning to the picture of the density $n(\vec{r},t)$ and phase $\theta(\vec{r},t)$ and substituting $\Psi(\vec{r},t) = \sqrt{n(\vec{r},t)}\exp(i\theta(\vec{r},t))$ into (3.3) we obtain

$$\frac{\partial}{\partial t}n + \frac{\hbar}{m}\nabla\left(n\nabla\theta\right) = 0, \tag{3.4a}$$

$$\frac{\partial}{\partial t}\theta + \left[\frac{\hbar\left(\nabla\theta\right)^2}{2m} + \frac{1}{\hbar}\left[V_{ext}(\vec{r}) + \mu + gn\right] - \frac{\hbar}{2m}\frac{\nabla^2\sqrt{n}}{\sqrt{n}}\right] = 0. \tag{3.4b}$$

The first equation is nothing else than the continuity equation, where $\frac{\hbar}{m}n\nabla\theta = n\vec{v} = \vec{j}$ is the current. The second equation is the Euler equation and it describes the energy transport. The last term in this equation is called the quantum pressure. It scales as $\hbar^2/2ml^2$, where $l$ is a typical distance characterizing density variations and it is negligible comparing to the classical pressure when $l \ll \xi = \hbar/\sqrt{mng}$.

Up to now the written equations do not contain dimensionality explicitly. However, we are interested in one-dimensional systems and we denote the one-dimensional density $n_1$ to underline the reduction of dimensionality. In the limit of slowly varying functions, the quantum pressure term can be neglected and equations (3.4) take the form:

$$\frac{\partial}{\partial t}n_1 + \frac{\partial}{\partial z}\left(n_1 v\right) = 0, \tag{3.5a}$$

$$\frac{\partial}{\partial t}n_1 v + \frac{\partial}{\partial z}\left[\frac{1}{2}mv^2 + V_{ext}(z) + \mu\left(n_1(z)\right)\right] = 0, \tag{3.5b}$$

where $n_1(z,t)$ and $v(z,t)$ are the 1D density and velocity, respectively. Eqs. (3.5) are more general than the derivation presented above. They hold even when the Gross-Pitaevskii approach could not be applied. In equations (3.5) $V_{ext}$ is the external potential defined in (1.15), and $\mu(n_1)$ is the equation of state of the system. The condition of smooth functions is used in these equations, and the last term in the left-hand side of Eq. (3.4b) is neglected. Hydrodynamics describes well collective oscillations if local equilibrium exists. This requires the applicability of the Local Density Approximation (LDA) along the $z$-axis

$$\mu_{LDA}\left(n_1\left(z\right)\right) + V_{ext}(z) = \mu. \tag{3.6}$$

where $\mu$ is the global chemical potential. The LDA assumes that the condensate is almost uniform and the local chemical potential $\mu_{LDA}$ at the point $z$ is equal to the chemical potential in a homogeneous system that has the same density $n_1(z)$. Thus, we have to calculate the chemical potential $\mu(n_1)$ of a homogeneous system.

## 3.2. Lieb-Liniger model

A system of $N$ identical bosons with contact interaction is described by the Hamiltonian of the Lieb-Liniger model [28, 29]

$$\hat{H} = -\frac{\hbar^2}{2m}\sum_{j=1}^{N}\frac{\partial^2}{\partial x_j^2} + g\sum_{j>k=1}^{N}\delta(x_j - x_k). \tag{3.7}$$

The bosons are put on a ring of circumference $L$, and periodic boundary conditions are imposed:

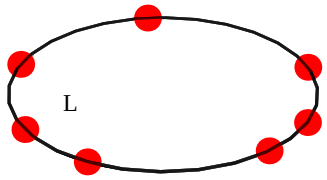


Particles on a ring of circumference $L$ with periodic boundary conditions

$$\psi(x_1, x_2, \ldots, x_i, \ldots, x_N) = \psi(x_1, x_2, \ldots, x_i + L, \ldots, x_N). \tag{3.8}$$

The eigenfunctions of the Hamiltonian (3.7) obey the bosonic symmetry, Eq. (1.19).

## 3.3. Bethe equations

First let us consider the Tonks-Girardeau case, where $g \to \infty$. In this section we set that $n_1$ stays constant, whereas $L \to \infty$. For the Tonks-Girardeau limit of the model (3.7) we can write down exact wave-functions [28]:

$$\psi(x_1, x_2, \ldots, x_N) = \frac{1}{\sqrt{N!}}\det[\exp(ik_j x_i)]\Pi_{i>j}\,\mathrm{sign}(x_i - x_j), \tag{3.9}$$

where all rapidities $k_j$ are different. The energy and momentum of the system can be calculated as follows:

$$E_N = \frac{\hbar^2}{2m}\sum_{j=1}^{N}k_j^2, \tag{3.10a}$$

$$P = \hbar\sum_{j=1}^{N}k_j. \tag{3.10b}$$

From the condition (3.8) we get $N$ equations, called the Bethe equations:

$$\exp(ik_j L) = (-1)^{N-1}, \qquad j = 1, \ldots, N. \tag{3.11}$$

This system of equations can be easily solved:

$$k_j = \frac{2\pi n_j}{L}, \tag{3.12}$$

where

$$n_j = j - \frac{N+1}{2}. \tag{3.13}$$

Thus, we have for the ground state energy

$$E_N = \frac{\hbar^2}{2m}\frac{\pi^2}{3}\frac{N\left(N^2-1\right)}{L^2}, \tag{3.14a}$$

the momentum

$$P_N = 0, \tag{3.14b}$$

and the chemical potential

$$\mu = E_{N+1} - E_N = \frac{\hbar^2}{2m}\frac{\pi^2(N^2+N)}{L^2} \approx \frac{\hbar^2}{2m}\pi^2 n_1^2. \tag{3.14c}$$

Now we write the Bethe equations for an arbitrary coupling [28]:

$$Lk_i = \sum_{j=1}^{N}\theta(k_i - k_j) + 2\pi\left(j - \frac{N+1}{2}\right), \tag{3.15}$$

where

$$\theta(k) = i\ln\left(\frac{i\frac{2mg}{\hbar^2}+k}{i\frac{2mg}{\hbar^2}-k}\right). \tag{3.16}$$

This is the set of $N$ non-linear algebraic equations.

Let us calculate the correction to the Tonks-Girardeau limit in $1/g$, where $g \to \infty$. To first order in $1/g$, we get an expression for quasi-momenta

$$k_j^{(1)} = k_j^{(0)}\left(1 - 2\gamma^{-1}\right) \tag{3.17}$$

and expressions for thermodynamical quantities

$$E_N = \frac{\hbar^2}{2m}\frac{\pi^2}{3}\frac{N(N^2-1)}{L^2}\left(1 - 4\gamma^{-1}\right), \tag{3.18a}$$

$$P_N = 0, \tag{3.18b}$$

$$\mu = E_{N+1} - E_N = \frac{\hbar^2}{2m}\frac{\pi^2}{3}\left(\frac{3N^2+3N}{L^2} - \frac{4(4N^3+6N^2+2N)}{gL^3}\right) \approx \frac{\hbar^2}{2m}\pi^2 n_1^2\left(1 - \frac{16}{3\gamma}\right). \tag{3.18c}$$

## 3.4. Lieb-Liniger equations

Let us consider the system in the ground state. Subtracting from the $i$-th equation (3.15) the $i+1$-st we obtain the following equation:

$$L(k_{i+1}-k_i)=\sum_{j=1}^{N}\left(\theta(k_i-k_j)-\theta(k_{i+1}-k_j)\right)+2\pi. \tag{3.19}$$

Let us introduce the density function

$$\rho(k_j)=\frac{1}{L(k_{j+1}-k_j)}. \tag{3.20}$$

In Ref. [28] the authors prove several important statements: positivity of $\rho$, existence of a unique solution bounded from above and from below for any $\gamma>0$. Also note that the quantity

$$\theta(k_{i+1}-k_j)=\theta((k_{i+1}-k_i)+k_i-k_j)=\theta\left(\frac{1}{L\rho(k_i)}+k_{i+1}-k_j\right), \tag{3.21}$$

in the $L\to\infty$ limit can be written as

$$\theta(k_{i+1}-k_j)=\theta(k_i-k_j)+\theta'(k_i-k_j)\frac{1}{L\rho(k_i)}+o\left(\frac{1}{L^2}\right), \tag{3.22}$$

where $\theta'(k)=4mg/\hbar^2((2mg/\hbar^2)^2+k^2)$. The sums in Eq. (3.19) can be transformed as

$$\frac{1}{L}\sum_{i=1}^{N}f(k_i)\to\int_{-\Lambda}^{\Lambda}f(k)\rho(k)dk,\qquad L\to\infty. \tag{3.23}$$

Here, $\Lambda=-k_1=k_N$ is the maximum value of rapidities. It depends on the interaction parameter $\gamma$ and will be determined later. Thus, the set of equations (3.19) takes the form of the Fredholm integral equation of second kind in the continuous limit:

$$\rho(k)-\frac{1}{2\pi}\int_{-\Lambda}^{\Lambda}K(\kappa,k)\rho(\kappa)d\kappa=\frac{1}{2\pi}, \tag{3.24}$$

where $K(\kappa,k)=4mg/\hbar^2((2mg/\hbar^2)^2+(\kappa-k)^2)$ is the Fredholm kernel. The parameter $\Lambda$ can be determined from the normalization condition

$$\int_{-\Lambda}^{\Lambda}\rho(k)dk=\frac{N}{L}=n_1. \tag{3.25}$$

In the canonical ensemble the energy can be calculated as

$$E_0=\frac{\hbar^2}{2m}\sum_{i=1}^{N}k_i^2\to L\int_{-\Lambda}^{\Lambda}\rho(k)k^2dk\qquad L\to\infty. \tag{3.26}$$

Following Ref. [28] we rescale variables:

$$k = \Lambda z, \qquad g = \Lambda\lambda, \qquad \rho(\Lambda z) = g(z). \tag{3.27}$$

In these variables equations (3.24), (3.25), (3.26) take the form of Lieb-Liniger equations [28, 29]:

$$g(z) - \frac{1}{2\pi}\int_{-1}^{1} \frac{2\lambda}{\lambda^2 + (z-y)^2} g(y)dy = \frac{1}{2\pi}, \tag{3.28a}$$

$$\gamma \int_{-1}^{1} g(x)dx = \lambda, \tag{3.28b}$$

$$e(\gamma) \equiv \frac{E_0}{\frac{\hbar^2}{2m}Ln_1^3} = \frac{\gamma^3}{\lambda^3}\int_{-1}^{1} g(x)x^2 dx. \tag{3.28c}$$

In these equations the dimensionless parameter

$$\gamma = \frac{mg}{\hbar^2 n_1} \tag{3.29}$$

is introduced. We denote the energy density $E_0/N$ as $\epsilon$. This system of equations should be solved in the following way. First one has to find the function $g(z)$ from equation (3.28a) for a given parameter $\lambda$. Using equation (3.28b) we find $\gamma$ as a function of $\lambda$. And then, finally, we calculate the energy per particle from equation (3.28c) for a given interaction parameter $\gamma$. From equations (3.28a, 3.28b) one easily recovers equations (3.24), (3.25) taking into account Eq. (3.27) and using the relation

$$\Lambda = n_1\frac{\gamma}{\lambda} = n_1\left(\int_{-1}^{1} g(z)dz\right)^{-1}. \tag{3.30}$$

## 3.5. Solution of Lieb-Liniger equations for repulsive interaction

We now start with the Lieb-Liniger equations (3.28). The solution to these equations can be represented by power series. Since $g(z)$ is an even function, only even terms will be present in the expansion:

$$g(z) = \sum_{n=0}^{\infty} g_{2n} z^{2n}. \tag{3.31}$$

Following [38], let us present the kernel of equation (3.28a) in the form:

$$\frac{1}{\lambda^2+(z-y)^2}=\frac{1}{\lambda^2+y^2}\left(1-\frac{2zy}{\lambda^2+y^2}+\frac{z^2}{\lambda^2+y^2}\right)^{-1}=\sum_{n=0}^{\infty}\sum_{m=0}^{n}(-1)^{n-m}C_n^m\frac{2^m z^{2n-m}y^m}{(\lambda^2+y^2)^{n+1}},\tag{3.32}$$

where $C_n^m=n!/m!(n-m!)$. Thus, we have

$$\int_{-1}^{1}g(y)\frac{1}{\lambda^2+(y-z)^2}dy=\sum_{k=0}^{\infty}\sum_{n=0}^{\infty}\sum_{m=0}^{n}g_{2k}\frac{2^{2m+1}}{(2m)!(k-m)!}\times\frac{\partial^{m+k}}{\partial s^{m+k}}\left[\sum_{l}^{k+m}\frac{(-1)^{l+1}\lambda^{2(l-1)}}{2(m+k-l)+1}+(-1)^{m+k}\lambda^{2(m+k)-1}\arctan\frac{1}{\lambda}\right]y^{2n}.\tag{3.33}$$

After transformation we obtain equations

$$1-(2\pi-4\arctan\frac{1}{\lambda})g_0+4\lambda\sum_{n=0}^{\infty}g_n\left(\sum_{m}^{n}\frac{(-1)^{m+1}\lambda^{2m-2}}{2n-2m+1}+(-1)^n\lambda^{2n-1}\arctan\frac{1}{\lambda}\right)=0,\tag{3.34a}$$

$$2\pi g_k=4\lambda\sum_{n=k+1}^{\infty}\sum_{m=0}^{k}g_n\frac{2^{2m}}{(2m)!(k-m)!}\frac{\partial^{s+k}}{\partial s^{m+k}}\sum_{l=0}^{m+n}\frac{(-1)^{l+1}s^{l+1}}{2(m+n-l)+1}+4\lambda\sum_{n=0}^{\infty}\sum_{m=0}^{k}g_k\frac{2^{2m}}{(2m)!(k-m)!}\frac{\partial^{m+k}}{\partial s^{m+k}}(-1)^{m+n}\lambda^{2(m+n)-1}\arctan\frac{1}{\lambda}.\tag{3.34b}$$

The solution was exact so far. The dependence of the energy per particle on the interaction parameter $\gamma$, calculated numerically from the Lieb-Liniger equations (red curve) and finite-$N$ results calculated directly from the Bethe equations, are shown in Fig. 13. It is clearly seen that the curves for finite $N$ are below the Lieb-Liniger result and approach it in the limit $N\to\infty$. Finite $N$ curves approach the Lieb-Liniger result rather fast. For $N=31$ there is practically no difference between the former and the latter.

### 3.5.1. Weak coupling regime

In the weak coupling limit ($\gamma\to 0$) the kernel of equation (3.28a) become singular. One can recognize a representation of the Dirac $\delta$-function in this kernel. Still, if the parameter $\lambda$ is small (but nonzero) we can find a solution. This solution $g(z)$ is unbounded and behaves as $\lambda^{-1}$. So, the studies of this limit become hard as we do not have a regular solution at

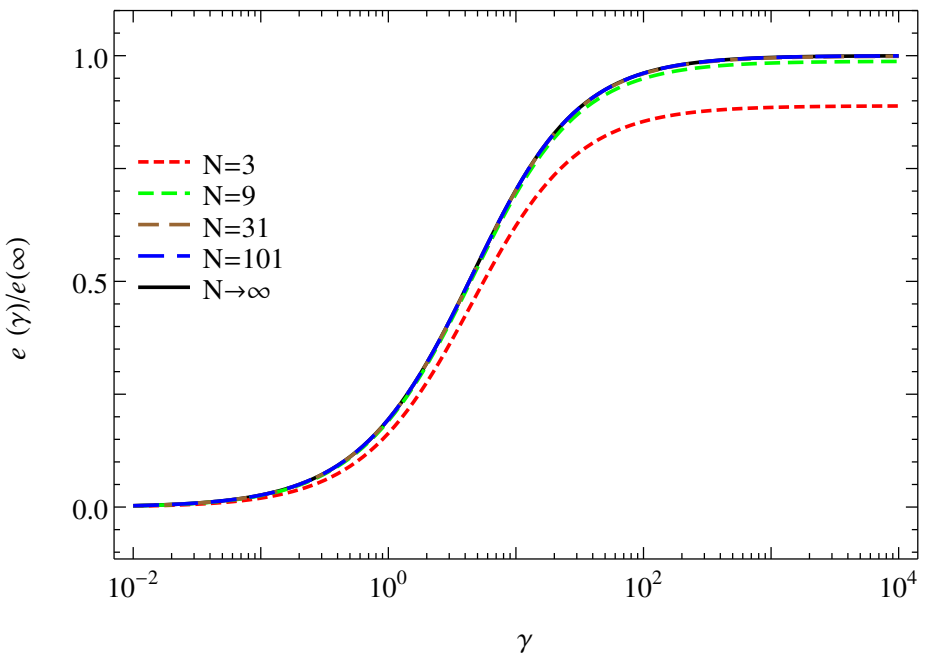


Figure 13: Energy per particle (3.28) calculated numerically for the different $N$, as a function of $\gamma$. The energy per particle is normalized on the $e(\infty) = \pi^2/3$. For $N = 31$ result is indistinguishable from the one in the thermodynamic limit.

$\gamma = 0$, which we can perturb. The coefficients $g_k$ have the form $g_k = \sum_{l=-1}^{\infty} \lambda^l g_k^{(l)}$, where the upper index $l$ determines the order of approximation.

To the first order in powers of $\lambda$, we have $g_k^{(-1)} = -(2k-3)!!/2\pi\lambda(2k)!!$, where $(-3)!! = -1$, and $(-1)!! = 1$. Therefore, we have

$$g(z) \approx -\frac{1}{2\pi\lambda} \sum_{k=0}^{\infty} \frac{(2k-3)!!}{(2k)!!} z^{2k}. \tag{3.35}$$

Equation (3.35) represents the Taylor expansion of the function

$$g(z) \approx -\frac{\sqrt{1-z^2}}{2\pi\lambda}. \tag{3.36}$$

Substituting this expression into the normalization condition (3.28b) we obtain the parameter $\lambda = \frac{\sqrt{\gamma}}{2}$. Hence, we have

$$\epsilon(\gamma) = \gamma. \tag{3.37}$$

Equation (3.37) is the first order of the series in the parameter $\gamma$. Taking into account the next term in $\epsilon(\gamma)$ we get

$$\epsilon(\gamma) = \gamma \left(1 - \frac{4}{3\pi}\sqrt{\gamma}\right). \tag{3.38}$$

### 3.5.2. Strong coupling regime (Tonks-Girardeau gas)

The Tonks-Girardeau gas is the Lieb-Liniger gas in the limit $\gamma \to \infty$. This limit can be studied relatively easily compared to the weak coupling regime. The kernel of Eq. (3.28a) goes to zero, and to the leading order we have:

$$g_{\lambda=\infty}(z) = \frac{1}{2\pi}. \tag{3.39}$$

Due to this, we can look for the solution of equation (3.28a) in the form:

$$g_\lambda(z) = g_{\lambda=\infty}(z) + \sum_{n=1}^{\infty} \lambda^{-n} g^{(n)}(z), \tag{3.40}$$

which leads to the relation:

$$\sum_{n=0}^{\infty} \lambda^{-n} g^{(n)}(z) - \frac{1}{\pi} \sum_{k=0,n=0}^{\infty,\infty} \int_{-1}^{1} dy (y-z)^{2k} g^{(n)}(y) \lambda^{-n-2k-1} = \frac{1}{2\pi}. \tag{3.41}$$

Equating expressions that have the same power of $\lambda$ we obtain a recurrent formula for $g^{(n)}(z)$

$$g^{(n)}(z) = \frac{1}{\pi} \sum_{k=0}^{[\frac{n}{2}]} \int_{-1}^{1} dy (y-z)^{2k} g^{(n-2k-1)}(y), \tag{3.42}$$

where $n \geq 1$, and $[x]$ denotes the floor function, i.e. the largest integer smaller than $x$. This gives us the energy density per particle

$$e(\gamma) = \frac{\pi^2}{3} \left(1 - \frac{4}{\gamma}\right) + O(\gamma^2). \tag{3.43}$$

This formula can be calculated more precisely [39]:

$$e(\gamma) = \frac{\pi^2}{3} \left(1 - \frac{4}{\gamma} + \frac{12}{\gamma^2} + (\pi^2 - 15)\frac{32}{15\gamma^3}\right) + O(\gamma^{-4}). \tag{3.44}$$

The Tonks-Girargeau regime is interesting because the exact wave-function can be constructed as

$$\psi(x_1, x_2, \ldots, x_N) = \frac{1}{\sqrt{N!}} \det\left[\psi_{j_P}^{HO}(x_i)\right] \prod_{i>k=1}^{N} \mathrm{sign}(x_i - x_k). \tag{3.45}$$

In the determinant all indexes $j_P$ should be different. They do not necessarily belong to the set $1, \ldots, N$, but in the ground state $j_P = j$.

## 3.6. Speed of sound

In the grand canonical ensemble the energy is calculated from the formula

$$E_N = \frac{\hbar^2}{2m}\sum_{i=1}^{N} k_i^2 - \mu, \tag{3.46}$$

where $\mu$ is the chemical potential.

The pressure of a 1D gas can be calculated using the expression

$$P = -\left(\frac{\partial E_0}{\partial L}\right)_{S,N} = -\left(\frac{\partial F}{\partial L}\right)_{T,N}, \tag{3.47}$$

where $E_0$ is the energy given by expression (3.10a), $S$ is the entropy of the system, $F = E_0 - TS$ is the Helmholtz free energy, $T$ is the absolute temperature. The pressure is

$$P = \frac{\hbar^2}{2m} n_1^3 \left(2e(\gamma) - \gamma e'(\gamma)\right). \tag{3.48}$$

The thermodynamic definition of the sound velocity is the following

$$v_s = \sqrt{-\frac{L}{mn_1}\left(\frac{\partial P}{\partial L}\right)_{N,S}}. \tag{3.49}$$

Now we can rewrite this definition in terms of the dimensionless parameter $\gamma = \frac{2}{a_{1D}n_1} = \frac{2L}{a_{1D}N}$ and $E_0 = \frac{\hbar^2}{2ma_{1D}^2} 4N\gamma^{-2}e(\gamma)$. The derivative can be rewritten as $\frac{\partial}{\partial L} = \frac{2}{a_{1D}N}\frac{\partial}{\partial \gamma}$. Hence, equation (3.49) takes the following form at $T = 0$:

$$v_s = \sqrt{-\frac{2}{mn_1^2 a_{1D}}\left(\frac{\partial P}{\partial \gamma}\right)_N}. \tag{3.50}$$

Finally, we obtain the following formula:

$$v_s = \frac{\hbar}{ma_{1D}}\left[2e''(\gamma) - 8\gamma^{-1}e'(\gamma) + 12\gamma^{-2}e(\gamma)\right]^{\frac{1}{2}}, \tag{3.51}$$

where the derivative "$\prime$" means the derivative with respect to $\gamma$. In Eq. (3.51) the chemical potential is given as $\mu(\gamma) = \left(\frac{\partial E_0}{\partial N}\right)_L$. Together with equation (3.28c) this leads to the formula

$$\mu(\gamma) = \frac{\hbar^2}{2m}\frac{4}{a_{1D}^2}\gamma^{-2}\left(3e(\gamma) - \gamma e'(\gamma)\right). \tag{3.52}$$

The dependence of the speed of sound on the interaction parameter $\gamma$ is shown in Fig. 14. In this figure the speed of sound $v_s$ is given in units of the Fermi velocity $v_F = \frac{\hbar}{m}\pi n_1$. The upper curve corresponds to the the speed of sound for the attractive interactions and the lower one to the repulsive interactions. In the Tonks-Girardeau limit and in the super-Tonks-Girardeau limit the speed of sound goes to $v_F$.

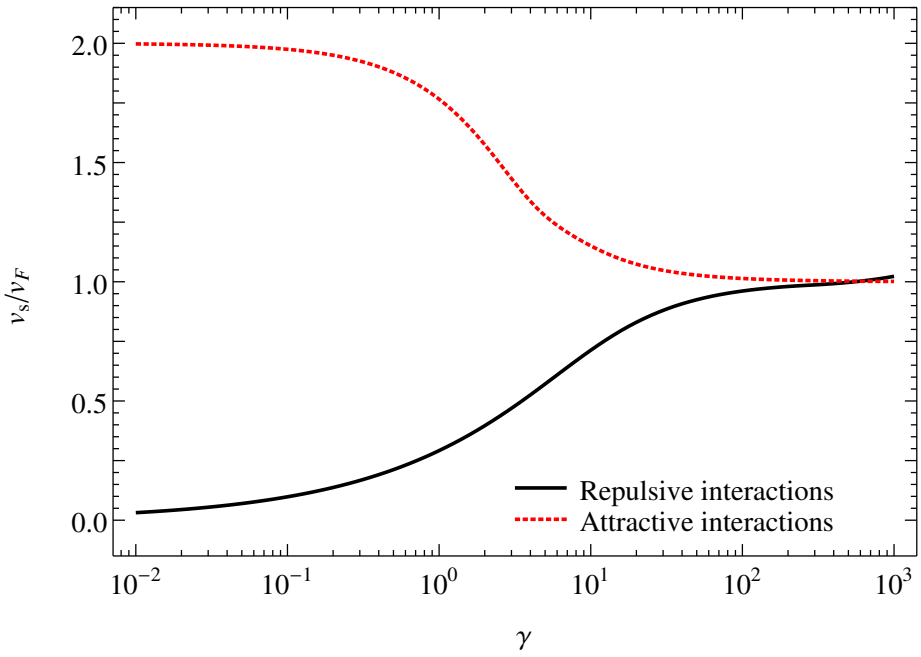


Figure 14: Speed of sound as a function of $\gamma$. Black solid curve: repulsive interactions, red dashed: attractive interactions.

### 3.6.1. Speed of sound in the Tonks-Girardeau limit

Let us calculate the speed of sound in this limit. We can calculate the speed of sound directly using expression (3.51), but it is more interesting to see all steps and expressions for pressure. We are going to use equations (3.18a) and (3.49). Thus we have

$$P = \frac{\hbar^2}{m}\frac{\pi^2}{3}n_1^3\left(1 - 6\gamma^{-1}\right). \tag{3.53}$$

The next step is to calculate the sound velocity using (3.50):

$$v_s^2 = \frac{\hbar^2}{m^2}\pi^2 n_1^2\left(1 - 8\gamma^{-1}\right). \tag{3.54}$$

### 3.6.2. Speed of sound in the weak coupling limit

Using equation (3.47) with the ground state energy $E_0$ following from Eq. (3.28c) and $e(\gamma)$ from Eq. (3.38) one calculates the pressure in the weak coupling limit:

$$P = \frac{\hbar^2}{2m}\gamma n_1^3\left(1 - \frac{2}{3\pi}\sqrt{\gamma}\right). \tag{3.55}$$

The speed of sound is then given by:

$$v_s^2 = \frac{\hbar^2}{m^2} n_1^2 \gamma \left(1 - \frac{1}{2\pi}\sqrt{\gamma}\right). \tag{3.56}$$

We remark that in this limit the speed of sound has a non-analytic expansion.

## 3.7. Solution to the Lieb-Liniger equations for attractive interaction

We now start with equations similar to the Lieb-Liniger equations [23, 28, 29]:

$$g(z) + \frac{1}{2\pi}\int_{-1}^{1} \frac{2\lambda}{\lambda^2 + (z-y)^2} g(y)dy = \frac{1}{2\pi}, \tag{3.57a}$$

$$\gamma \int_{-1}^{1} g(x)dx = \lambda, \tag{3.57b}$$

$$e(\gamma) = \frac{\gamma^3}{\lambda^3}\int_{-1}^{1} g(x)x^2 dx. \tag{3.57c}$$

These equations are similar to equations (3.28a), (3.28b), (3.28c). However, the sign in front of the integral in Eq. (3.28a) is different. The solution to these equations shows us that in the attractive case the parameters $\lambda$ and $\gamma$ are negative. These equations are written not for the bound state, in which all rapidities $k_i$ are complex, and even not for the cluster state, where only some of the rapidities are complex and some are real. Equations (3.57a, 3.57b, 3.57c) describe the so-called gas state, which is characterized by only real rapidities, and is adiabatic continuation of the repulsive bound state through $g = \infty$. The dependence of the energy per particle on the interaction parameter, calculated numerically, is represented by the black curve in Fig. 15. In the super-Tonks-Girargeau limit, $\gamma \to -\infty$, the energy density goes to $\pi^2/3$, merging with the repulsive branch shown in Fig. 13. As it will be shown later (in Eq. (3.63)) in the opposite limit, $\gamma \to -0$, the energy density per particle $e(\gamma)$ goes to $4\pi^2/3$. Fig. 15 also shows the dependence of the energy per particle on $\gamma$ for finite $N$ systems. Like in the repulsive case, the energy density is smaller then the Lieb-Liniger energy density. However, one can see that already for $N = 31$ the energy density is non-distinguishable from the energy density from the Lieb-Liniger equations (3.57).

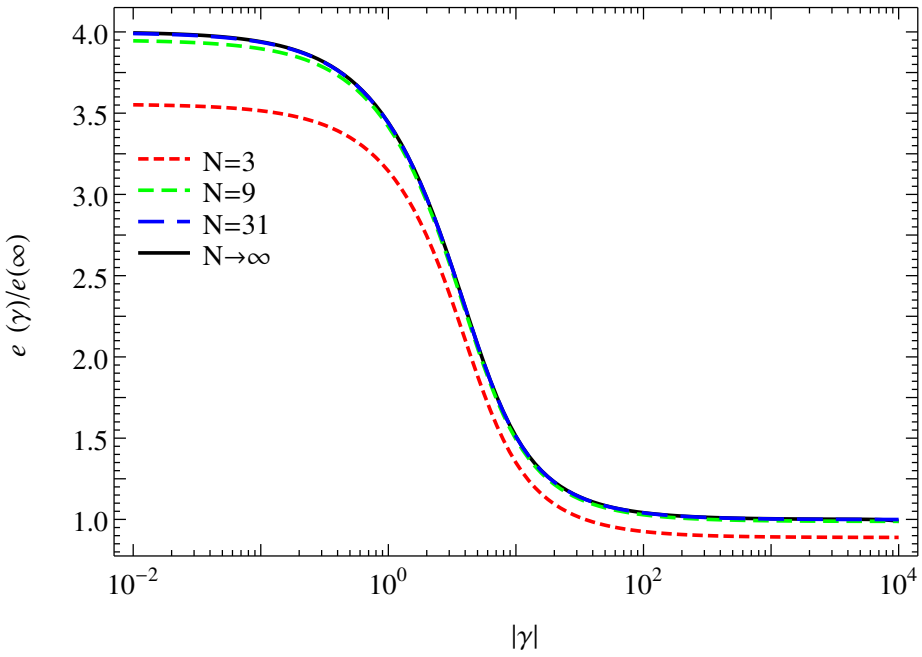


Figure 15: Energy per particle (3.57) calculated numerically for the different $N$, as a function of $\gamma$. The energy per particle is normalized on the $e(\infty) = \pi^2/3$. For $N = 31$ result is indistinguishable from the one in the thermodynamic limit.

### 3.7.1. Strong attractive regime (super-Tonks-Girardeau gas)

The super-Tonks-Girardeau gas is the gas state, which is a highly excited meta-stable state of attractive Lieb-Liniger gas in the limit $\gamma \to -\infty$. The kernel of Eq. (3.57a) goes to zero, so that to zero order $g_{\lambda=\infty}(z) = \frac{1}{2\pi}$. This result shows that the distribution function is a continuous function at $\gamma = \pm\infty$. Due to this, we can search for the solution of Eq. (3.57a) in the form:

$$g_\lambda(z) = g_{\lambda=\infty}(z) + \sum_{n=1}^{\infty} \lambda^{-n} g^{(n)}(z), \tag{3.58}$$

which leads to an expression

$$\sum_{n=0}^{\infty} \lambda^{-n} g^{(n)}(z) + \frac{1}{\pi} \sum_{k=0,n=0}^{\infty,\infty} \int_{-1}^{1} dy (y-z)^{2k} g^{(n)}(y) \lambda^{-n-2k-1} = \frac{1}{2\pi}. \tag{3.59}$$

Equating terms with the same powers of $\lambda$ we obtain a recurrent formula for $g^{(n)}(z)$

$$g^{(n)}(z) = -\frac{1}{\pi} \sum_{k=0}^{\left[\frac{n}{2}\right]} \int_{-1}^{1} dy (y-z)^{2k} g^{(n-2k-1)}(y), \tag{3.60}$$

where $n \geq 1$, and $[x]$ denotes the floor function, i.e. the largest integer smaller than $x$. Using Eq.(3.57c) we can calculate the energy per particle

$$e(\gamma) = \frac{\pi^2}{3}\left(1 + \frac{4}{\gamma}\right) + O(\gamma^2). \tag{3.61}$$

Comparing (3.61) with Eq. (3.43) we conclude that the energy per particle is also a continuous function of $\gamma$ at $\gamma = \pm\infty$. This fact can be used as the argument that equations (3.57) indeed describes the gas state, rather than some other state. This for sure cannot be a description of the bound state because in the $g \to \infty$ limit the energy of this bound state $E_0(\gamma)$ goes to $-\infty$ as $\gamma^2$.

### 3.7.2. Weak attractive regime

In the $|\gamma| \to 0$ limit (and $\gamma < 0$) the kernel of equation (3.57a) becomes singular. One can recognize a representation of the $\delta$-function in this kernel. Thus, equation (3.57a) in this limit goes to $g(z) = -g(z) + 1/2\pi$. This leads to

$$g(z) = \frac{1}{4\pi}. \tag{3.62}$$

Hence, the energy per particle to the leading order in $\gamma$ is

$$e(\gamma) = \frac{4\pi^2}{3}. \tag{3.63}$$

It is important to emphasise that this is not the ground state energy, but the energy of the so-called gas state characterised by the presence of real rapidities. This state thus does not contain bound states. The densities of energy in the weak attractive regime and in the weak repulsive regime are not adiabatically connected with each other (see expressions (3.63) and (3.38)).

## 3.8. Breathing mode frequency in the repulsive regime

It is possible to calculate the breathing mode frequency using the Local Density Approximation. Since $V_{ext}(z) = m\omega_z^2 z^2/2$, one has $\mu_{LDA} = m\omega_z^2 \left(Z^2 - z^2\right)/2$, where $Z$ is the Thomas-Fermi radius [40]. From Eqs. (3.28a) – (3.28c) we obtain the energy density per particle $e$ and the chemical potential $\mu$ as functions of the parameter $\gamma = mg/\hbar^2 n_1 = 2/\left|a_{1D}\right| n_1$.

Inverting the dependence of the chemical potential on the parameter $\gamma$, one can consider the normalization condition

$$\int_{-Z}^{Z} n_1\left(\mu(z)\right) dz = N, \tag{3.64}$$

as the equation which determines the Thomas-Fermi radius. Expressing the chemical potential in units of $\hbar^2/2ma_{1D}^2$, we get the dimensionless chemical potential

$$\tilde{\mu}_{LDA}(z) = \frac{2\mu m a_{1D}^2}{\hbar^2} = \frac{m\omega_z^2 a_{1D}^2\left(Z^2 - z^2\right)}{\hbar^2} = \frac{a_{1D}^2\left(Z^2 - z^2\right)}{a_z^4}. \tag{3.65}$$

This leads to the equation

$$\int_{-Z}^{Z} n_1\left(\frac{a_{1D}^2\left(Z^2 - z^2\right)}{a_z^4}\right) dz = N. \tag{3.66}$$

Changing the variables to $t = z/Z$, and $\tilde{Z} = Z a_{1D}/a_z^2$ we get the following equation:

$$2\tilde{Z}\int_0^1 n_1\left(\tilde{Z}^2\left(1 - t^2\right)\right) dt = N\frac{|a_{1D}|}{a_z^2}. \tag{3.67}$$

Multiplying the left and right parts of this equation by $a_{1D}$ we obtain:

$$2\tilde{Z}\int_0^1 |a_{1D}|\, n_1\left(\tilde{Z}^2\left(1 - t^2\right)\right) dt = N\left(\frac{a_{1D}}{a_z}\right)^2. \tag{3.68}$$

In terms of the interaction parameter $\gamma$ equation (3.68) has the form:

$$4\tilde{Z}\int_0^1 \gamma^{-1}\left(\tilde{Z}^2\left(1 - t^2\right)\right) dt = N\left(\frac{a_{1D}}{a_z}\right)^2. \tag{3.69}$$

The breathing mode frequency can be calculated from equation (2.23) [20, 32]. It is more convenient to rewrite Eq. (2.23) following from (1.53) in the form:

$$\frac{\omega^2}{\omega_z^2} = -4\frac{\langle z^2\rangle}{\Lambda\frac{\partial\langle z^2\rangle}{\partial\Lambda}}, \tag{3.70}$$

Using the results obtained in sections 3.5.1 and 3.5.2 we present analytics in the limits $\gamma \to 0$ and $\gamma \to \infty$ in the next sections.

### 3.8.1. Breathing mode in the Tonks-Girardeau limit

First we make the analysis of the Tonks-Girardeau gas based on formula (3.43). We investigate the leading order in $1/\gamma$, and then go to subleading orders. The chemical potential is related to the particle density as

$$\mu = \frac{\partial E_0}{\partial N} = \frac{\partial\left(n_1\epsilon(n_1)\right)}{\partial n_1}, \tag{3.71}$$

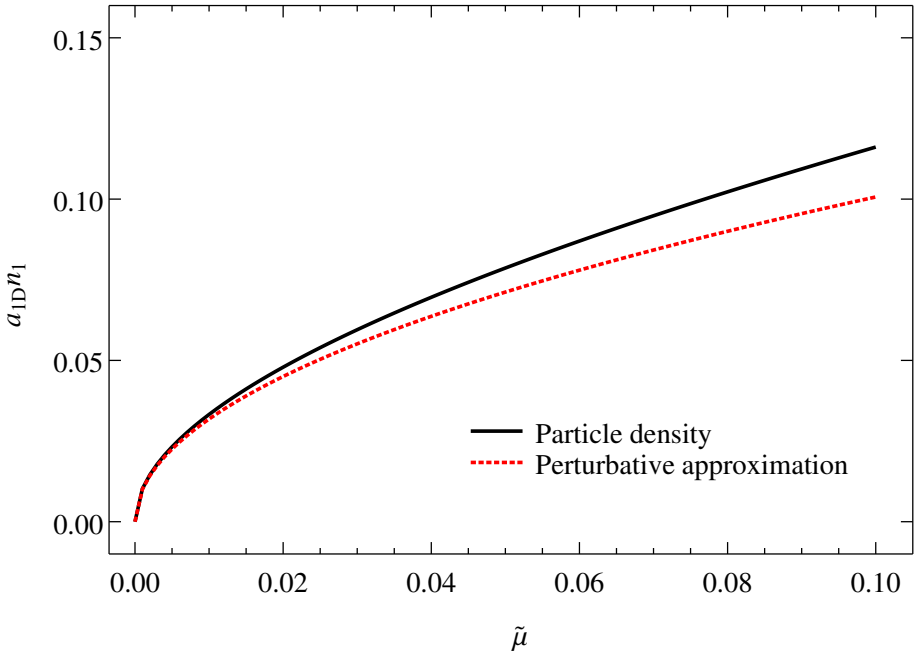


(a)

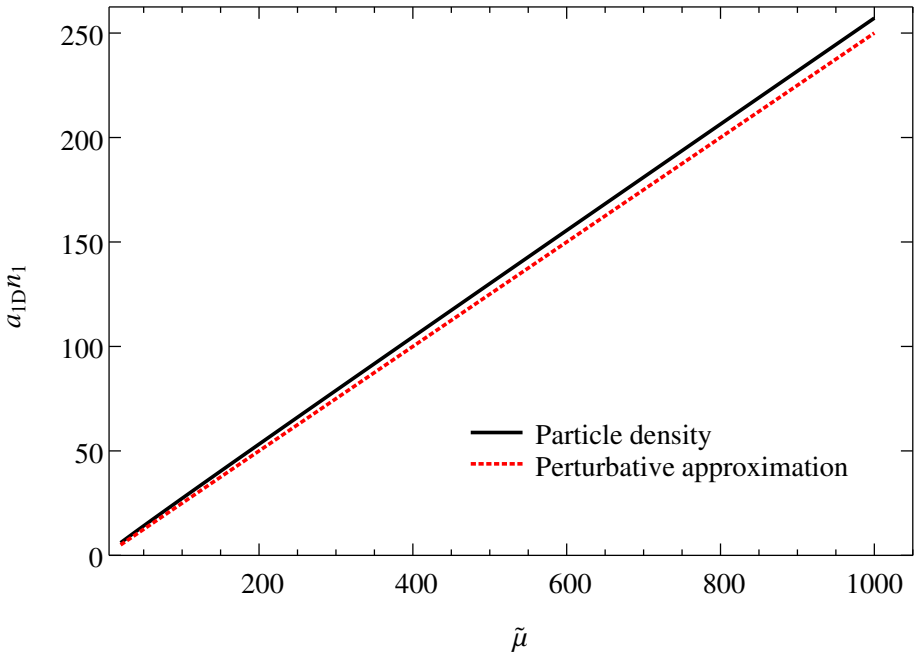


(b)

Figure 16: The quantity $|a_{1D}|\, n_1$ as a a function of the dimensionless chemical potential $\tilde{\mu}$ (calculated using Eq. (3.71)) in the Lieb-Liniger theory: (a) Tonks-Girardeau regime (b) weak coupling regime

where $\epsilon = \frac{\hbar^2}{2m} n_1^2 e(\gamma)$. This implies that the local chemical potential (3.65) is $\tilde{\mu} = \pi^2 (a_{1D} n_1)^2$.

Inverting this relation one gets the dependence of the local particle density on the local chemical potential

$$|a_{1D}|\, n_1 = \frac{\sqrt{\tilde{\mu}}}{\pi} = \frac{|a_{1D}|\,\sqrt{Z^2 - z^2}}{\pi a_z^2}. \tag{3.72}$$

The dependence of the density $|a_{1D}|\, n_1$ on the chemical potential $\tilde{\mu}$ is shown in the right panel in Fig. 16. The blue curve shows analytical approximation of equation (3.72), the red curve is the numerical result obtained from the solution to the Lieb-Liniger equations.

Let us introduce the dimensionless Thomas-Fermi radius

$$\tilde{Z} = \frac{Z\,|a_{1D}|}{a_z^2}. \tag{3.73}$$

We can determine the Thomas-Fermi radius from the normalization condition (3.68)

$$2\tilde{Z}\int_0^1 \frac{1}{\pi}\sqrt{\tilde{Z}^2\,(1-t^2)}dt = N\left(\frac{a_{1D}}{a_z}\right)^2. \tag{3.74}$$

Thus we get

$$\tilde{Z} = \sqrt{2N\left(\frac{a_{1D}}{a_z}\right)^2}. \tag{3.75}$$

The dependence of the Thomas-Fermi radius on the interaction parameter $N\left(\frac{a_{1D}}{a_z}\right)^2$ is shown in the left panel of Fig. 17. Now one has to calculate the mean square radius and its derivative with respect to $\omega_z^2$.

$$\left\langle z^2\right\rangle = \frac{Z^4}{a_z^2\pi}\frac{\pi}{8} = \frac{N^2 a_z^2}{2}, \tag{3.76}$$

$$\omega_z^2\frac{\partial\left\langle z^2\right\rangle}{\partial\omega_z^2} = -\frac{1}{2}\frac{N^2a_z^2}{2}. \tag{3.77}$$

This leads to the result

$$\omega^2 = 4\omega_z^2 \qquad \text{for } \gamma\to\infty. \tag{3.78}$$

Before going to subleading orders, we have to make an analysis of the present result. We get Eq. (3.78) in the limit $\gamma\to\infty$, which was realized by setting $g\to\infty$. We used the local density and the Thomas-Fermi approximations for the calculation of the breathing mode frequency. In this approximations we get the Thomas-Fermi radius $Z = \sqrt{2N}a_z$ and the density profile is $n_1(z) = \sqrt{2N}\sqrt{1-(z/Z)^2}/a_z\pi$. The limit $\gamma\to\infty$ should be interpreted as $mg/\hbar^2 n_1 = mga_z\pi/\hbar^2\sqrt{2N}\to\infty$. In this sense, in order to investigate the thermodynamic limit for a non-homogeneous system one should take into account that the ratio $\hbar^2\sqrt{2N}/a_z\pi mg = \sqrt{2N}\,|a_{1D}|/2\pi a_z$ has to be small.

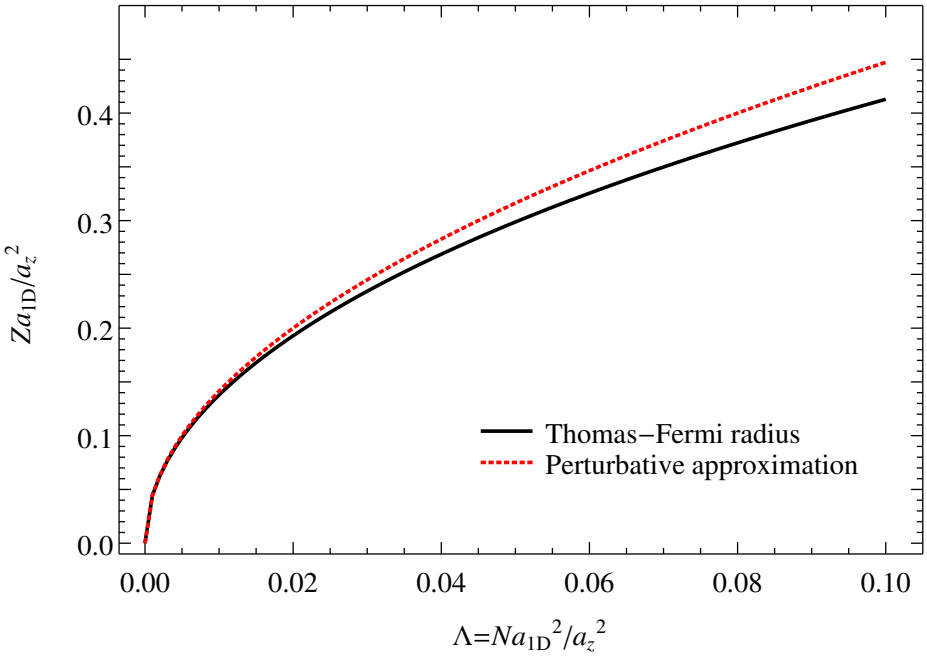


(a)

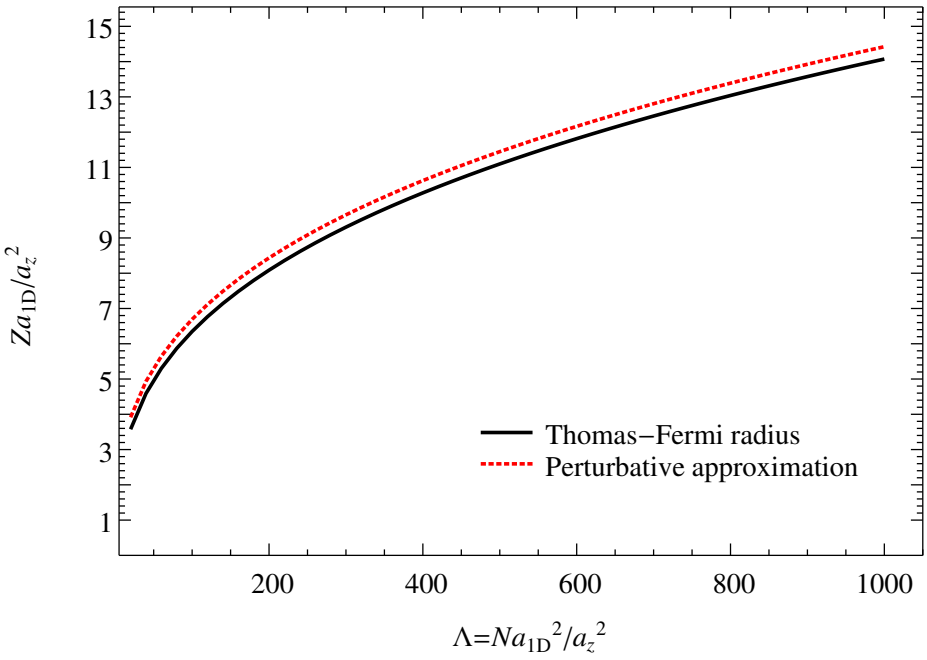


(b)

Figure 17: The dependence of the dimentionless Thomas-Fermi radius $\tilde{Z}$ (Eq. (3.73)) on $N\left(\frac{a_{1D}}{a_z}\right)^2$ for repulsive interactions: (a) Tonks-Girardeau regime ($\Lambda \ll 1$) (b) Thomas-Fermi regime ($\Lambda \gg 1$)

Now we analyse how good is the LDA approximation. We can do this because it is

possible to construct the exact wave-function of the system in the Tonks-Giradeau limit. In this limit there exists the so-called boson-fermion mapping [41], and the ground state wave-function is given by the expression

$$\psi(x_1,\ldots,x_N) = \frac{1}{\sqrt{N!}} \det\left[\psi_i^{HO}(x_j)\right] \prod_{i>j=1}^{N} \mathrm{sign}(x_i - x_j). \tag{3.79}$$

From this ground state wave-function we can determine the density distribution using the formula

$$n_1(x)^{exact} = \iiint \psi(x, x_2, \ldots, x_N)^2 \prod_{k=2}^{N} dx_k. \tag{3.80}$$

The ground state density in the Tonks-Girardeau limit reads as follows:

$$n_1(x)^{exact} = \frac{1}{N} \sum_{i=1}^{N} \left|\psi_i^{HO}(x_j)\right|^2. \tag{3.81}$$

The exact density distribution and the one calculated in the LDA approximation for $N = 5$, 10, 20 and 50 particles are plotted in Fig. 18. We can see that the more particles are in the trap, the better is the LDA (see also Ref. [30]).

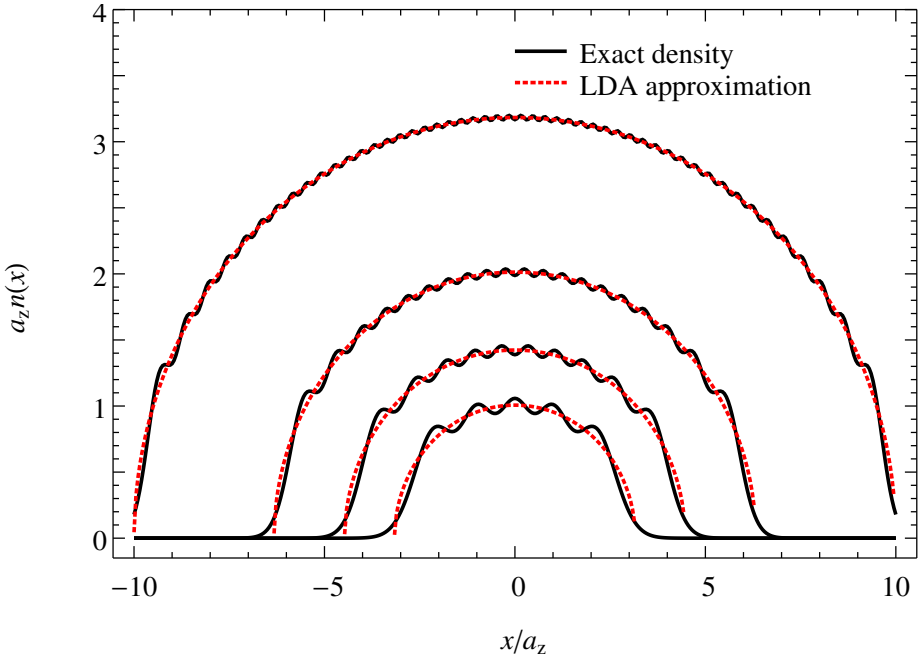


Figure 18: Densities distribution in the Tonks-Girardeau regime for $N = 5$, 10, 20 and 50 particles (bottom to top). Black curves: exact result, red dashed curves - LDA approximation.

Now we can calculate the first-order correction in $\frac{1}{g}$. Taking into account first subleading term in Eq. (3.43) we get

$$\tilde{\mu} = \pi^2 \left(n_1 a_{1D}\right)^2 - \frac{8\pi^2}{3} \left(|a_{1D}|\, n_1\right)^3 . \tag{3.82}$$

Inverting this relation we obtain a dependence of the particle density on the local chemical potential

$$|a_{1D}|\, n_1 = \frac{\sqrt{\tilde{\mu}}}{\pi} + \frac{4\tilde{\mu}}{3\pi^2}. \tag{3.83}$$

The next step is to calculate the Thomas-Fermi radius using Eq. (3.65) from the normalization condition

$$\int_{-Z}^{Z} \left( \frac{\sqrt{Z^2 - z^2}}{a_z^2 \pi} + \frac{4a_{1D}}{3} \frac{(Z^2 - z^2)}{\pi^2 a_z^4} \right) dz = N. \tag{3.84}$$

Hence, the Thomas-Fermi radius is

$$Z = \sqrt{2N} a_z - \frac{32N}{9\pi^2} \left|a_{1D}\right| , \tag{3.85}$$

and the density profile is

$$n_1 = \frac{Z}{a_z^2 \pi} \sqrt{1 - \left(\frac{z}{Z}\right)^2} + \frac{4\left|a_{1D}\right| Z^2}{3\pi^2 a_z^4} \left(1 - \left(\frac{z}{Z}\right)^2\right). \tag{3.86}$$

Let us now calculate the first subleading term in $1/g$ for the breathing mode using (2.23). Now we have to calculate the mean square radius and it's derivative with respect to $\omega_z^2$.

$$\left\langle z^2 \right\rangle = \frac{N^2 \hbar}{2m\omega_z} + \frac{16\hbar^2 (N)^{\frac{5}{2}} \sqrt{2\hbar}}{15mg\pi^2 \sqrt{m\omega_z}}, \tag{3.87}$$

and

$$\frac{\partial \left\langle z^2 \right\rangle}{\partial \omega_z^2} = -\frac{1}{2} \frac{N^2 \hbar}{2m\omega_z^3} + \frac{1}{4} \frac{16\hbar^2 (N)^{\frac{5}{2}} \sqrt{2\hbar}}{15mg\pi^2 \omega_z^2 \sqrt{m\omega_z}}. \tag{3.88}$$

This leads to (see also Ref. [35]):

$$\omega^2 = 4 \left(1 - \frac{32\sqrt{2N}\left|a_{1D}\right|}{15\pi^2 a_z}\right) \omega_z^2, \qquad \gamma \to \infty \tag{3.89}$$

The dependence of $\left(\frac{\omega}{\omega_z}\right)^2$ on $N\left(\frac{a_{1D}}{a_z}\right)^2$ was calculated numerically in Ref. [16]. We reproduce this dependence and display it in Fig. 19. One can see that the asymptotic expansions are rather good approximations for small and large values of $\Lambda$.

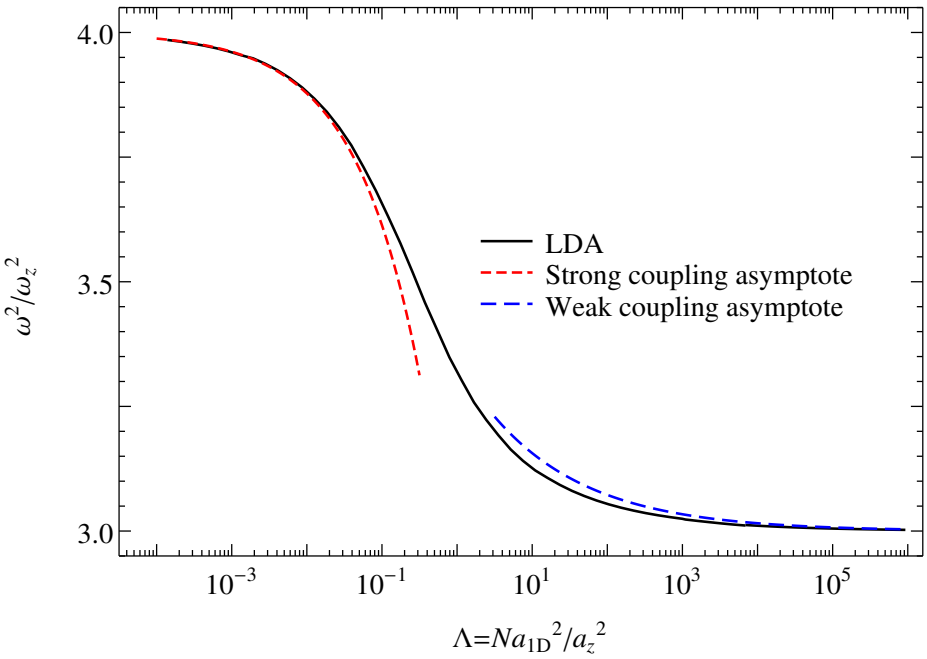


Figure 19: The ratio $\omega^2/\omega_z^2$ as a function of the LDA parameter $\Lambda = Na_{1D}^2/a_z^2$ obtained from Eqs. (3.70) and (3.64). Colored dashed curves are the weak and strong coupling asymptotes ((3.96) and (3.89), respectively).

### 3.8.2. Breathing mode frequency in the weak coupling limit

We now investigate the $\gamma \to 0$ limit. This limit we realize through $g \to 0$, with the number of particles $N$ and trap frequency $\omega_z$ remaining constant. In this limit the energy per particle could be calculated using (3.38):

$$\epsilon = \frac{\hbar^2}{2m} n_1^2 \gamma \left(1 - \frac{4}{3\pi}\sqrt{\gamma}\right), \tag{3.90}$$

and the chemical potential calculated from Eq. (3.71) is

$$\tilde{\mu} = 8\gamma^{-1} - \frac{8}{\pi}\gamma^{-\frac{1}{2}}. \tag{3.91}$$

We then find the local density

$$n_1 = \frac{\mu}{2a_{1D}^2 \frac{mg}{\hbar^2}} + \frac{1}{\pi}\sqrt{\frac{\mu}{2a_{1D}^2}} = \frac{Z^2 - z^2}{2a_z^4 \frac{mg}{\hbar^2}} + \frac{1}{\pi}\sqrt{\frac{Z^2 - z^2}{2a_z^4}}. \tag{3.92}$$

From normalization condition we determine the Thomas-Fermi radius:

$$Z = \left(\frac{3a_z^4}{|a_{1D}|}N\right)^{\frac{1}{3}} - \frac{a_z^2}{2\sqrt{2}|a_{1D}|}. \tag{3.93}$$

The dependence of the Thomas-Fermi radius on the parameter $N\left(\frac{a_{1D}}{a_z}\right)^2$ is shown in the right panel of Fig. 17.

The density profiles for twenty five particles and different values of the interaction parameter $\Lambda$ are shown in Fig. 20.

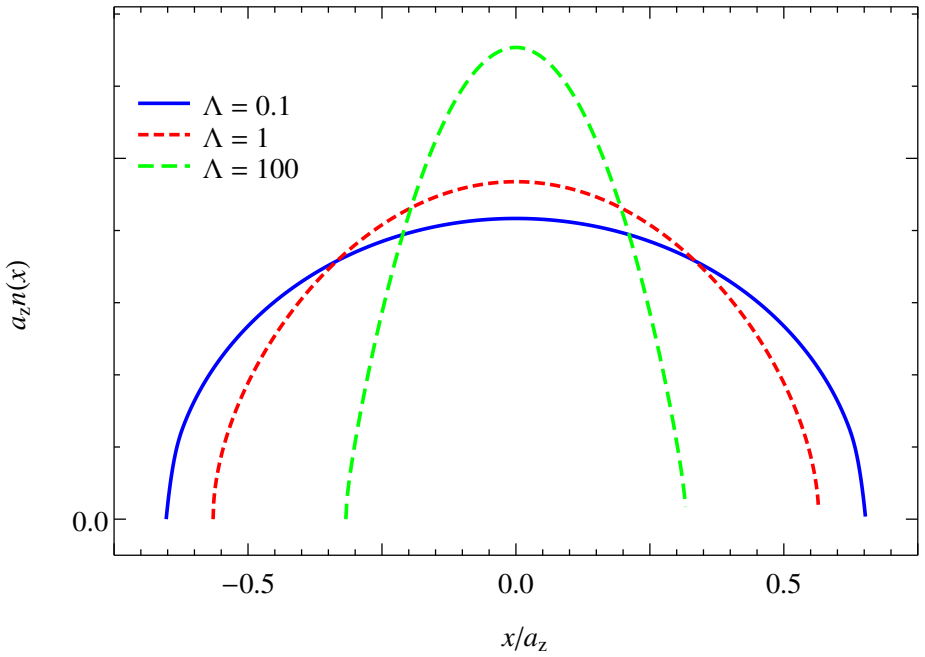


Figure 20: Profiles of density calculated in the hydrodynamic approach (dashed) for various values of the interaction parameter $\Lambda = N\left(\frac{a_{1D}}{a_z}\right)^2$. In the Tonks-Girardeau regime, $\Lambda \ll 1$, the density profile is a semi-circle. In the Thomas-Fermi regime, $\Lambda \gg 1$, the density profile is an inverted parabola.

Now, when all parameters of the system are determined, we can calculate the breathing mode frequency from Eq. (2.23)

$$\langle z^2\rangle = \frac{2Z^5}{15a_z^4\frac{mg}{\hbar^2}} - \frac{Z^4}{8\sqrt{2}a_z^2} = \frac{1}{5}3^{\frac{2}{3}}a_z^{\frac{8}{3}}|a_{1D}|^{-\frac{2}{3}}N^{\frac{5}{3}} - \frac{1}{8\sqrt{2}}3^{\frac{1}{3}}a_z^{\frac{10}{3}}|a_{1D}|^{-\frac{4}{3}}N^{\frac{4}{3}}, \tag{3.94}$$

$$\omega_z^2\frac{\partial\langle z^2\rangle}{\partial\omega_z^2} = -\frac{1}{5}3^{-\frac{1}{3}}a_z^{\frac{8}{3}}|a_{1D}|^{-\frac{2}{3}}N^{\frac{5}{3}} - \frac{5}{32\sqrt{2}}3^{-\frac{2}{3}}a_z^{\frac{10}{3}}|a_{1D}|^{-\frac{4}{3}}N^{\frac{4}{3}}, \tag{3.95}$$

$$\omega^2 = \omega_z^2\left(3 + \frac{5}{32\sqrt{2}}3^{\frac{2}{3}}\left(\frac{a_z}{a_{1D}}\right)^{\frac{2}{3}}N^{-\frac{1}{3}}\right); \qquad \text{for } \gamma \to 0 \tag{3.96}$$

Let us discuss the applicability of this result. In the weak-coupling limit ($\Lambda \gg 1$) the applicability of the Thomas-Fermi approximation is limited. The Laplacian of the density profile in the central part of the cloud is omitted in this approach in Eq. (3.6), and the applicability

of the LDA coincides with the applicability of the Thomas-Fermi approximation. The bound of applicability of the approach is given by the condition

$$\xi \sim a_z, \tag{3.97}$$

where $\xi$ is a the healing length

$$\xi = \frac{\hbar}{\sqrt{m n_1 g}}. \tag{3.98}$$

This leads to the condition $N\frac{a_z}{a_{1D}} \sim 1$. Thus, the limit of applicability of the LDA is $N\left(\frac{a_{1D}}{a_z}\right)^2 \sim N^3$. Comparing this bound with Figures 7 and 19 one can conclude that the coefficient of proportionality is approximately $\frac{1}{81}$, and finally the approach is applicable for

$$\Lambda \leq \frac{1}{81} N^3. \tag{3.99}$$

## 3.9. Breathing mode frequency for attractive interactions

In Section 3.7 calculations were made for a homogeneous system. For a trapped system the coordinate dependence of the particle density plays a crucial role. In this case the interaction parameter introduced in section 3.4 depends on the coordinate. Near the edge of the cloud (close to the Thomas-Fermi radius) the particle density is small, which implies that $\gamma$ is very large. In other words $\gamma(z) \to \infty, z \to Z$. In the trap center the particle density reaches its maximum and $\gamma$ is the smallest. The dependence of $\gamma_0 = \gamma(0) = 2/\left(a_{1D} n_1(0)\right)$ on the LDA parameter $\Lambda$ for the repulsive (blue) and the attractive (red) interaction is shown in Fig. 21.

Now we can calculate the frequency of the breathing mode oscillations in the same way as in Section 3.8. In the LDA we calculate the Thomas-Fermi radius using equation (3.68) and then use expression (2.23) to calculate the breathing mode frequency.

### 3.9.1. Breathing mode frequency at the strongly attractive regime

First we make an analysis of the super-Tonks-Girardeau gas based on equation (3.61). We investigate the leading order in $1/\gamma$, and then find the first subleading correction. The

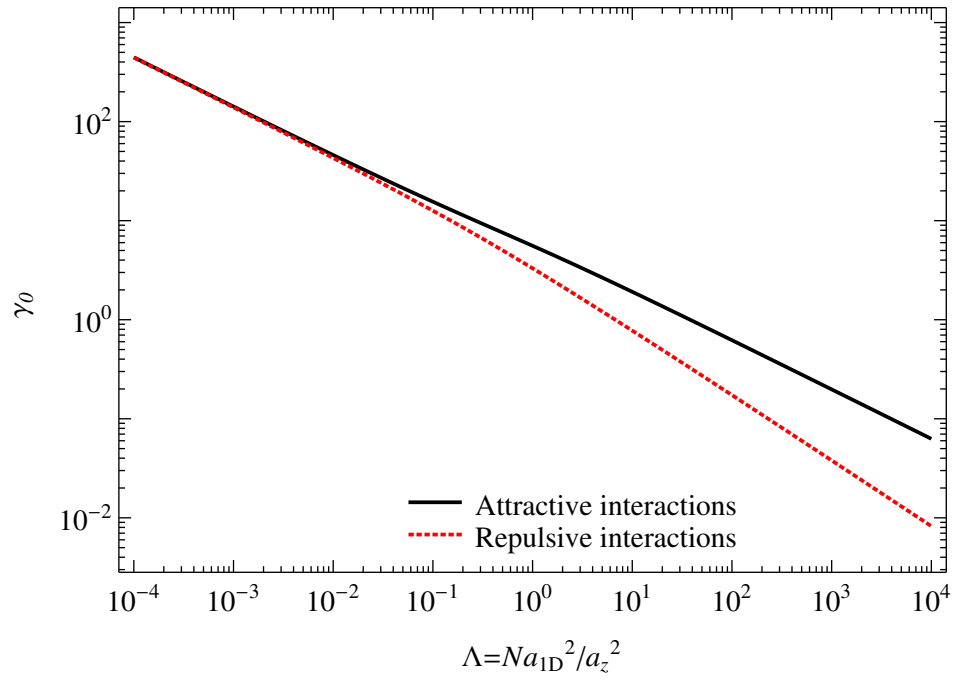


Figure 21: Interaction parameter in the trap center $\gamma_0$ as a function of $N\left(\frac{a_{1D}}{a_z}\right)^2$. Black curve corresponds to repulsive interactions and red curve to attractive interactions.

chemical potential is connected with the particle density by the relation (3.71). This leads to the local chemical potential $\tilde{\mu} = \pi^2(a_{1D}n_1)^2$. Inverting this relation we get the dependence of the local particle density on the local chemical potential:

$$a_{1D}n_1 = \frac{\sqrt{\tilde{\mu}}}{\pi} = \frac{a_{1D}\sqrt{(Z^2 - z^2)}}{\pi a_z^2}. \tag{3.100}$$

Now we can determine the Thomas-Fermi radius from the normalization condition (3.68):

$$2\tilde{Z}\int_0^1 \frac{1}{\pi}\sqrt{\tilde{Z}^2\,(1-t^2)}dt = N\left(\frac{a_{1D}}{a_z}\right)^2. \tag{3.101}$$

Thus we get $\tilde{Z} = \frac{Za_{1D}}{a_z^2} = \sqrt{2N\left(\frac{a_{1D}}{a_z}\right)^2}$. Now one has to calculate the mean square radius and its derivative with respect to $\omega_z^2$:

$$\left\langle z^2\right\rangle = \int_{-Z}^{Z} z^2 n_1(z)dz = \frac{N^2\hbar}{2m\omega_z}, \tag{3.102a}$$

and

$$\frac{\partial\left\langle z^2\right\rangle}{\partial\omega_z^2} = -\frac{1}{2}\frac{N^2\hbar}{2m\omega_z^3}. \tag{3.102b}$$

This leads to the result

$$\omega^2 = 4\omega_z^2 \qquad \text{for the } \gamma \to \infty \tag{3.103}$$

One can conclude that at $\gamma = \pm\infty$ the breathing mode frequency is an analytic function of the parameter $N\left(\frac{a_{1D}}{a_z}\right)^2$.

### 3.9.2. Breathing mode frequency in the weakly attractive regime

We now investigate the $\gamma \to 0$ limit, ($\gamma < 0$). In this limit the energy per particle can be calculated using (3.63). Using Eq. (3.71) we get

$$a_{1D} n_1 = \frac{\sqrt{\tilde{\mu}}}{2\pi} = \frac{a_{1D}\sqrt{Z^2 - z^2}}{2\pi a_z^2}. \tag{3.104}$$

This density profile is written for the gas state defined in sections 3.7.1 and 3.7.2. We can see that both in the Tonks-Girardeau and the weak attractive regimes, the cloud density profile is a semi-circle because the chemical potential is quadratic in density. However the coefficients for these cases are different from each other (compare Eqs. (3.104) and (3.72)). Thus, the Thomas-Fermi radius in the weak attractive regime is different from the one in the Tonks-Girardeau regime. Now we determine the Thomas-Fermi radius from the normalization condition (3.68):

$$2\tilde{Z}\int_0^1 \frac{1}{2\pi}\sqrt{\tilde{Z}^2\left(1-t^2\right)}dt = N\left(\frac{a_{1D}}{a_z}\right)^2. \tag{3.105}$$

Hence we get $\tilde{Z} = Z a_{1D}/a_z^2 = \sqrt{4N\left(\frac{a_{1D}}{a_z}\right)^2}$. One then calculates the mean square radius and its derivative with respect to $\omega_z^2$:

$$\left\langle z^2 \right\rangle = \int_{-Z}^{Z} z^2 n_1(z) dz = \frac{Z^4}{a_z^2 2\pi}\frac{\pi}{8} = \frac{N^2\hbar}{m\omega_z}, \tag{3.106a}$$

and

$$\frac{\partial\left\langle z^2\right\rangle}{\partial\omega_z^2} = -\frac{N^2\hbar}{2m\omega_z^3}. \tag{3.106b}$$

This leads to the result:

$$\omega^2 = 4\omega_z^2 \qquad \text{for } \gamma \to 0 \tag{3.107}$$

Contrary to the case of weak repulsive interactions, (section 3.8.2), where $\left(\frac{\omega}{\omega_z}\right)^2 \to 3$, in the case of weak attractive interaction we have $\left(\frac{\omega}{\omega_z}\right)^2 \to 4$.

## 3.10. Perturbation theory for a gas close to the Tonks-Girargeau regime

The perturbation theory also gives a possibility to calculate the leading order correction to the ground state energy and the chemical potential close to the Tonks-Girardeau limit [42]. This can be done by mapping the strongly interacting bosons with pairwise interaction strength $\alpha$ onto weakly-interacting fermions with $1/\alpha$ interaction strength [41]. The fermion system obeys the Schrödinger equation

$$\left[\sum_{i=1}^{N}\left(-\frac{\hbar^2}{2m}\frac{\partial^2}{\partial x_i^2}+\frac{m\omega_z^2}{2}x_i^2\right)+\hat{V}\right]\Psi^f=E\Psi^f, \tag{3.108}$$

where the operator $\hat{V}$ has the matrix elements

$$\langle\Psi^f\left|\hat{V}\right|\Phi^f\rangle=-\frac{4}{\alpha}\sum_{i<j}\int_{-\infty}^{\infty}\lim_{r_{ij}\to 0}\frac{\partial\Psi^f}{\partial r_{ij}}\frac{\partial\Phi^f}{\partial r_{ij}}dR_{ij}dx_1\ldots dx_N, \tag{3.109}$$

with $r_{ij}=x_i-x_j$, and $R_{ij}=\frac{x_i+x_j}{2}$ being the relative and center-of-mass coordinates. In Eq. (3.109) the integration goes over the $R_{ij}$ and we take the $r_{ij}\to 0$ limit. This gives the ground state energy:

$$E_{gs}=\frac{1}{2}N^2\hbar\omega_z+\left\langle\Psi^f\left|\hat{V}\right|\Psi^f\right\rangle+O(\frac{1}{\alpha^2}). \tag{3.110}$$

Thus, $\langle\Psi^f\left|\hat{V}\right|\Psi^f\rangle=\sum_{k<l}(v_{klkl}-v_{kllk})$, where

$$v_{klmn}=-\frac{1}{\alpha}\int\lim_{r_{12}\to 0}\frac{\partial\psi_k^*(x_1)\psi_l^*(x_2)}{\partial r_{12}}\frac{\partial\psi_m(x_1)\psi_n(x_2)}{\partial r_{12}}dR_{12}. \tag{3.111}$$

This leads to the final result (see also Ref. [42]):

$$\frac{E_{gs}}{\hbar\omega_z}=\frac{1}{2}N^2+\frac{1}{\alpha}\sqrt{\frac{2}{\pi^3}}\sum_{l=1}^{N-1}\frac{\Gamma\left(l-\frac{1}{2}\right)}{\Gamma(l+1)}\sum_{k=0}^{l-1}\frac{(l-k)^2\Gamma\left(k-\frac{1}{2}\right)}{\Gamma(k+1)}{}_3F_2\left(\frac{3}{2},-k,-l;\frac{3}{2}-k,\frac{3}{2}-l;1\right). \tag{3.112}$$

The second excited level is doubly degenerated. The first state is related to the center of mass motion (second exited center of mass state) and its energy is

$$E_{CM}=E_{gs}+2\omega_z. \tag{3.113}$$

Let us take the energy of the second state. We have to use the degenerate perturbation theory to do so. Let us take two states as a basis for the perturbation theory and then diagonalise

the secular matrix. We choose the states with the quantum numbers $0, 1, 2, \ldots, N-2, N+1$ and $0, 1, 2, \ldots, N-3, N-1, N$. Let us denote the first set of the quantum numbers as $2\alpha$ and the second set as $2\beta$. Energies of the $2\alpha$ and $2\beta$ states are

$$\frac{E_{2\alpha}}{\hbar\omega_z} = \frac{1}{2}N^2+2+\frac{1}{\alpha}\sqrt{\frac{2}{\pi^3}}\sum_{l=1}^{N-2}\frac{\Gamma\left(l-\frac{1}{2}\right)}{\Gamma(l+1)}\sum_{k=0}^{l-1}\frac{(l-k)^2\Gamma\left(k-\frac{1}{2}\right)}{\Gamma(k+1)}{}_3F_2\left(\frac{3}{2},-k,-l;\frac{3}{2}-k,\frac{3}{2}-l;1\right)$$
$$+\frac{1}{\alpha}\sqrt{\frac{2}{\pi^3}}\frac{\Gamma\left(N+\frac{1}{2}\right)}{\Gamma(N+2)}\sum_{k=0}^{N-2}\frac{(N+1-k)^2\Gamma\left(k-\frac{1}{2}\right)}{\Gamma(k+1)}{}_3F_2\left(\frac{3}{2},-k,-N-1;\frac{3}{2}-k,\frac{3}{2}-N-1;1\right), \tag{3.114}$$

$$\frac{E_{2\beta}}{\hbar\omega_z} = \frac{1}{2}N^2+2+\frac{1}{\alpha}\sqrt{\frac{2}{\pi^3}}\sum_{l=1}^{N-3}\frac{\Gamma\left(l-\frac{1}{2}\right)}{\Gamma(l+1)}\sum_{k=0}^{l-1}\frac{(l-k)^2\Gamma\left(k-\frac{1}{2}\right)}{\Gamma(k+1)}{}_3F_2\left(\frac{3}{2},-k,-l;\frac{3}{2}-k,\frac{3}{2}-l;1\right)$$
$$+\frac{1}{\alpha}\sqrt{\frac{2}{\pi^3}}\frac{\Gamma\left(N-\frac{3}{2}\right)}{\Gamma(N)}\sum_{k=0}^{N-3}\frac{(N-1-k)^2\Gamma\left(k-\frac{1}{2}\right)}{\Gamma(k+1)}{}_3F_2\left(\frac{3}{2},-k,-N+1;\frac{3}{2}-k,\frac{3}{2}-N+1;1\right)$$
$$+\frac{1}{\alpha}\sqrt{\frac{2}{\pi^3}}\frac{\Gamma\left(N-\frac{1}{2}\right)}{\Gamma(N+1)}\sum_{k=0}^{N-3}\frac{(N-k)^2\Gamma\left(k-\frac{1}{2}\right)}{\Gamma(k+1)}{}_3F_2\left(\frac{3}{2},-k,-N;\frac{3}{2}-k,\frac{3}{2}-N;1\right)$$
$$+\frac{1}{\alpha}\sqrt{\frac{2}{\pi^3}}\frac{\Gamma\left(N-\frac{1}{2}\right)}{\Gamma(N+1)}\frac{\Gamma\left(N-\frac{3}{2}\right)}{\Gamma(N)}{}_3F_2\left(\frac{3}{2},-N-1,-N;\frac{5}{2}-N,\frac{3}{2}-N;1\right). \tag{3.115}$$

The difference of the energy of the $2\alpha$ ($2\beta$) state from the ground state energy is:

$$\frac{E_{2\alpha}-E_{gs}}{\hbar\omega_z}-2 = \frac{1}{\alpha}\sqrt{\frac{2}{\pi^3}}\frac{\Gamma\left(N+\frac{1}{2}\right)}{\Gamma(N+2)}\sum_{k=0}^{N-2}\frac{(N+1-k)^2\Gamma\left(k-\frac{1}{2}\right)}{\Gamma(k+1)}{}_3F_2\left(\frac{3}{2},-k,-N-1;\frac{3}{2}-k,\frac{3}{2}-N-1;1\right)$$
$$-\frac{1}{\alpha}\sqrt{\frac{2}{\pi^3}}\frac{\Gamma\left(N-\frac{3}{2}\right)}{\Gamma(N)}\sum_{k=0}^{N-2}\frac{(N-1-k)^2\Gamma\left(k-\frac{1}{2}\right)}{\Gamma(k+1)}{}_3F_2\left(\frac{3}{2},-k,-N+1;\frac{3}{2}-k,\frac{5}{2}-N;1\right), \tag{3.116}$$

$$\frac{E_{2\beta}-E_{gs}}{\hbar\omega_z}-2 = \frac{1}{\alpha}\sqrt{\frac{2}{\pi^3}}\frac{\Gamma\left(N-\frac{1}{2}\right)}{\Gamma(N+1)}\sum_{k=0}^{N-3}\frac{(N-k)^2\Gamma\left(k-\frac{1}{2}\right)}{\Gamma(k+1)}{}_3F_2\left(\frac{3}{2},-k,-N;\frac{3}{2}-k,\frac{3}{2}-N;1\right)$$
$$-\frac{1}{\alpha}\sqrt{\frac{2}{\pi^3}}\frac{\Gamma\left(N-\frac{5}{2}\right)}{\Gamma(N-1)}\sum_{k=0}^{N-3}\frac{(N-2-k)^2\Gamma\left(k-\frac{1}{2}\right)}{\Gamma(k+1)}{}_3F_2\left(\frac{3}{2},-k,-N+2;\frac{3}{2}-k,\frac{7}{2}-N;1\right)$$
$$+\frac{1}{\alpha}\sqrt{\frac{2}{\pi^3}}\frac{\Gamma\left(N-\frac{1}{2}\right)}{\Gamma(N+1)}\frac{\Gamma\left(N-\frac{3}{2}\right)}{\Gamma(N)}{}_3F_2\left(\frac{3}{2},-N+1,-N;\frac{5}{2}-N,\frac{3}{2}-N;1\right)$$
$$-\frac{1}{\alpha}\sqrt{\frac{2}{\pi^3}}\frac{\Gamma\left(N-\frac{3}{2}\right)}{\Gamma(N)}\frac{\Gamma\left(N-\frac{5}{2}\right)}{\Gamma(N-1)}{}_3F_2\left(\frac{3}{2},-N+2,-N+1;\frac{7}{2}-N,\frac{5}{2}-N;1\right). \tag{3.117}$$

The $2\alpha$ and $2\beta$–states are orthogonal to each other. From these states one can construct two physical states: the first state describes the center of mass oscillations and the second state is the breathing mode. These states are connected with the $2\alpha$ and $2\beta$–states by an orthogonal transformation. The main property of the center of mass oscillation state is that the energy difference of this state from the ground state energy is equal to $2\hbar\omega_z$, and does not depend on the interaction strength:

$$\psi_{CM} = c_1\psi_{2\alpha} + c_2\psi_{2\beta}, \tag{3.118a}$$

$$\psi_{BM} = c_2\psi_{2\alpha} - c_1\psi_{2\beta}, \tag{3.118b}$$

where $c_1 = \sqrt{\frac{2\hbar\omega_z + E_{gs} - E_{2\alpha}}{E_{2\beta} - E_{2\alpha}}}$, and $c_2 = -\sqrt{\frac{E_{2\beta} - 2\hbar\omega_z - E_{gs}}{E_{2\beta} - E_{2\alpha}}}$. Using $\psi_{BM}$ one can calculate the energy of the breathing mode

$$E_{BM} = E_{2\alpha} + E_{2\beta} - E_{gs} - 2\hbar\omega_z. \tag{3.119}$$

### 3.10.1. Comparison of the perturbation result with the two-particle exact expansion

Using equation (2.12) one can find the expansion of the breathing mode frequency in $\frac{1}{\alpha}$ in the Tonks-Girargeau limit. The energy of the ground state and the state corresponding to the the breathing mode oscillations are

$$\frac{E_{gs}}{\hbar\omega_z} = \frac{1}{2}N^2 - \frac{\sqrt{2}}{\alpha}\frac{2}{\sqrt{\pi}}, \tag{3.120a}$$

$$\frac{E_{BM}}{\hbar\omega_z} = \frac{1}{2}N^2 + 2 - \frac{\sqrt{2}}{\alpha}\frac{3}{\sqrt{\pi}}, \tag{3.120b}$$

The breathing mode frequency is

$$\frac{\omega}{\hbar\omega_z} = 2 - \frac{\sqrt{2}}{\alpha}\frac{1}{\sqrt{\pi}}. \tag{3.120c}$$

Expressions (3.120) can be compared with (3.119). Since due to equations (3.116) and (3.117) we have

$$\frac{E_{gs}}{\hbar\omega_z} = \frac{1}{2}N^2 - \frac{\sqrt{2}}{\alpha}\frac{2}{\sqrt{\pi}}, \tag{3.121}$$

$$\frac{E_{2\alpha}}{\hbar\omega_z} = \frac{1}{2}N^2 + 2 - \frac{1}{\alpha}\frac{9}{2\sqrt{2\pi}}, \tag{3.122}$$

$$\frac{E_{2\beta}}{\hbar\omega_z} = \frac{1}{2}N^2 + 2 - \frac{1}{\alpha}\frac{11}{2\sqrt{2\pi}}, \tag{3.123}$$

we get the following result:

$$\frac{\omega}{\hbar\omega_z} = 2 - \frac{1}{\alpha}\sqrt{\frac{2}{\pi}}. \tag{3.124}$$

This result coincides with expression (3.120c).

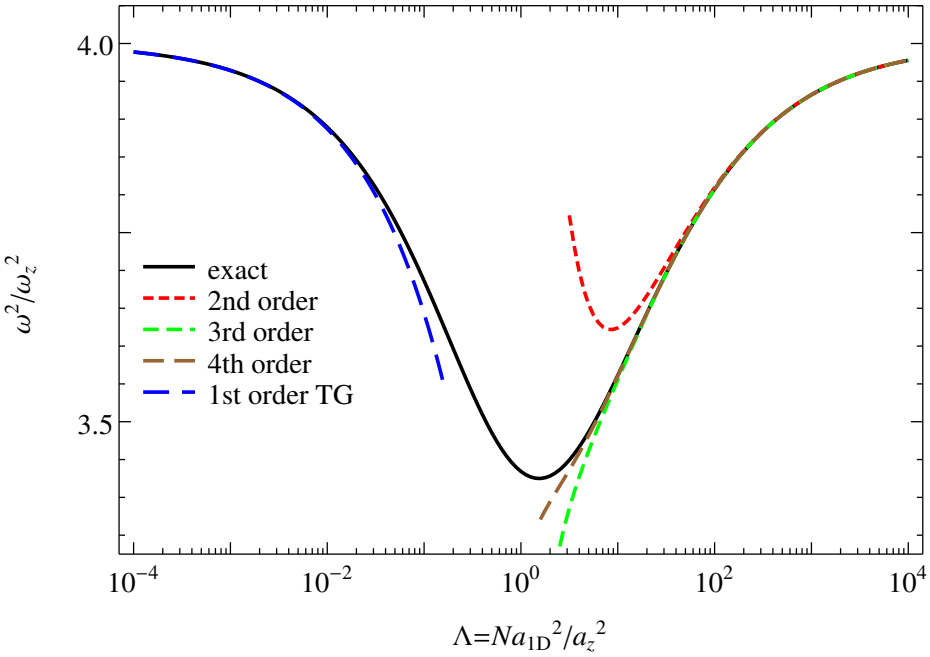


Figure 22: Breathing mode frequency and its perturbation approximations of different orders.

The two particle breathing mode frequency for the repulsive regime and its perturbation expansion are shown in Fig. 22. In the Tonks-Girargeau regime the first order perturbation approximation gives a good result when $N\left(\frac{a_{1D}}{a_z}\right)^2 < 0.1$, and for the weak-coupling regime the perturbation result works when $N\left(\frac{a_{1D}}{a_z}\right)^2 > 5$.

### 3.10.2. Finite $N$ Tonks-Girardeau expansions

Using equation (3.119) it is possible to calculate the leading order term of the expansion in $1/\alpha$ for the breathing mode frequency $\omega$. It can be done for any finite value of $N$. The summation of the terms in equations (3.112, 3.116, 3.117) and the use of equation (3.119)

give the following result [43]:

$$\left(\frac{\omega}{\omega_z}\right)^2 = 4\left(1 - \frac{3\sqrt{2N}}{\pi\sqrt{\pi}}\frac{\Gamma(N-\frac{5}{2})\Gamma(N+\frac{1}{2})}{\Gamma(N)\Gamma(N+2)}{}_3F_2\left[\begin{matrix}\frac{3}{2}, 1-N, -N \\ \frac{7}{2}-N, \frac{1}{2}-N\end{matrix}; 1\right]\sqrt{N\left(\frac{a_{1D}}{a_z}\right)^2}\right). \tag{3.125}$$

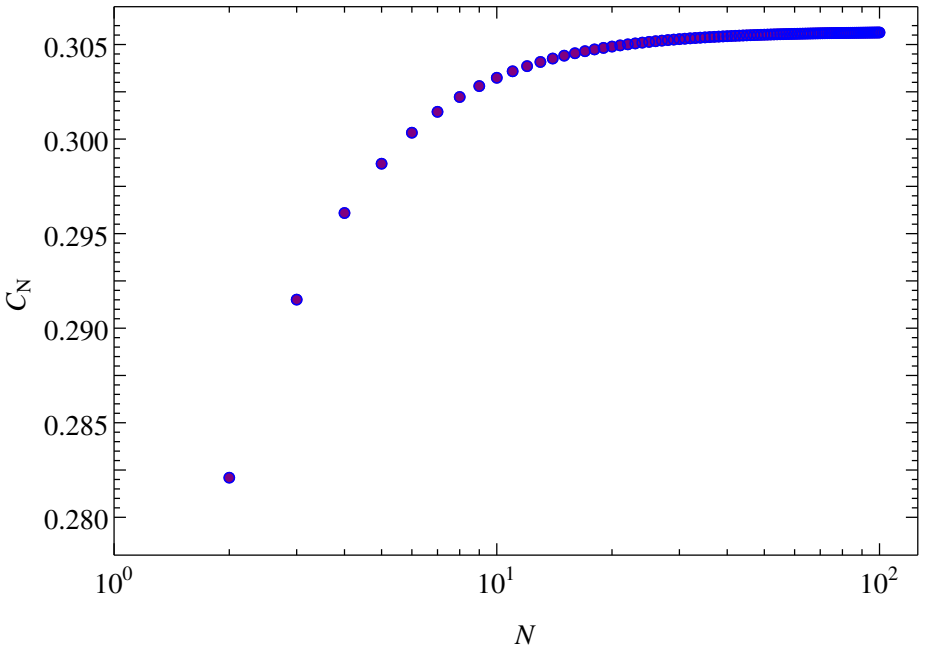


Figure 23: First coefficient of the breathing mode expansion. With larger $N$ it goes to the asymptotic value $32\sqrt{2}/15\pi^2$.

Now we can compare the asymptotic expansion (3.89) based on the LDA with the expansion based on perturbative calculations and the boson-fermion mapping (3.125). The dependence of the first coefficient of this expansion on the number of particles is shown in Fig. 23. We can clearly see the difference in the first coefficient of the expansion. The LDA expansion gives the coefficient $32\sqrt{2}/15\pi^2$ while the perturbative result depends on $N$. The coefficient for $N = 2$ is $1/2\sqrt{\pi}$. The difference between these LDA and perturbative coefficients is small and does not exceed 8%.

## 3.11. Temporal behavior of the momentum distribution of the Tonks-Girardeau gas

Let us now consider the Tonks-Girardeau gas in a parabolic trap, with the time-dependent trap frequency:

$$\omega_z(t) = \begin{cases} \omega_{z,-} & \text{if } t < 0, \\ \omega_{z,+} & \text{if } t > 0, \end{cases} \tag{3.126}$$

The exact wave-functions are known:

$$\psi(x_1, \ldots, x_N; t) = \frac{1}{\sqrt{N!}} \det\left[\phi_i(x_j; t)\right] \prod_{1 \le j < k}^{N} \mathrm{sign}(x_j - x_k), \tag{3.127}$$

where the single-particle wave-functions $\phi_i(x_j, t)$ satisfy the Schrödinger equation with the potential $V_{ext}(x,t) = m\omega_z^2(t)x^2/2$. It has the scaling symmetry [44]:

$$\phi_i(x;t) = \frac{1}{\sqrt{b(t)}} \phi_i\left(\frac{x}{b(t)}; 0\right) \exp\left(i\frac{mx^2\dot{b}(t)}{2\hbar b(t)} - E_j\tau(t)\right), \tag{3.128}$$

where $\tau(t) = \int_0^t \frac{1}{b^2(t')}dt'$, and $E_j$ are eigenvalues of harmonic oscillator with frequency $\omega_{z,-}$. Hence, $E_j = \omega_{z,-}^2\left(j + \frac{1}{2}\right)$. The scaling function $b(t)$ has to satisfy the equation [44]:

$$\ddot{b} + \omega^2(t)b = \frac{\omega_{z,-}^2}{b^3} \tag{3.129}$$

with initial conditions $b(0) = 1$ and $\dot{b}(0) = 0$. Thus, we get scaling properties for the wave-function

$$\psi(x_1, \ldots, x_N; t) = b^{-\frac{N}{2}} \psi\left(\frac{x_1}{b}, \ldots, \frac{x_N}{b}; 0\right) \exp\left(\frac{im\dot{b}}{\hbar b}\sum_{j=1}^{N} x_j^2 - i\sum_{j=1}^{N} E_j\tau\right). \tag{3.130}$$

Now we can investigate the time evolution of the density and momentum distributions. The density profile is connected with the one-body density matrix by the relation $n_1(x;t) = g_1(x,x;t)$, where

$$g_1(x,y;t) = N \iiint_{-\infty}^{\infty} \psi^*(x, x_2, \ldots, x_N; t)\psi(y, x_2, \ldots, x_N; t)dx_2 \cdots dx_N. \tag{3.131}$$

Using equation (3.130) we get

$$g_1(x,y;t) = \frac{1}{b} g_1\left(\frac{x}{b}, \frac{y}{b}; 0\right) \exp\left(-\frac{m\dot{b}}{\hbar b}(x^2 - y^2)\right). \tag{3.132}$$

Equation (3.132) follows from the Bose-Fermi mapping and does not depend on temperature. This formula yields the exact evolution of the Tonks-Girardeau density profile:

$$n_1(x;t) = \frac{1}{b(t)} g_1\left(\frac{x}{b}, \frac{x}{b}; 0\right) = \frac{1}{b(t)} n_1\left(\frac{x}{b}; 0\right). \tag{3.133}$$

It is also interesting to investigate the time evolution of the momentum distribution

$$n_1(p;t) = \iint_{-\infty,-\infty}^{\infty,\infty} \exp\left(i\frac{p(x-y)}{\hbar}\right) g_1(x,y;t)dxdy, \tag{3.134}$$

or after changing the variables, $x/b \to x$ and $y/b \to y$, we have:

$$n_1(p;t) = b\iint_{-\infty,-\infty}^{\infty,\infty} \exp\left(ib\left[\frac{m\dot{b}}{\hbar}(x^2-y^2) - \frac{p(x-y)}{\hbar}\right]\right) g_1(x,y;0)dxdy. \tag{3.135}$$

### 3.11.1. One-particle correlation functions

Now let us calculate the exact expression for the one-particle correlation function $g_1$ defined by equation (3.131). The wave-function of the system is $\psi(x_1,\ldots,x_N;t) = \frac{1}{\sqrt{N!}}\det\left[\phi_i(x_j;t)\right]$, so that one can write the expression for $g_1$:

$$g_1(x,y;t) = \frac{1}{N}\sum_{i=1}^{N} \phi_i^*(x;t)\phi_i(y;t). \tag{3.136}$$

For the Tonks-Girargeau gas the wave-function is given by equation (3.45), and $g_1$ can be written as [45]

$$g_1(x,y;t) = \frac{1}{N}\sum_{i,j=1}^{N,N} \phi_i^*(x;t)A_{i,j}(x,y;t)\phi_j(y;t), \tag{3.137}$$

where the matrix

$$A(x,y;t) = \left(P(x,y)^{-1}\right)^T \det\left[P_{i,j}(x,y;t)\right], \tag{3.138}$$

and

$$P_{i,j}(x,y;t) = \delta_{i,j} - 2\int_x^y \phi_j^*(z;t)\phi_i(z;t)dz. \tag{3.139}$$

In the $y \to x$ limit expressions (3.136) and (3.137) tend to the same function $n_1(x)$ (3.81). Using expression (3.137) is not the most productive way to calculate the one-body density matrix. Interestingly, it was noticed in Ref. [12, 46] that the wave-function can be rewritten in the form

$$\psi(x_1,\ldots,x_N) = \frac{1}{C_N}\prod_{k=1}^{N}\exp(-x_k^2)\prod_{1\le j<k\le N}|x_j - x_k|, \tag{3.140}$$

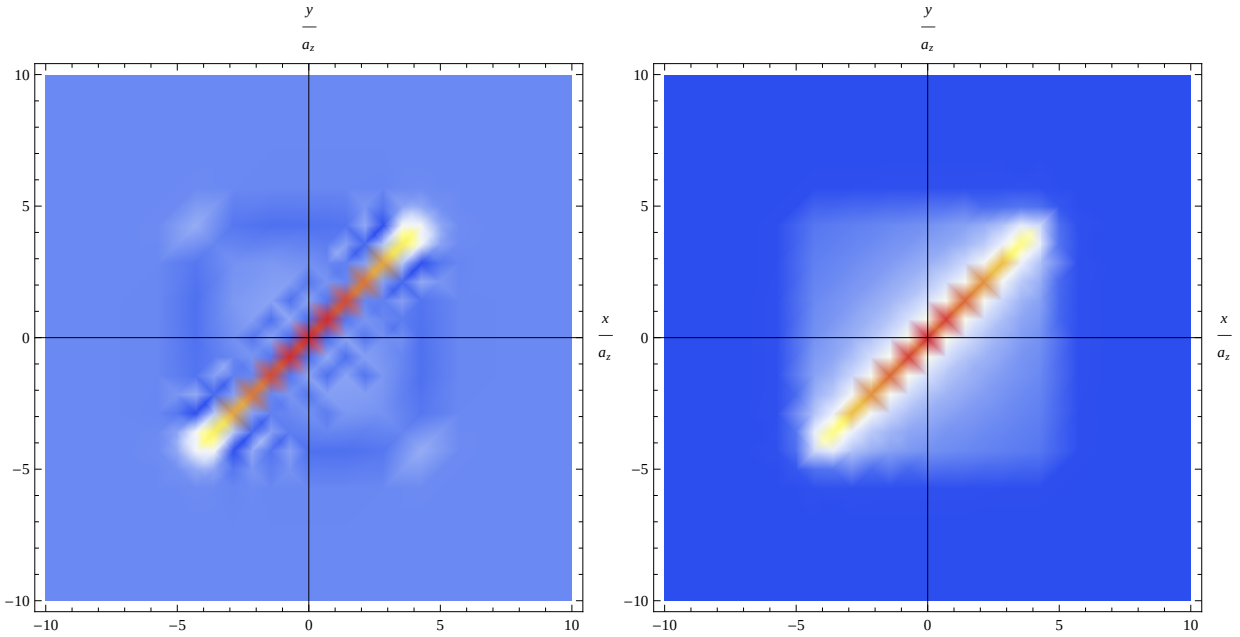


Figure 24: One-particle correlation functions for trapped free fermions and Tonks-Girargeau bosons for $N = 11$.

where $C_N^2 = N! \prod_{k=1}^{N-1} 2^{-k} \sqrt{\pi} k!$. This makes it possible to write the one-body density matrix as [46]

$$g_1(x,y) = \frac{2^{N-1}}{\sqrt{N}\Gamma(N)} \exp\left(-\frac{x^2+y^2}{2}\right) \times \det\left[\frac{2^{\frac{j+k}{2}}}{2\sqrt{\pi\Gamma(j)\Gamma(k)}}\beta_{j,k}(x,y)\right]_{j,k=1,\ldots,N-1}, \quad (3.141)$$

where $\beta_{j,k}(x,y) = \int_{-\infty}^{+\infty} dt \exp(-t^2)|x-t||t-y|t^{j+k-2}$. The integrals can be calculated explicitly:

$$\beta_{j,k}(x,y) = \tilde{\beta}_{j,k}(x,y) - 2\,\mathrm{sign}(y-x)\left[xy\mu_{j+k-2}(x,y) - (x+y)\mu_{j+k-1}(x,y) + \mu_{j+k}(x,y)\right], \quad (3.142)$$

where

$$\tilde{\beta}_{j,k}(x,y) = \begin{cases} \Gamma\left(\frac{j+k-1}{2}\right) xy + \Gamma\left(\frac{j+k+1}{2}\right), & \text{if } j+k \text{ is even;} \\ -\Gamma\left(\frac{j+k}{2}\right)(x+y), & \text{if } i+k \text{ is odd,} \end{cases} \quad (3.143)$$

and

$$\mu_{j+k-2}(x,y) = \frac{y^{m+1}\exp(-y^2)}{m+1} {}_1F_1\left(1; \frac{m+3}{2}; y^2\right) - \frac{x^{m+1}\exp(-x^2)}{m+1} {}_1F_1\left(1; \frac{m+3}{2}; x^2\right). \quad (3.144)$$

The one-body correlation functions for free fermions (left) and the Tonks-Girerdeau bosons (right) are shown in Fig. 24. For free fermions the main contribution to the one-body

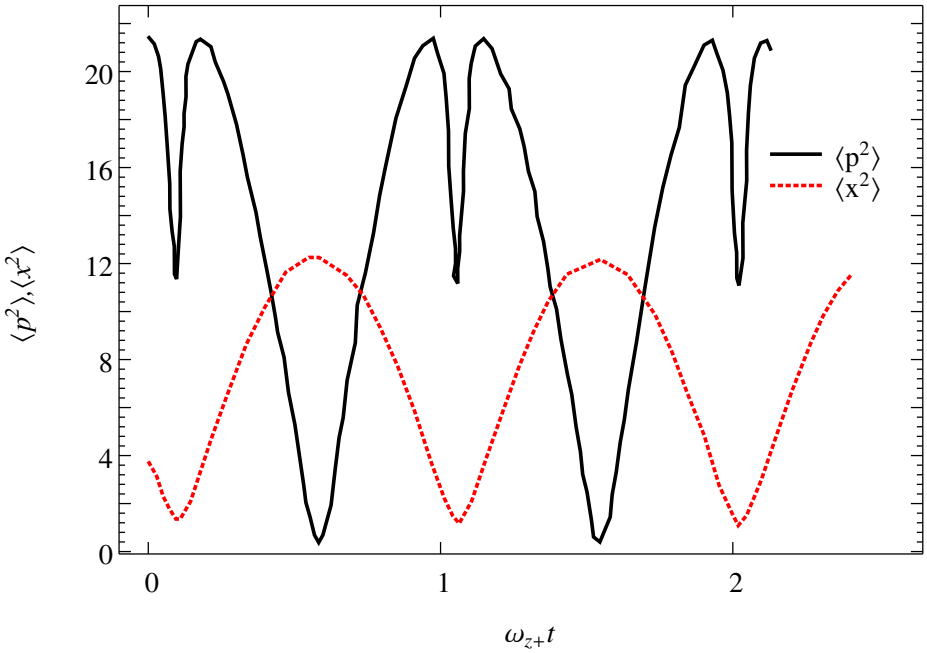


Figure 25: The time-evolution of the half-width for free fermions. Black curve: momentum space, red dashed curve: coordinate space. The strength of quench is $\omega_{z,+}/\omega_{z,-} = 115.4/15.6$.

correlation function comes from the near-diagonal region $x = y$ with maximum at the point $x = y = 0$. For the Tonks-Girardeau bosons the one-body correlation function looks similar. The main contribution comes from the nearly diagonal region, $x = y$, with maximum at the point $x = y = 0$, but in general $g_1(x, y)$ is a positive function at any $x$ and $y$.

The time evolution of the half-width of the free fermion system in the coordinate and momentum spaces after the excitation are shown in Fig. 25. The number of particles $N = 11$. The excitation frequency is $\omega_{z,+} = 115.4/15.6\,\omega_{z,-}$. The periods of oscillation in the coordinate space and in the momentum space are equal. In the coordinate space the time evolution of the average cloud size $\langle z^2 \rangle$ is proportional to the scaling function $b(t)$.

The time evolution of the half-width of the Tonks-Girardeau gas in the coordinate and momentum space after the excitation is shown in Fig. 26. The number of particles is $N = 11$. The excitation frequency is $\omega_{z,+} = 7/9\,\omega_{z,-}$. The periods of oscillation in coordinate space and in the momentum space are equal. The half-width of oscillation in the coordinate space is nothing else than the scaling function $b(t)$, as in the case of free fermions. The expansion starts at the moment of time $\tau\omega_{z,-} = 2\pi \times 1.541$. After the expansion starts, the half-width

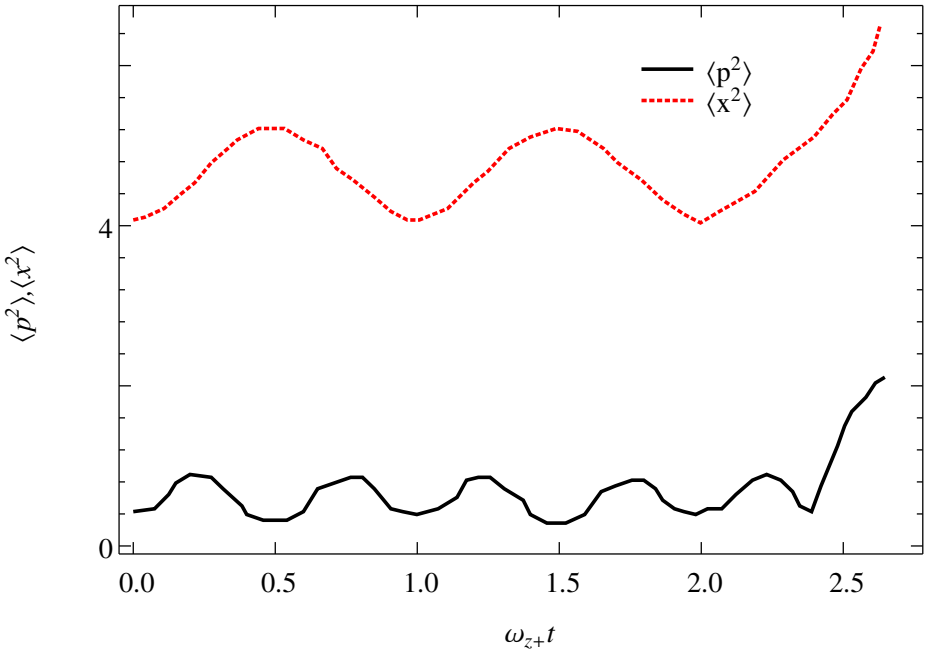


Figure 26: The time-evolution of the half-width for the Tonks-Girargeau gas. Black curve: momentum space, red dashed curve: coordinate space. The strength of quench is $\omega_{z,+}/\omega_{z,-} = 7/9$.

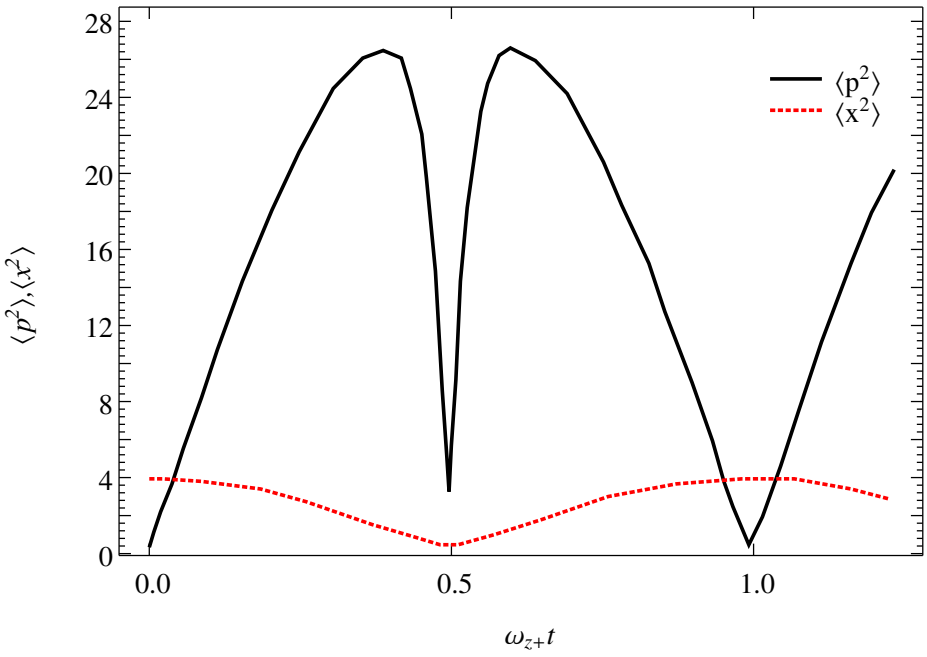


Figure 27: The time-evolution of the half-width of the Tonks-Girargeau gas. Black curve: momentum space, red dashed curve: coordinate space. The strength of quench is $\omega_{z,+}/\omega_{z,-} = 115.4/15.6$

in the coordinate space grows linearly. The half-width in the momentum space goes to a constant.

The time evolution of the half-width of the Tonks-Girardeau gas in the coordinate and momentum space after the excitation is also shown in Fig. 27. The number of particles is $N = 11$. The excitation frequency is $\omega_{z,+} = 115.4/15.6\,\omega_{z,-}$. The periods of oscillation in the coordinate space and in the momentum spaces are equal to each other.

# 4. Thomas-Fermi to Gaussian regime crossover

In a trapped non-interacting gas the energies of all states are proportional to the trapping frequency $\omega_z$. The second energy level is twice degenerate and has the energy $2\hbar\omega_z$. One of these states is connected with the center of mass motion. The second one determines the frequency of breathing oscillations. It is clear that the breathing oscillation frequency for the non-interacting gas is $2\omega_z$. In the Thomas-Fermi regime the breathing mode frequency is $\sqrt{3}\omega_z$. This means that there should be a crossover in the breathing mode frequency from the value $\sqrt{3}\omega_z$ to $2\omega_z$ in the region of weak interaction. Such a crossover appears also for the Coulomb interactions in one-dimensional systems [31]. We describe this crossover within the Hartree approximation which reduces the many-body problem to an effective one-body problem, where interactions are taken into account by the effective mean-field potential. We use the Hartree approximation for the ground state wave-function in the calculation of the breathing mode frequency. In the regime of very weak coupling the ground state density profile is gaussian-like. Thus, we call this regime Gaussian. We compare the results obtained from equation (1.48) with those from Eq. (3.70).

## 4.1. Hartree approximation

The Hartree approximation is one of the most powerful and, at the same time, simple methods. It was applied before for the calculation of the expansion dynamics [47], breathing mode of the fermion Colagero model [48], for the Coulomb gas [31], and it is shown to be in good agreement with the exact solution. Let us find the ground state wave-function in the Hartree approximation:

$$\psi_{gs}(x_1, x_2, \ldots, x_N) = \psi_0(x_1)\psi_0(x_2)\cdots\psi_0(x_N), \tag{4.1}$$

where $\psi_0$ is the one-particle wave function normalized to unity. The ground state wave-function can be obtained from the Ritz variational method. It consists of minimisation of the energy functional with respect to the one-particle wave-function

$$F[\psi_0] = \langle\psi_{gs}|\hat{H}|\psi_{gs}\rangle - \nu\langle\psi_{gs}|\psi_{gs}\rangle, \tag{4.2}$$

where $\nu$ is a Lagrange multiplier.

$$\frac{\delta F}{\delta \psi_0^*(x_k)} = 0 \tag{4.3}$$

Thus we obtain the following equation for the ground state wave-function

$$\left[-\frac{1}{2}\frac{\partial^2}{\partial x^2} + \frac{x^2}{2} + \alpha(N-1)\left|\psi_0(x)\right|^2\right]\psi_0(x) = \epsilon\psi_0(x). \tag{4.4}$$

It is important to mention that the solution to Eq. (4.4) depends on a single parameter $\alpha(N-1)$.

We introduce the potential, kinetic and interaction energies as follows:

$$E_{pot} = N\frac{m\omega_z^2}{2}\int_{-\infty}^{\infty} z^2\psi_0(z)^2 dz \tag{4.5a}$$

$$E_{kin} = N\frac{\hbar^2}{2m}\int_{-\infty}^{\infty}\left(\frac{\partial\psi_0(z)}{\partial z}\right)^2 dz \tag{4.5b}$$

$$E_{int} = \frac{N(N-1)}{2}g\int_{-\infty}^{\infty}\psi_0(z)^4 dz \tag{4.5c}$$

Equation (4.4) does not have analytical solutions and it is possible to find the ground state numerically. We thus solve the Gross-Pitaevskii equation numerically, starting from a trial wave-function. The algorithm simulates the relaxation of the system to the ground state in the imaginary time. The ground-state density profiles for 25 particles with various values of the interaction parameter $\lambda$ are shown in Fig. 28. In the Thomas-Fermi regime we see a good agreement between the results given by different approaches. However, in the Gaussian regime the LDA approximation does not give correct results.

It is possible to calculate the breathing oscillation frequency in the Hartree approximation using the wave-function from the numerical solution of equation (4.4) and the sum rules. The frequency of the breathing mode for two particles and the one calculated in the Hartree approximation are shown in Fig. 29. The former curve is universal: it depends on the parameter $\lambda$ only and does not depend on the number of particles. With larger $N$ the applicability range of the Hartree approximation grows. The more particles the larger is the interaction strength at which the breathing mode follows the Hartree solution. This was confirmed by the Diffusion Monte Carlo (DMC) simulations for the finite $N$ (shown as coloured points). The DMC simulations were performed in collaboration with Gregory Astrakharchik [49]. We can see that in the weak coupling limit the parameter $\lambda = -a_{1D}/Na_z$ is a unique parameter

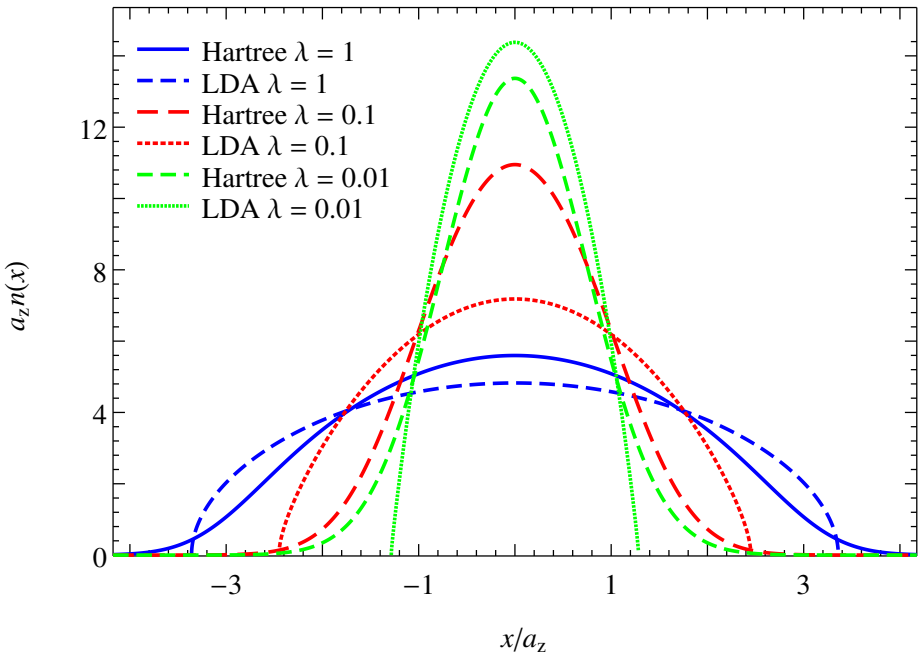


Figure 28: Ground state densities for various values of the parameter $\lambda = -a_{1D}/Na_z$ in the Hartree approximation with sum rules, compared with the results of the LDA.

which determines the system properties. Diffusive Monte Carlo simulations represent an appropriate tool for problems like this. Typically, calculation time grows as a third power of the discretization step. The derivatives can be calculated with the quadratic accuracy using symmetric schemes, whereas the accuracy over the discretization parameter is linear.

## 4.2. Perturbative analysis for the Gaussian regime

We can consider a set of $N$ uncoupled harmonic oscillators as the unperturbed problem and treat the weak interparticle interaction as perturbation. Thus the unperturbed eigenstates are

$$\psi_{i_1,i_2,\ldots,i_N}(x_1, x_2, \ldots, x_N) = \frac{1}{\sqrt{N!}} \sum_{\{P\}} \phi_{i_1}(x_1)\phi_{i_2}(x_2)\cdots\phi_{i_N}(x_N), \tag{4.6}$$

with the corresponding energies

$$E_{i_1,i_2,\ldots,i_N} = \hbar\omega_z \sum_{k=1}^{N} \left(\frac{1}{2} + i_k\right). \tag{4.7}$$

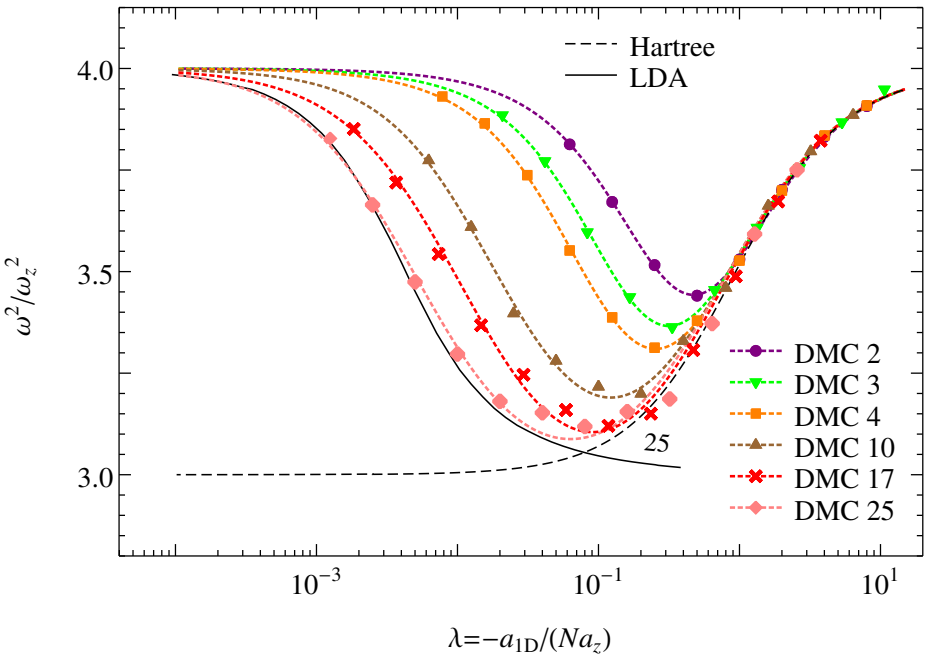


Figure 29: The dependence of the breathing mode frequency versus interaction parameter $\lambda = -a_{1D}/Na_z$ and the Hartree approximation with the sum rule (1.53) (black, dashed). Colored points are results of DMC. Connecting lines are Pade approximations.

.

So, one can use the perturbation theory for calculating the ground state energy

$$\frac{E_{gs}}{\hbar\omega_z} = \frac{1}{2}N + \langle\psi_{0,0,\ldots,0}\,|V|\,\psi_{0,0,\ldots,0}\rangle\,. \tag{4.8}$$

We notice that all coordinates enter expression (4.8) in the same way, so that the first order perturbation correction to the energy is

$$\begin{aligned}\langle\psi_{0,0,\ldots,0}\,|V|\,\psi_{0,0,\ldots,0}\rangle &= \frac{N(N-1)}{2}\alpha\,\langle\psi_{0,0,\ldots,0}\,|\delta(x_1-x_2)|\,\psi_{0,0,\ldots,0}\rangle \\ &= \frac{N(N-1)}{2}\alpha\int_{-\infty}^{\infty}\psi_0^4(x)dx = \frac{N(N-1)}{2\sqrt{2\pi}}\alpha.\end{aligned} \tag{4.9}$$

The first order correction to the ground state wave-function is

$$\psi_{gs} = \psi_{0,0,\ldots,0} + \alpha\sum_{n_1,n_2,n_1+n_2=odd}^{\infty,\infty}\frac{(-1)^{\frac{n_1+n_2}{2}}2^{\frac{n_1+n_2-1}{2}}\Gamma\left(\frac{n_1+n_2+1}{2}\right)}{\sqrt{2^{n_1+n_2}n_1!n_2!\pi(n_1+n_2)}}\psi_{n_1,n_2,0,..,0}. \tag{4.10}$$

The second order perturbation correction to the ground state energy is

$$\sum_{n_1,n_2,\ldots,n_N} \frac{\left|\left\langle \psi_{0,0,\ldots,0} \left| \hat{V} \right| \psi_{n_1,n_2,\ldots,n_N} \right\rangle\right|^2}{E_0 - E_{n_1+n_2+\ldots+n_N}} = \frac{N(N-1)}{2}\alpha^2 \sum_{n_1,n_2,\ldots,n_N} \frac{\left|\langle \psi_{0,0,\ldots,0} \left| \delta(x_1-x_2) \right| \psi_{n_1,n_2,\ldots,n_N} \rangle\right|^2}{E_0 - E_{n_1+n_2+\ldots+n_N}}$$

$$= \frac{N(N-1)}{2}\alpha^2 \sum_{n_1,n_2,\ldots,n_N} \frac{\left|\iint \psi_0(x_1)\psi_0(x_2)\delta(x_1-x_2)\psi_{n_1}(x_1)\psi_{n_2}(x_2)dx_1dx_2\right|^2}{E_0 - E_{n_1+n_2+\ldots+n_N}} \delta_{n_3,0}\cdots\delta_{n_N,0}$$

$$= 2\alpha^2 \sum_{n_1,n_2} \frac{\left|\int \psi_0(x)^2\psi_{n_1}(x)\psi_{n_2}(x)dx\right|^2}{E_0 - E_{n_1+n_2}}$$

$$= -2\alpha^2 \sum_{n_1,n_2,n_1+n_2=odd}^{\infty,\infty} \left| \frac{\Gamma\left(\frac{n_1+n_2+1}{2}\right)}{\sqrt{2n_1!n_2!\pi}} \right|^2 \frac{1}{n_1+n_2} = -\alpha^2 \frac{\ln(4)}{2\pi}. \quad (4.11)$$

Let us calculate the energy of the breathing mode. The non-perturbed system has two states with energy $2\omega_z$. Their quantum numbers are $2,0,0,0,\ldots,0$ and $1,1,0,0,\ldots,0$. Let us denote these states $2\alpha$ and $2\beta$. In principle, in order to find the energy of the breathing mode one has to solve a secular equation, but now it is possible to avoid this procedure. The states $2\alpha$ and $2\beta$ are connected to the breathing state and center-of-mass oscillation with an orthogonal transformation which does not change the trace of the secular matrix. Since the center-of-mass oscillation has frequency $2\omega_z$, the breathing mode has frequency $2\omega_z + V_{2\alpha,2\alpha} + V_{2\beta,2\beta} - 2V_{gs,gs}$, in analogy to the result of Eq. (3.119):

$$V_{2\alpha,2\alpha} = \frac{(N-1)(2N-1)}{4\sqrt{2\pi}}\alpha, \quad (4.12a)$$

$$V_{2\beta,2\beta} = \frac{2N^2-2N-1}{4\sqrt{2\pi}}\alpha. \quad (4.12b)$$

This leads to

$$\frac{E_{BM}}{\omega_z} = \frac{1}{2}N + 2 + \frac{4N^2-5N}{4\sqrt{2\pi}}\alpha. \quad (4.13)$$

Finally, we get the breathing mode frequency:

$$\frac{\omega}{\omega_z} = 2 - \frac{N}{4\sqrt{2\pi}}\alpha. \quad (4.14)$$

This result coincides with (2.22) when $N = 2$.

Now we calculate the first order correction to the breathing mode using sum rules [20, 32].

$$\left\langle \sum_{n=1}^{N} x_n^2 \right\rangle = N \left\langle x_1^2 \right\rangle = N \iiint_{-\infty}^{\infty} x_1^2 \psi_{gs}^2 dx_1 dx_2 \cdots dx_N$$

$$= N \iiint_{-\infty}^{\infty} x_1^2 \left( \psi_{0,0,\ldots,0}^2 + 2\alpha \psi_{0,0,\ldots,0} \sum_{n_1,n_2}^{n_1+n_2=odd} \frac{V_{\{0\},\{n_1,n_2\}}}{E_0 - E_{n_1,n_2}} \psi_{n1,n2,0,..,0} \right) dx_1 dx_2 \cdots dx_N$$

$$= N\frac{a_z^2}{2} + 2Na_z^2\alpha \sum_{n_1,n_2}^{n_1+n_2=odd} \frac{V_{\{0\},\{n_1,n_2\}}}{E_0 - E_{n_1,n_2}} \delta_{n_2,0} \frac{1}{\sqrt{N}} \int \psi_0(x_1) x_1^2 \psi_{n_1}(x_1) dx_1$$

$$= N\frac{a_z^2}{2} + 2Na_z^2\alpha \sum_{n_1=2}^{odd} \frac{V_{\{0\},\{n_1\}}}{E_0 - E_{n_1}} \frac{1}{\sqrt{N}} \frac{1}{\sqrt{2}} \delta_{n_1,2} = N\frac{a_z^2}{2} + Na_z^2\alpha \frac{N-1}{4\sqrt{2\pi}}, \quad (4.15)$$

$$\omega_z^2 \frac{\partial}{\partial \omega_z^2} \left\langle \sum_{n=1}^{N} x_n^2 \right\rangle = -\frac{1}{2} N \frac{a_z^2}{2} + \left( -\frac{3}{4} \right) Na_z^2\alpha \frac{N-1}{4\sqrt{2\pi}}. \quad (4.16)$$

Thus, we arrive at the result

$$\left( \frac{\omega}{\omega_z} \right)^2 = 4 \left( 1 - \alpha \frac{N-1}{4\sqrt{2\pi}} \right). \quad (4.17)$$

When $N = 2$ this result coincides with the two-particle result given by (2.28).

It is also important to analyze what we get if instead of the operator $\sum_{n=1}^{N} x_i^2$ take the operator $\sum_{n=1}^{N} x_i^2 - N x_{CM}^2$. This will improve our result as this operator does not excite the center-of-mass motion. It is always possible to separate the center-of-mass motion from the collective modes [50, 51].

$$\left\langle \sum_{n=1}^{N} x_n^2 - N x_{CM}^2 \right\rangle = (N-1)\frac{a_z^2}{2} + Na_z^2\alpha \frac{N-1}{4\sqrt{2\pi}}, \quad (4.18)$$

$$\omega_z^2 \frac{\partial}{\partial \omega_z^2} \left\langle \sum_{n=1}^{N} x_n^2 - N x_{CM}^2 \right\rangle = -\frac{1}{2}(N-1)\frac{a_z^2}{2} + \left( -\frac{3}{4} \right) Na_z^2\alpha \frac{N-1}{4\sqrt{2\pi}}. \quad (4.19)$$

Thus, we obtain

$$\left( \frac{\omega}{\omega_z} \right)^2 = 4 \left( 1 - \frac{N}{N-1} \alpha \frac{N-1}{4\sqrt{2\pi}} \right) = 4 \left( 1 - \alpha \frac{N}{4\sqrt{2\pi}} \right). \quad (4.20)$$

When $N = 2$ this result coincides with the two-particle result given by (2.30).

### 4.2.1. Secular equation and exact diagonalization

It is always possible to expand the wave-function over a complete basis. Let us choose the free boson wave-functions as a basis

$$\psi(x_1, x_2, \ldots, x_N) = \sum_{n_1 \le n_2 \le \ldots \le n_N} c_{n_1,n_2,\ldots,n_N} \sum_{\{P\}} \psi_{n_1}(x_{P_1}) \psi_{n_2}(x_{P_2}) \cdots \psi_{n_N}(x_{P_N}), \tag{4.21}$$

where $c_{n_1,n_2,\ldots,n_N}$ are coefficients of the expansion. The normalization condition is

$$\sum_{n_1 \le n_2 \le \ldots \le n_N} c^2_{n_1,n_2,\ldots,n_N} = 1. \tag{4.22}$$

Thus, the Schrödinger equation takes the form:

$$\left[\hat{H}^{HO} + \alpha \hat{V}\right] \psi(x_1, x_2, \ldots, x_N) = E\psi(x_1, x_2, \ldots, x_N). \tag{4.23}$$

Multiplying this equation by $\sum_{\{P\}} \psi_{m_1}(x_{P_1}) \psi_{m_2}(x_{P_2}) \cdots \psi_{m_N}(x_{P_N})$ we get the following formula:

$$\left(E_{n_1,n_2,\ldots,n_N} - E\right) c_{n_1,n_2,\ldots,n_N} \delta_{n_1,m_1} \delta_{n_2,m_2} \cdots \delta_{n_N,m_N} + \alpha V_{n_1,n_2,\ldots,n_N;m_1,m_2,\ldots,m_N} c_{n_1,n_2,\ldots,n_N} = 0. \tag{4.24}$$

This is a problem of finding eigenfunctions and eigenvalues in the $l_2$ space. Eigenvalues of the secular matrix are the energies of the states, and the eigenfunctions are the wave-functions. This problem has no analytical solution and the only thing which can be done is to truncate the state space. After truncating we get a finite-dimension problem which is easily solvable.

Two and three–particle results for the solution of the secular equation are shown in Fig. 30. The states with energies less than $20\hbar\omega_z$ were chosen as a basis for the expansion. For two particles the basis contains 441 functions and for three particles there are 1831 functions in the basis. The purple and red dashed curves show the first-order expansion (4.20) for two and three particles and the orange dashed curve is the 8-th order expansion of the breathing mode frequency for two particles. It is clear that this approach works better than the perturbation theory, but still it has the convergence radius which is smaller than the position of the breathing mode frequency minimum. This means that there is a region of the parameters where the wave-function cannot be properly expanded over the truncated space and an infinite number of functions is needed for the correct expansion.

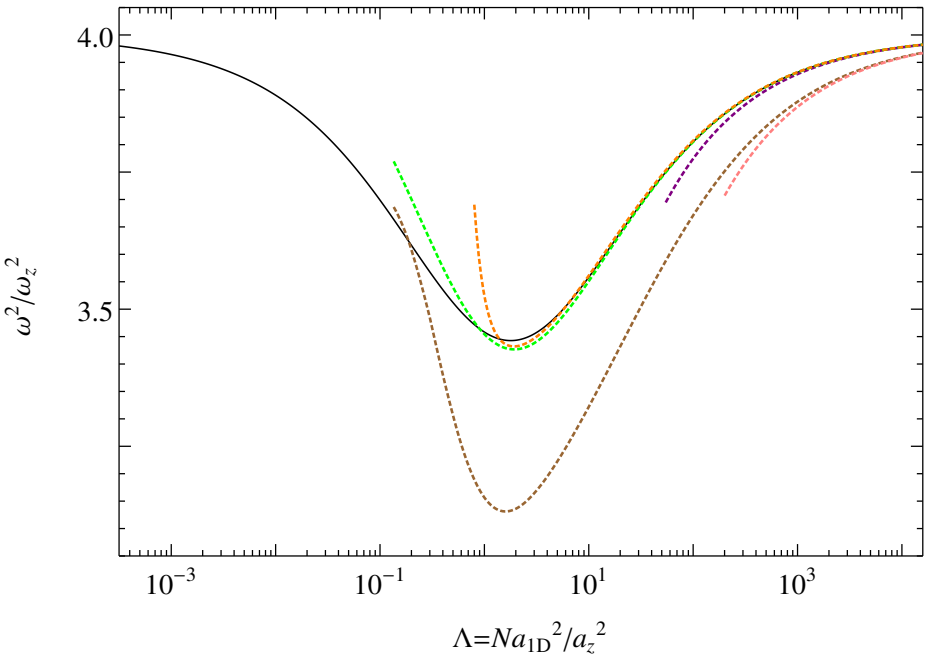


Figure 30: The ratio $\omega^2/\omega_z^2$, as a function of the LDA parameter $\Lambda = Na_{1D}^2/a_z^2$. The solid black curve is the exact solution. The brown and green dashed curves are secular results. The purple and red dashed curves are the first-order perturbation expansions. The orange dashed curve is eights-order perturbation expansions.

## 4.3. Comparison of two sum rules

The dependence of the breathing mode frequency calculated with Eq. (1.41) on the interaction strength of two particles is shown in Fig. 31. The exact solution for the two particle system (see Sec. 2) is shown with violet dashed curve. The breathing mode frequency calculated in the scaling approximation (1.41) is plotted with green dashed curve. The same results obtained with exclusion of the center-of-mass motion terms are shown in orange dashed curves. The scaling approach with the exclusion of the center-of-mass motion gives a correct asymptotic behaviour in the weak coupling regime. The black and dashed red curves represent the sum rules and the scaling formula used within the Hartree approximation (see Sec. 4.1). These two results are indistinguishable under the small computation accuracy in the thermodynamic limit, and as it is shown in Fig. 32 have big deviations for the finite-size systems. In the Gaussian both sum rules lead us to the same result, while in the Tonks-Girargeau regime Eq. (1.41) describes the crossover incorrectly.

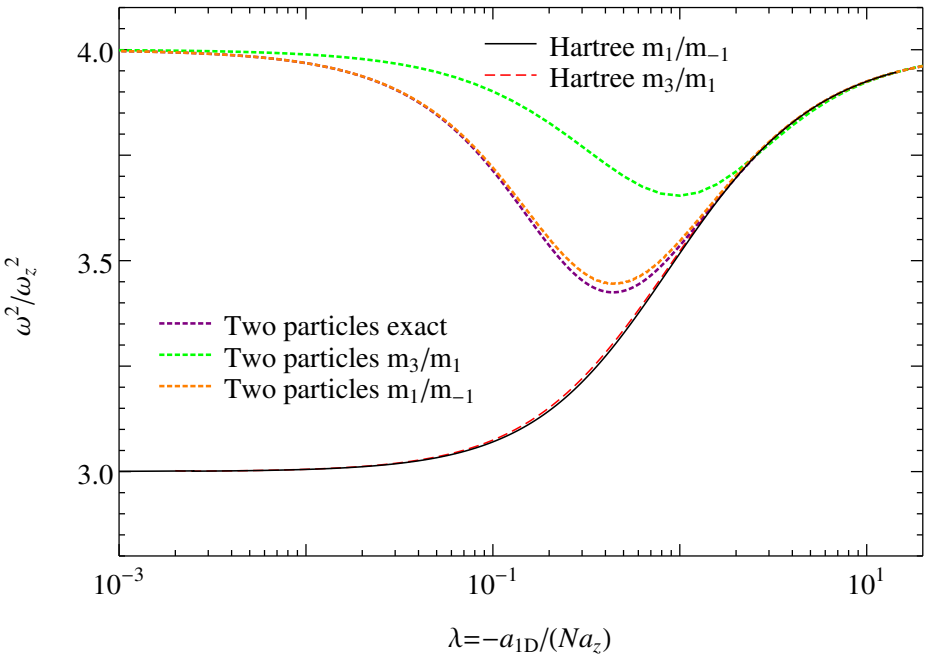


Figure 31: Comparison of the ratio $\omega^2/\omega_z^2$ calculated from Eq. (1.41) with the one from Eq. (1.53) for two particles and for the Hartree solution. The exact $\omega^2/\omega_z^2$ value for the two-particle system is plotted with the black solid curve.

Let us prove that the breathing mode frequency calculated in the Hartree approximation with expressions (1.48) and (3.70) are not equal to each other. First we rewrite Eq. (3.70) in terms of the potential energy:

$$\frac{\omega^2}{\omega_z^2} = 4\left(1 - \frac{\lambda E'_{pot}}{\lambda E'_{pot} - 2E_{pot}}\right) \tag{4.25}$$

Now let us consider the difference of expression (1.48) from (3.70):

$$\frac{\omega^2_{(1,-1)} - \omega^2_{(3,1)}}{\omega_z^2} = -\frac{2E_{pot}E_{int} + 2\lambda E_{pot}E'_{int} + \lambda E_{int}E'_{pot}}{2E_{pot}(\lambda E'_{pot} - 2E_{pot})} \tag{4.26}$$

If both sum rules give the same result, then equation (4.26) gives 0. If it is so, then

$$\frac{(\lambda E_{int})'}{\lambda E_{int}} = -\frac{1}{2}\frac{E'_{pot}}{E_{pot}} \tag{4.27}$$

This equation has to be correct for any $\lambda$. So, one can consider Eq. (4.27) as a differential equation. The solution to this equation is

$$(\lambda E_{int})^{-2} = CE_{pot}, \tag{4.28}$$

where $C$ is a constant which should not depend on $\lambda$.

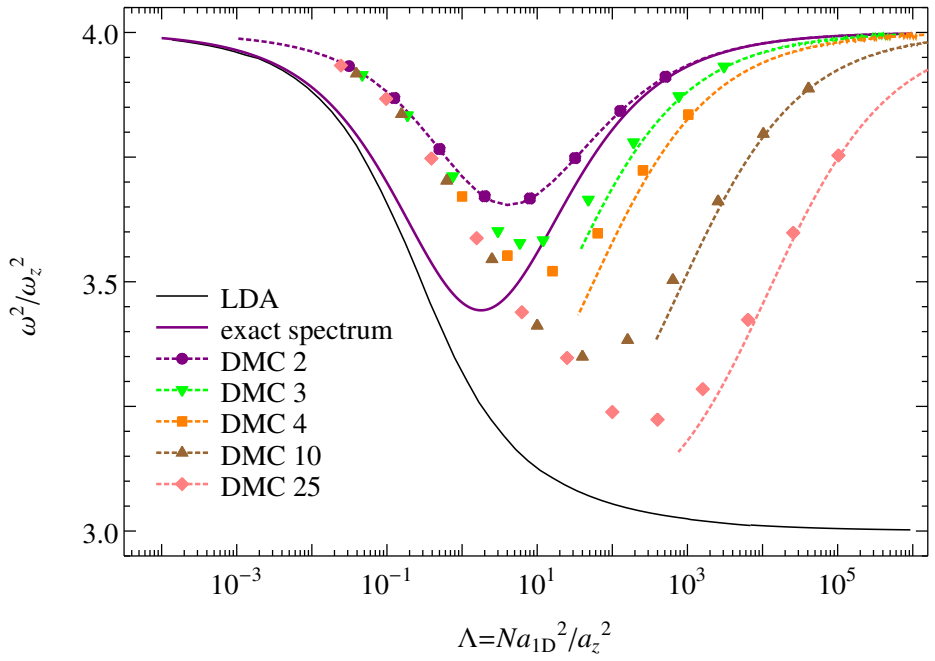


Figure 32: The ratio $\omega^2/\omega_z^2$ as a function of the LDA parameter $\Lambda = Na_{1\mathrm{D}}^2/a_z^2$. Colored symbols are data points obtained with Eq. (1.41) and diffusion Monte Carlo (DMC) simulations for $N = 2, 3, 4, 10, 25$ (top to bottom). The dashed violet curve is the breathing mode for two particles calculated with the operator $Q_c$ (1.23). Dashed colored curves: Hartree approximation for a given particle number. The exact solution for two particles (see Sec. 2) is shown with the violet dashed curve.

Let us calculate this constant in two asymptotic regimes where analytical solutions exists. Namely, in the Gaussian and Thomas-Fermi regimes. In the Gaussian regime we have

$$E_{pot} = \frac{1}{4}, \tag{4.29}$$

and

$$(\lambda E_{int})^2 = 2\pi. \tag{4.30}$$

Thus, in the Gaussian regime $C = 8\pi \approx 25.13$. In the Thomas-Fermi regime

$$E_{pot} = \frac{3^{\frac{2}{3}}}{10}\lambda^{-\frac{2}{3}}, \tag{4.31}$$

and

$$(\lambda E_{int})^2 = \frac{3^{\frac{2}{3}}}{5}\lambda^{-\frac{2}{3}}. \tag{4.32}$$

Therefore $C = \frac{250}{9} \approx 27.78$. We therefore see that $C$ depends on the interaction strength $\lambda$, which contradicts Eq. (4.28), and therefore the assumption that the difference of expression

(1.48) from (3.70) is equal to zero is incorrect. Thus, we prove that expressions (1.48) and (3.70) are not equal to each other. The difference between the breathing mode frequency calculated using expressions (1.48) and (3.70) with high precision is plotted in Fig. 33.

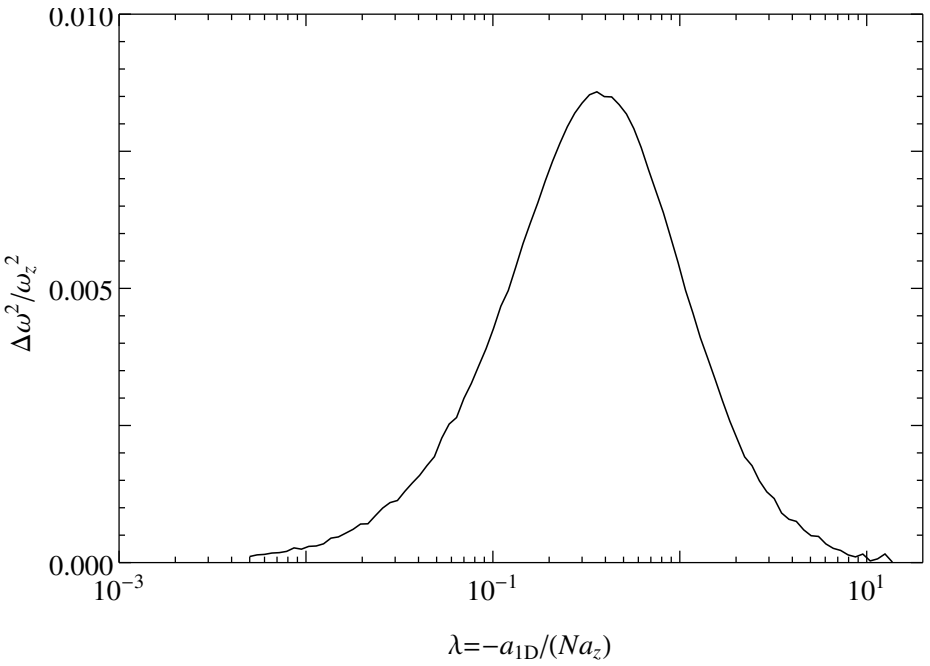


Figure 33: The difference between the breathing mode frequencies calculated with the $(1,-1)$ and $(3,1)$ sum rules for arbitrary values of the parameter $\lambda = -a_{1D}/(Na_z)$ in the Hartree approximation.

## 4.4. Regimes of a trapped one-dimensional gas

Summarising sections 3 and 4 we build a schematic plot which explains regimes of a one-dimensional gas and crossovers between them.

The TF BEC to TG crossover is associated to an interplay of the parameters $\lambda$ and $N^{-3/2}$, (see Fig. 34). It may not be captured within the Hartree approximation, which does not contain $N^{-3/2}$ as a parameter independent of $\lambda$. Instead, we may use the LDA [16]. It is only valid in the large $N$ limit and is based on the assumption that the local chemical potential at the point $z$ is equal to the chemical potential of a homogeneous system that has the same density $n(z)$. Therefore $\mu_{\rm loc}(n(z)) = V(Z) - V(z)$ for $|z| \leq Z$ and it vanishes for $|z| > Z$ in the model (1.17). Here $Z$ is the Thomas-Fermi radius of the gas cloud, whose

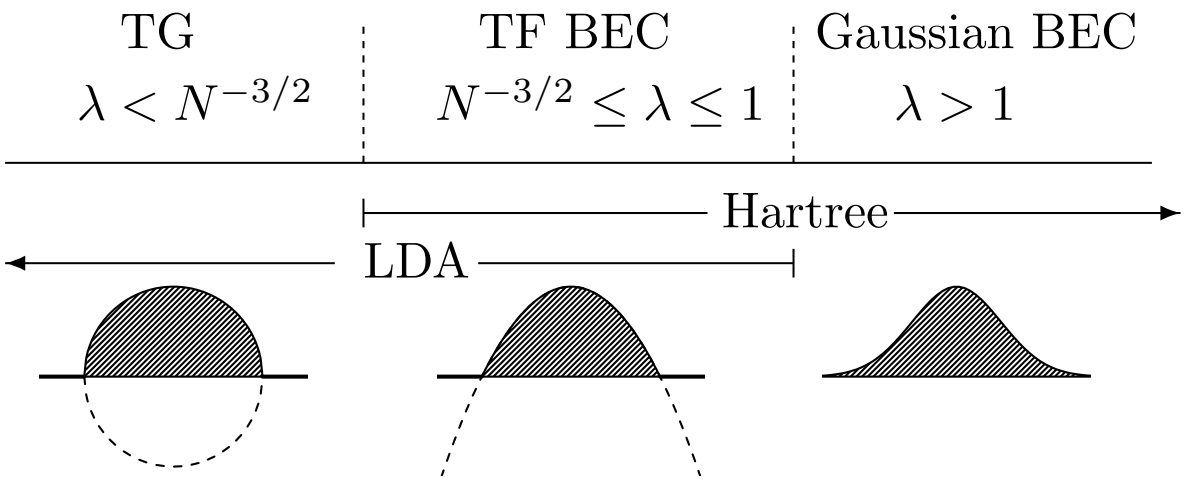


Figure 34: The Tonks-Girardeau (TG), the Thomas-Fermi Bose-Einstein condensate (TF BEC), and the Gaussian BEC regimes of the repulsive Lieb-Liniger gas in a parabolic trap, Eq. (1.17), are shown as a function of the Hartree parameter $\lambda = -a_{1D}/(Na_z)$ for a given $N$. Density profiles are semicircle, inverted parabola, and the Gaussian deep in these regimes, respectively. The local density approximation (LDA) parameter $\Lambda$ is related to $\lambda$ as $\Lambda = N^3\lambda^2$. The TG and the TF BEC regimes are separated with $\Lambda = 1$.

value is set by the normalization condition $\int_{-Z}^{Z} dz\, n(\mu_{\rm loc}(z)) = N$. The dependence of $\mu_{\rm loc}$ on $n$ in the homogeneous Lieb-Liniger model (Eq. (1.17) with $V = 0$) was found in Ref. [28]. Using Eq. (1.53) with $\langle Q_c \rangle = \langle Q_0 \rangle = \int dz\, z^2 n(z)$ we get $\omega/\omega_z$ readily. The result depends on $a_{1D}, a_z$, and $N$ through a single parameter $\Lambda = Na_{1D}^2/a_z^2 = N^3\lambda^2$ within LDA [16, 52, 53].

The Thomas-Fermi BEC to the Gaussian regime crossover is associated only with the interaction parameter $\lambda$. It is described in the Hartree approximation by the Gross-Pitaevskii equation. Deeply in the TF BEC regime, where the chemical potential $\mu$ is large compared to the energy spacing $\hbar\omega_z$, the kinetic energy term can be omitted and we have a parabolic density distribution

$$n_H(z) = N\frac{(9\lambda)^{\frac{1}{3}}}{4a_z}\left(1 - \frac{z^2}{Z^2}\right)\theta\left(1 - \frac{z^2}{Z^2}\right), \quad \lambda \to 0. \tag{4.33}$$

Here $\theta$ is the Heaviside step function, and the Thomas-Fermi radius is $Z/a_z = (3/\lambda)^{1/3}$. Thus, the Hartree approximation and the LDA are compatible with each other in the Thomas-Fermi region, where the breathing mode frequency is $\sqrt{3}\omega_z$.

# 5. Comparison of theory with experiments

*"It doesn't matter how beautiful your theory is, it doesn't matter how smart you are. If it doesn't agree with experiment, it's wrong."*

*Richard P. Feynman*

The first experiment on measuring the breathing mode was reported in Ref. [13]. In this experiment the breathing mode frequency was measured in two regimes and it was clearly shown that it is different in these regimes. In this chapter we compare our theoretical results with more recent experimental data from Refs. [14, 15]. We find an excellent quantitative agreement with the data from the experiment [14]. However, there exists a mismatch between the zero-temperature theory and the experimental data of Ref. [15]. Therefore, we provide a finite temperature analysis and estimate the relevant temperature scales.

## 5.1. Comparison with $^{133}Cs$ experiment

This section is dedicated to the analysis of the data from the experiment described in Refs. [14, 22]. It is extremely hard to make measurements in highly-exited many-body states because of their short lifetime. Therefore, for such measurements one can use cold atoms in the 1D geomtry for getting a metastable state called the super-Tonks-Girardeau state (sTG) decoupled the from thermal bath. This state is obtained by using Feshbach and confinement-induced resonances to tune the interparticle interaction to infinitely attractive [14]. It is long-lived [54] because in order to form a bound state the atoms have to approach each other at an atomic distance. However, the probability of this is extremely small because of an effective fermionisation [55, 56].

In the experiment [14, 22] bosonic $^{133}Cs$ atoms were placed in an optical lattice with retro-reflected laser beams confining the atoms to an array of $1D$-tubes (see Fig. 35) and creating a one-dimensional gas in each tube by using the condition $\omega_\perp \gg \omega_z$. The tubes contained $10^4$ atoms [14]. In the central tube the number of atoms reached $8 - 25$. In this experiment typical scattering lengths for the Tonks-Girardeau and the super-Tonks-Girardeau regime are $a_{3D} \sim 875a_0$ (TG) and $a_{3D} \sim 2300a_0$ (sTG), where $a_0 \approx 0.529$ Å is

the Bohr radius. The trap frequencies are $\omega_\perp \approx 2\pi \times 13.1$ kHz, $\omega_z \approx 2\pi \times 15.4$ Hz in the repulsive regime and $\omega_z \approx 2\pi \times (22.4 \div 52.3 \div 115.6)$ Hz in the attractive regime.

First, we calculate values of physical quantities using data for cesium taken from Ref. [57]. Using the atomic mass of cesium $m_{Cs} = 2.20 \times 10^{-25}$ kg we calculate the perpendicular oscillatory length $a_\perp = 1440.33 a_0 = 7.61 \times 10^{-8}$ m and the oscillatory length along the $z$-axis $a_z = 2.24 \times 10^{-6}$m in the repulsive regime and $a_z = (18.42 \div 12.05 \div 8.11) \times 10^{-7}$m in the attractive regime.

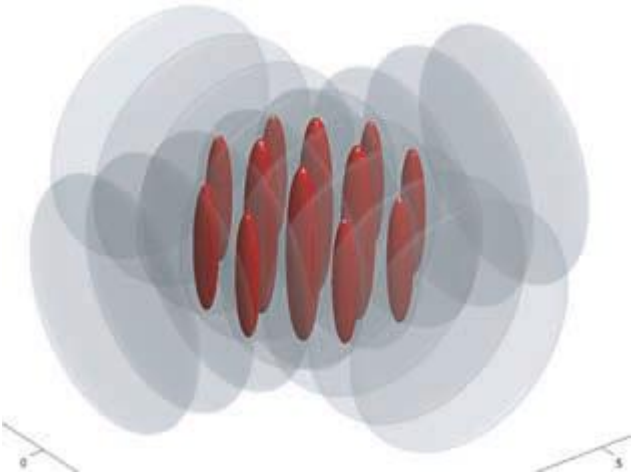

Figure 35: Laser beams holding $^{133}Cs$ in a trap. Red curves are equipotential surfaces.

If we assume that in the experiment the number of $^{133}Cs$ atoms in the central tube is fixed, then we can reproduce the values of all physical quantities such as the scattering length, the correlation length $\xi = (\hbar^2/2mgn)^{\frac{1}{2}} = \gamma^{\frac{1}{2}} a_{1\mathrm{D}}/2\sqrt{2}$ and the Thomas-Fermi radius $Z_{TF}$. These data for the repulsive interaction and the fixed number of particles $N = 25$ are presented in Tables I and II. The particles are distributed over the tubes according to the Thomas-Fermi law. The average over the whole system is $\langle N \rangle = 17$, but due to the measurement scheme the main signal comes from the central tubes, where $N = 25$.

We can reproduce the values of all the physical quantities such as the scattering length, the correlation length $\xi$ and the Thomas-Fermi radius $Z_{TF}$ for the attractive regime as well. We assume that in the central tube the number of $^{133}Cs$ atoms is fixed and is equal to $N = 11$. This set of data is presented in Table III. The numeration of points is similar to the one in the original paper [14] (see Fig. 3(A)). The point $1a$ was measured at the trap frequency $\omega_z \sim 2\pi \times 22.4$ Hz, $1b$ at $\omega_z \sim 2\pi \times 52.3$ Hz and points $1c - 6$ were measured at $\omega_z \sim 2\pi \times 115.6$ Hz.

The results for the attractive regime are presented in Fig. 36. The breathing mode calculated in the hydrodynamic approach is shown by the solid curve, the exact two particle solution is shown by the dashed curve, and the red squares are the experimental data. If we assume that the interaction parameter has a different effective value, we can then explain a

Table I: Table of data for the repulsive regime from experiment [14].

Data for the repulsive interaction first 7 points

| # | 1 | 2 | 3 | 4 | 5 | 6 | 7 |
|---|---|---|---|---|---|---|---|
| $N\left(\frac{a_{1D}}{a_z}\right)^2$ | $1.15 \times 10^{-4}$ | $1.49 \times 10^{-3}$ | $4.92 \times 10^{-3}$ | $9.22 \times 10^{-3}$ | $2.22 \times 10^{-2}$ | $1.12 \times 10^{-1}$ | $2.53 \times 10^{-1}$ |
| $\left(\frac{\omega}{\omega_z}\right)^2$ | 3.998 | 3.992 | 3.968 | 4.021 | 3.781 | 3.536 | 3.389 |
| $a_{1D}$, $\mu m$ | $5.79 \times 10^{-3}$ | $2.08 \times 10^{-2}$ | $3.78 \times 10^{-2}$ | $5.18 \times 10^{-2}$ | $8.04 \times 10^{-2}$ | 0.18 | 0.27 |
| $\gamma(0)$ | 456. | 129. | 71.1 | 52.0 | 33.3 | 14.7 | 9.80 |
| $n(0)$,$\mu m^{-1}$ | 0.757 | .741 | .744 | .743 | .746 | .754 | .752 |
| $n(0)^{-1}, \mu m$ | 1.32 | 1.35 | 1.34 | 1.34 | 1.34 | 1.33 | 1.33 |
| $T_d\sqrt{\gamma}$, $nK$ | 44.7 | 22.8 | 17.0 | 14.6 | 11.7 | 7.97 | 6.47 |
| $t$ | $7.35 \times 10^{-4}$ | $9.49 \times 10^{-3}$ | $3.13 \times 10^{-2}$ | $5.87 \times 10^{-2}$ | $1.42 \times 10^{-1}$ | $7.12 \times 10^{-1}$ | 1.61 |
| $\xi, \mu m$ | 0.0437 | 0.0838 | 0.113 | 0.132 | 0.164 | 0.244 | 0.300254 |
| $Z_{TF}, \mu m$ | 12.9 | 12.8 | 12.7 | 12.6 | 12.5 | 11.9 | 11.4 |

Table II: Table of data for the repulsive regime from experiment [14].

Data for the repulsive interaction second 7 points

| # | 8 | 9 | 10 | 11 | 12 | 13 | 14 |
|---|---|---|---|---|---|---|---|
| $N\left(\frac{a_{1D}}{a_z}\right)^2$ | 3.01 | 3.99 | 13.8 | 70.7 | 554. | 8937 | 11310 |
| $\left(\frac{\omega}{\omega_z}\right)^2$ | 3.246 | 3.192 | 3.060 | 3.265 | 3.429 | 3.669 | 3.732 |
| $a_{1D}$, $\mu m$ | 0.94 | 1.08 | 2.00 | 4.53 | 12.7 | 51.0 | 57.3 |
| $\gamma(0)$ | 2.116 | 1.800 | 0.796 | 0.129 | $3.30 \times 10^{-2}$ | $5.17 \times 10^{-3}$ | $4.42 \times 10^{-3}$ |
| $n(0)$,$\mu m^{-1}$ | 1.01 | 1.03 | 1.26 | 3.41 | 4.81 | 7.59 | 7.89 |
| $n(0)^{-1}, \mu m$ | 0.990 | 0.968 | 0.796 | 0.293 | 0.208 | 0.132 | 0.127 |
| $T_d\sqrt{\gamma}$, $nK$ | 5.41 | 5.22 | 5.14 | 15.28 | 15.28 | 15.13 | 15.12 |
| $t$ | 19 | 25 | 87 | 449 | 3529 | 56906 | 72018 |
| $N_{co}$ | 29 | 32 | 48 | 69 | 95 | 130 | 133 |
| $\xi, \mu m$ | 0.481 | 0.510 | 0.631 | 0.576 | 0.812 | 1.30 | 1.35 |
| $Z_{TF}, \mu m$ | 9.27 | 8.99 | 7.70 | 6.12 | 4.47 | 2.87 | 2.76 |

mismatch between theory and experiment by introducing a constant shift. Thus, we present

Table III: Table of data for the attractive regime from experiment [14].

| PIвЂЂhвЂ“ | $N\left(\frac{a_{1D}}{a_z}\right)^2$ | $a_{1D}$ $[\mu m]$ | $\xi$ $[\mu m]$ | $Z_{TF}$ $[\mu m]$ | $\gamma(0)$ | $n_1(0)$ $\left[\mu m^{-1}\right]$ |
|---|---|---|---|---|---|---|
| 1 a | $8.0 \times 10^{-4}$ | $1.57 \times 10^{-2}$ | $1.39 \times 10^{-1}$ | 8.70 | 158 | 0.80 |
| 1 b | $2.0 \times 10^{-3}$ | $1.02 \times 10^{-2}$ | $1.15 \times 10^{-1}$ | 5.72 | 100 | 1.21 |
| 1 c | $3.4 \times 10^{-3}$ | $1.42 \times 10^{-2}$ | $8.88 \times 10^{-2}$ | 3.86 | 77.7 | 1.80 |
| 2 | $8.9 \times 10^{-3}$ | $2.30 \times 10^{-2}$ | $1.13 \times 10^{-1}$ | 3.89 | 48.6 | 1.78 |
| 3 | $2.1 \times 10^{-2}$ | $3.54 \times 10^{-2}$ | $1.42 \times 10^{-1}$ | 3.94 | 32.1 | 1.75 |
| 4 | $6.0 \times 10^{-2}$ | $5.99 \times 10^{-2}$ | $1.87 \times 10^{-1}$ | 4.04 | 19.6 | 1.69 |
| 5 | $2.4 \times 10^{-1}$ | $1.19 \times 10^{-1}$ | $2.74 \times 10^{-1}$ | 4.25 | 10.4 | 1.59 |
| 6 | $6.5 \times 10^{-1}$ | $1.97 \times 10^{-1}$ | $3.62 \times 10^{-1}$ | 4.48 | 6.74 | 1.50 |

the experimental data shifted by a constant. This constant is taken from the best fit and is equal to 11.1.

Compiled data for the repulsive regime are presented in Fig. 37. Two universal scaling curves are plotted. The one obtained in the hydrodynamic approximation is shown by the black solid curve, and one for the weak coupling regime in the Hartree approximation is shown by the black dashed curve. This curve depends on $\lambda$, and for plotting it as a function of the parameter $\Lambda$ we used $N = 25$. The colored circles are the results of the Diffusive Monte Carlo simulations for $N = 2$, 3, 4, 10 and 25. Experimental points form Refs. [14] are reproduced, and we see a good agreement between theory the experiment.

## 5.2. Excitation probabilities in the Tonks-Girargeau regime

In the experiment [14] the super-Tonks-Girardeau regime was realized in the following way. The system was placed in the laser trap with the trapping frequency $\omega_{z,-} = 15.4$ Hz. Then the magnetic field was changed during 100 ms in such a way that the effective interaction became attractive. At the same time, the frequency of the laser trap was changed to $\omega_{z,+} = 115$ Hz. Thus, one can ask a question whether during this ramp higher levels were excited. We analyse this using the results from Ref. [58]. Before the ramp the system was in

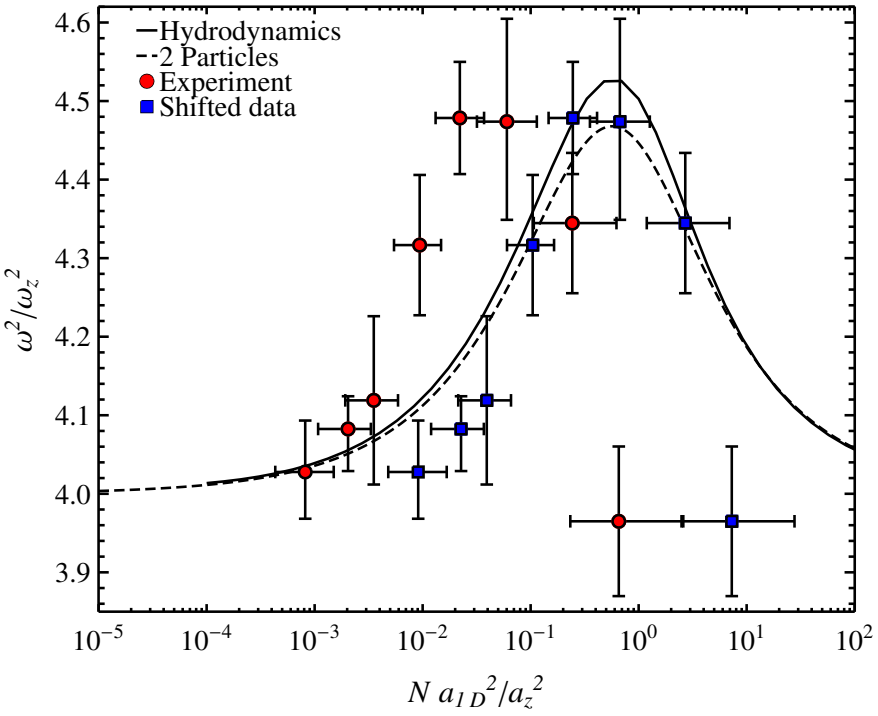


Figure 36: The breathing mode frequency in the attractive regime. The solid curve corresponds to the breathing mode from the hydrodynamic analytical solution, and the dashed one to the exact solution for two particles. The red points are experimental data and the blue points are rescaled data.

the ground state in a trap with frequency $\omega_{z,-}$. This means that $\psi(x) \to \phi_0(x)$ for $t \to -\infty$. At $t \to \pm\infty$ the stationary states are:

$$\phi_n(x; t \to \pm\infty) = \exp\left(-i\left(n + \frac{1}{2}\right)\omega_{z,\pm} t\right)\phi_n(x; \omega_{z,\pm}), \tag{5.1}$$

where $\phi_n(x; \omega_{z,\pm})$ is the $n$-th eigenfunction of the harmonic oscillator with frequency $\omega_{z,\pm}$:

$$\phi_n(x; \omega) = \frac{1}{\sqrt{2^n n!}}\left(\frac{\omega}{\pi}\right)^{\frac{1}{4}} \exp\left(-\frac{\omega x^2}{2}\right) H_n\left(\sqrt{\omega}x\right). \tag{5.2}$$

It is possible to calculate the excitation probabilities $W_{n,m} = |C_{n,m}|^2$, where $C_{n,m}$ are coefficients in the expansion of the wave-function $\phi_n(x; t \to +\infty)$ in the basis $\phi_m(x; t \to -\infty)$:

$$\phi_n(x; t \to +\infty) = \sum_{m=0}^{\infty} C_{n,m}\phi_m(x; t \to -\infty). \tag{5.3}$$

This leads to the excitation probabilities

$$W_{n,m} = \frac{\min(n,m)!}{\max(n,m)!}\left|P_{\frac{m+n}{2}}^{\frac{|n-m|}{2}}\left(\sqrt{1-\rho}\right)\right|\sqrt{1-\rho}, \tag{5.4}$$

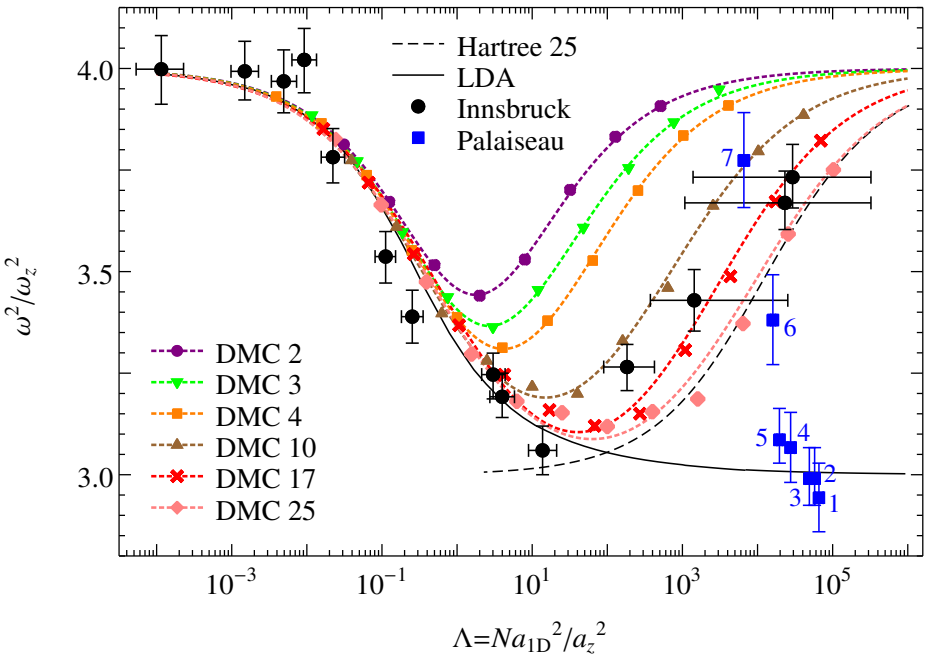


Figure 37: The ratio $\omega^2/\omega_z^2$, as a function of the LDA parameter $\Lambda = Na_{1D}^2/a_z^2$. The dashed (black) curve: the Hartree approximation for $N = 25$ in the equation $\Lambda = N^3\lambda^2$. The solid (black) curve: LDA. The TG regime corresponds to the $\Lambda < 1$, as defined in Fig. 34.

where the parameter $\rho$ is defined by the auxiliary scattering problem [58]

$$\ddot{\xi} + \omega(t)^2\xi = 0, \tag{5.5a}$$

$$\xi(t) \sim \exp(i\omega_{z,-}t) \qquad t \to -\infty. \tag{5.5b}$$

The trapping frequency $\omega(t) \to \omega_{z,+}$ when $t \to +\infty$. Therefore,

$$\xi(t) \to A_1 \exp(i\omega_{z,+}t) - A_2 \exp(-i\omega_{z,+}t) \qquad t \to +\infty, \tag{5.6}$$

where $A_1$ and $A_2$ are constants, which satisfy the condition $|A_1|^2 - |A_2|^2 = \omega_{z,-}/\omega_{z,+}$. The parameter $\rho$ is

$$\rho = \left|\frac{A_2}{A_1}\right|^2. \tag{5.7}$$

We are interested only in the excitation probability $W_{n,0}$. Expression (5.4) is significantly simplified for the case of $m = 0$:

$$W_{2n,0} = \frac{2n!}{2^n(n!)^2}\sqrt{1-\rho}\,\rho^n. \tag{5.8}$$

The excitation probabilities for an infinitely fast ramp and smooth ramp during the time 100 ms are shown in Fig. 39 in the left and right panels, respectively. If the ramp is made

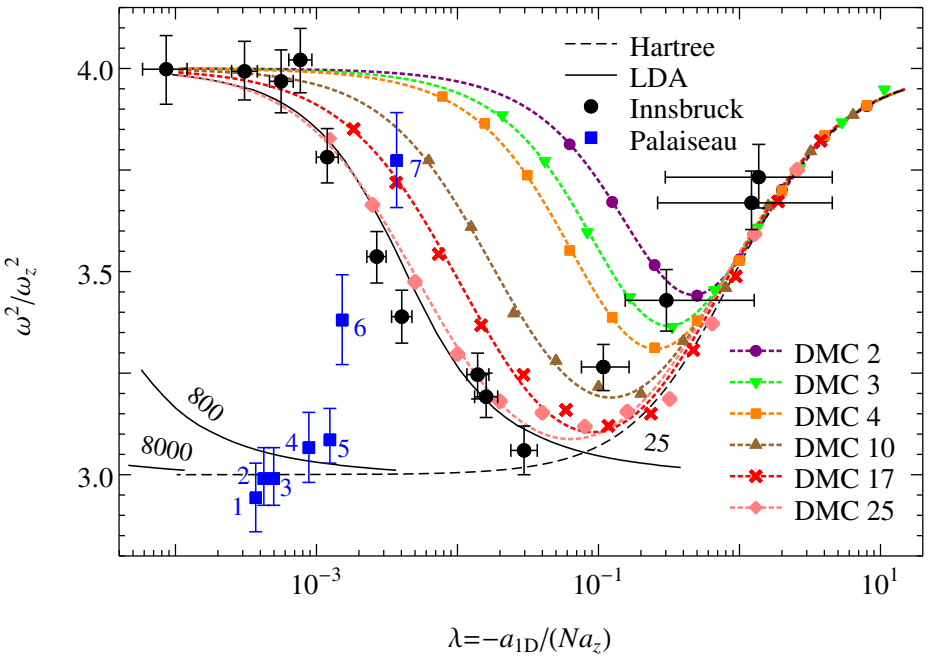


Figure 38: The ratio $\omega^2/\omega_z^2$ as a function of the Hartree parameter $\lambda = -a_{1D}/(Na_z)$. Dashed (black) curve: the Hartree approximation. Solid (black) curves: LDA for $N = 25$, 800, 8000. Dashed colored curves: interpolations for the data points obtained with diffusion Monte Carlo (DMC) simulations for $N = 2, 3, 4, 10, 17, 25$ (top to bottom). Large (black) circles: Innsbruck experiment [14], for which $N = 25$. Large (blue) boxes: Palaiseau experiment [15], for which $N$ is given in Table IV. The Gaussian BEC regime corresponds to $\lambda > 1$ as defined in Fig. 34. DMC and experimental data points are the same as in Fig. 37.

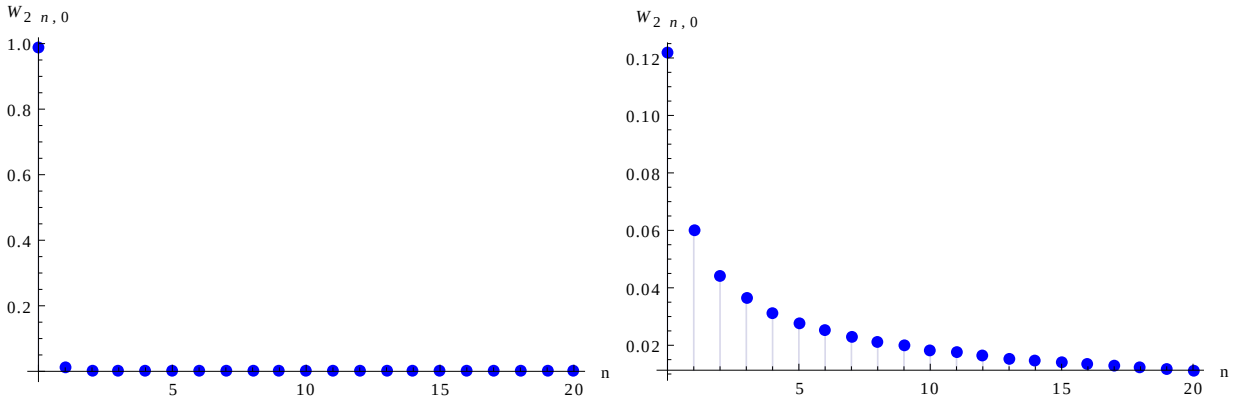


Figure 39: First 20 excitation probabilities $W_{2n,0}$ for smooth (right) and strong (left) ramps.

slowly the probability to excite high-energy levels is negligible, but if the ramp is strong, the probability to excite high-energy levels is large.

## 5.3. Comparison with $^{87}Rb$ experiment

The ETH (Zurich) experiment examined what happens with the breathing oscillations if the temperature of the 3D BEC prepared to be loaded into an array of 1D tubes gets higher [13]. The parameters $a_{1\mathrm{D}}$, $a_z$, and $N$ correspond to the TF BEC regime of the 1D gas. It was found that the breathing mode persists and the ratio $\omega^2/\omega_z^2$ grows from the value 3 to 4 (with the uncertainty about 0.1). These findings could be interpreted as an increase of $\omega$ due to the temperature increase, assuming that the 1D gas is in thermal equilibrium.

In this section we discuss the recently reported results of the Palaiseau group [15]. For $^{87}Rb$ atoms there is no accessible Feshbach resonance and the $3D$ scattering length is fixed, $a_{3D} = 103 \pm 5a_0 = 5.45 \pm 0.26$ nm. The perpendicular trapping frequency is $\omega_\perp = 2\pi \times 2.0$ kH, and $a_{1D} = -10.42\ \mu m$. The frequency $\omega_z = 2\pi \times 9.0$ Hz and $a_z = 3.59\ \mu m$. The data points from the Palaiseau group shown in Figs. 37 and 38 are taken from Fig. 3(a) of Ref. [15]. The parameters $a_{1\mathrm{D}}$, $a_z$, and $N$ correspond to the Thomas-Fermi BEC regime for all data points. We see that the frequencies for the first five of them match our theoretical predictions within the error bars. The frequencies for the last two are higher than the theory predicts.

In both experiments [14, 15] the temperature was claimed to be in the range of dozens of $nK$ during the measurements. In the $Cs$ experiment [14] the temperature was close to 10 nK. In the Palaiseau experiment the in situ density profile [15] indicates a temperature around 100 nK. The analysis of the raw data gives temperatures presented in Table IV.

For the $Rb$ experiments [15], a change of the 1D scattering length $a_{1D} = -a_\perp^2/a_{3D} \approx 10.42\mu m$ in wide range is hard, and the only parameter which can be easily tuned is the number of particles in the tube $N$. This gives a constant dimensionless temperature $t = \frac{2\hbar^2 k_B T}{mg^2} = \frac{ma_{1D}^2 k_B T}{2\hbar^2} \approx 972$. The classification of the regimes contains also the temperature of quantum degeneracy $T_Q = N\hbar\omega_z$ (see Ref. [55]). When the number of the particles is fixed the reduced temperature $t$ is proportional to the interaction parameter $\Lambda$:

$$t = \frac{\Lambda}{2N}\frac{k_B T}{\hbar\omega_z}. \tag{5.9}$$

For the $^{133}Cs$ experiment one has $t = 6.37\Lambda$ and $T_Q \approx 20\ nK$. We can see that for all points $T$ and $T_Q$ are of the same order, and for the last two $T < T_Q$.

Another classification [59] suggests to compare temperature with the temperature of quantum degeneracy $T_d = \hbar^2 n^2/2m = 2\hbar^2/ma_{1D}^2\gamma^2$ and with $T_d\sqrt{\gamma}$.

Table IV: Table of the data from the experiment [15].

| # | 1 | 2 | 3 | 4 | 5 | 6 | 7 |
|---|---|---|---|---|---|---|---|
| $N$ | 7817 | 6846 | 5826 | 3281 | 2328 | 1904 | 783 (1385) |
| $\left(\frac{\omega}{\omega_z}\right)^2$ | 2.944 | 2.990 | 2.990 | 3.06 | 3.08 | 3.38 | 3.77 |
| $T_Q$, $nK$ | 3376 | 2957 | 2516 | 1417 | 1005 | 822 | 338 (598) |
| $N\left(\frac{a_{1D}}{a_z}\right)^2$ | 65687 | 57531 | 48959 | 27576 | 19564 | 16003 | 6580 |
| $T_d$, $nK$ | 12125 | 9904 | 7864 | 3248 | 1495 | 958 | 181 (507) |
| $T_d\sqrt{\gamma}$, $nK$ | 654 | 562 | 473 | 244 | 136 | 98 | 28 (59) |
| $T_{co}$, nK | 1078 | 954 | 824 | 502 | 383 | 327 | 144 (225) |
| $\gamma(0)$ | 0.0027 | 0.0030 | 0.0034 | 0.0054 | 0.0079 | 0.0098 | 0.0238 |
| $n(0)_{exp}$, $\mu m^{-1}$ | 65.5 | 58.1 | 51.8 | 33.3 | 22.6 | 18.1 | 7.87 (13.4) |
| $n(0)_{LDA}$, $\mu m^{-1}$ | 81.2 | 74.4 | 66.8 | 45.6 | 36.2 | 31.7 | 17.5 |
| $n(0)^{-1}, \mu m$ | 0.0153 | 0.0172 | 0.0193 | 0.030 | 0.0442 | 0.0552 | 0.127 |
| $\frac{n(0)_{LDA}}{n(0)_{exp}}$ | 1.24 | 1.28 | 1.29 | 1.37 | 1.60 | 1.75 | 2.23 |
| $\xi, \mu m$ | 0.199 | 0.212 | 0.224 | 0.280 | 0.339 | 0.379 | 0.575 |
| $Z_{TF}, \mu m$ | 64.6 | 62.4 | 59.6 | 47.2 | 38.7 | 34.5 | 29.1 |
| $T_{bf}$, nK | 400 | 396 | 340 | 235 | 210 | 210 | 350 (190) |

The number of the particles and densities in Table IV were taken from the raw data [15].

The phase diagram of a 1D quantum gas [55, 59] is shown in Fig. 40. The black lines show edges of the Tonks-Girargeau regime. The dashed lines show the transition asymptotes $t = \gamma^{-2}$ and $t = \gamma^{-\frac{3}{2}}$.

The following analysis was implemented. For the parameters of the experiment [15] the density profiles were calculated in the LDA for a finite temperature. The local chemical potential was taken from the Yang-Yang solution [60] (see Sec. 5.4). The density in the center of the cloud was calculated for a broad range of temperatures. The dependence of the

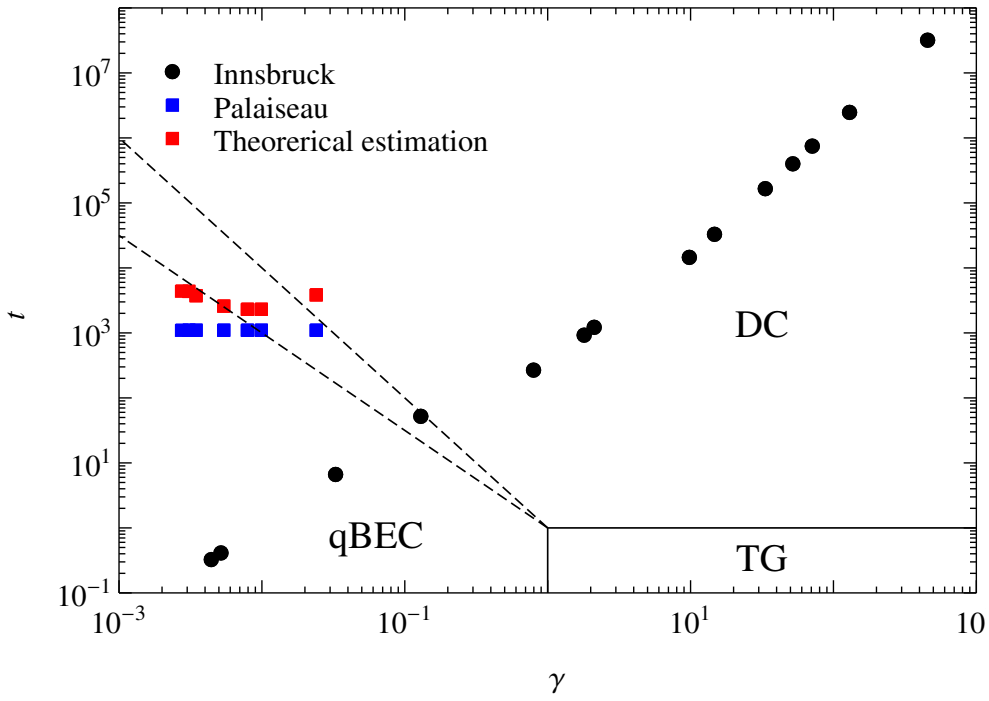


Figure 40: The phase diagram of a 1D quantum gas and the experimental data. The black circles and blue squares are experimental data from Refs. [14] and [15], respectively.

central density on temperature and interaction parameter is plotted in Fig. 41. We extract the best fitting temperature $T_{bf}$ from the comparison of this dependence with the densities measured in the experiment [15]. Our analysis indicates much higher temperatures than the one from the in situ density.

According to Ref. [59], the finite-temperature effects are relevant above $T_{\rm co} = 3N\hbar\omega_z/[k_B \ln(\Lambda/4)]$ for the range of parameters which was chosen in the experiment. We see from Table IV that $T/T_{\rm co}$ increases monotonically from the value $\approx 0.4$ for the first data point to $\approx 0.9$ for the last one. Note that $T_Q$ larger than $T_{\rm co}$ by nearly a factor of 3 (and, therefore, than $T$) for all data points. Thus, $T_Q$ may not define a crossover temperature in the experiment [15].

## 5.4. Thermodynamics of the Lieb-Liniger model. Yang-Yang solution

Thermodynamics of the system described by the Hamiltonian (3.7) is known [60]. For finite temperatures the Bethe hypothesis (3.15) holds. Let us introduce functions $L\rho(k)$ and

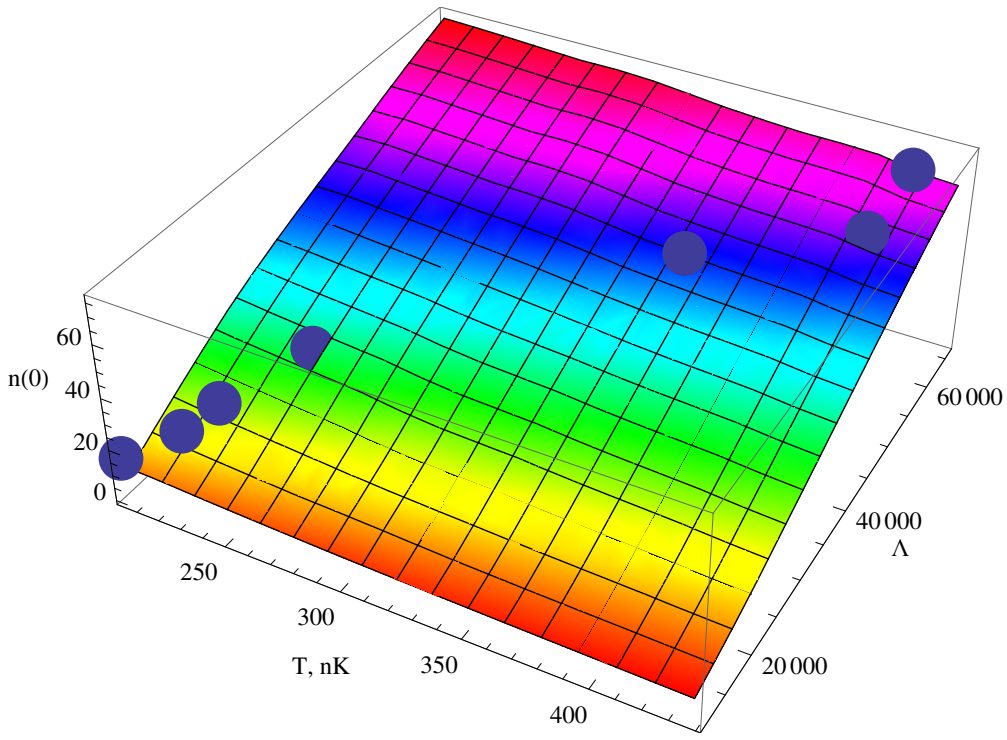


Figure 41: The dependence of the density in the center of the cloud on temperature and dimensionless interaction parameter $\Lambda$ in the region relevant for the experiment [15]. Blue spheres are experimental densities for a given interaction.

$L\rho_h(k)$ which show the number of the filled rapidities $k$'s and holes in the interval $k; k+dk$, correspondingly. Introducing the function $\epsilon(k)$ as $\exp(\epsilon(k)/T) = \frac{\rho_h}{\rho}$ we have

$$2\pi(\rho(k)+\rho_h(k)) = 2\pi\rho(k)(1+\exp(\epsilon(k)/T)) = 1 + 2g\int_{-\infty}^{\infty}\frac{\rho(k')}{g^2+(k-k')^2}dk' \tag{5.10}$$

The entropy $S$ and energy $E$ are defined as follows:

$$S/N = n_1^{-1}\int_{-\infty}^{\infty}\left((\rho(k)+\rho_h(k))\ln(\rho(k)+\rho_h(k)) - \rho(k)\ln(\rho(k)) - \rho_h(k)\ln(\rho_h(k))\right)dk \tag{5.11a}$$

$$E/N = n_1^{-1}\int_{-\infty}^{\infty}\rho(k)k^2dk \tag{5.11b}$$

$$n_1 = \int_{-\infty}^{\infty}\rho(k)dk \tag{5.11c}$$

From the condition of thermal equilibrium we get the following equation by minimizing the functional $\exp(S-E/T)$:

$$\epsilon(k) = -\mu + \frac{\hbar^2}{2m}k^2 - k_BT\int_{\infty}^{\infty}\frac{1}{\pi}\frac{g}{g^2+(k-q)^2}\ln(1+\exp(-\epsilon(q)/T))dq \tag{5.12}$$

The solution of equations (5.10) and (5.12) gives the dependence of the interaction parameter $\gamma$ on the chemical potential $\mu$ and temperature $T$. In our future calculations we will be interested in the dependence of $\mu$ on $\gamma$ at a fixed $T$. The dependence of density on the chemical potential for the dimensionless temperature $t = 1000$ is presented in Fig. 42. This picture is typical for the phase diagram at a finite temperature. Contrary to the case of $t = 0$ (see Sec. 3.4 and Fig. 16), the zero chemical potential does not imply zero density. For a given negative chemical potential the system has a finite density (see Fig. 42). The density far from the center of the trap is small, and thus the chemical potential is negative near the edges of the cloud. It can be described classically (see Sec. 5.5).

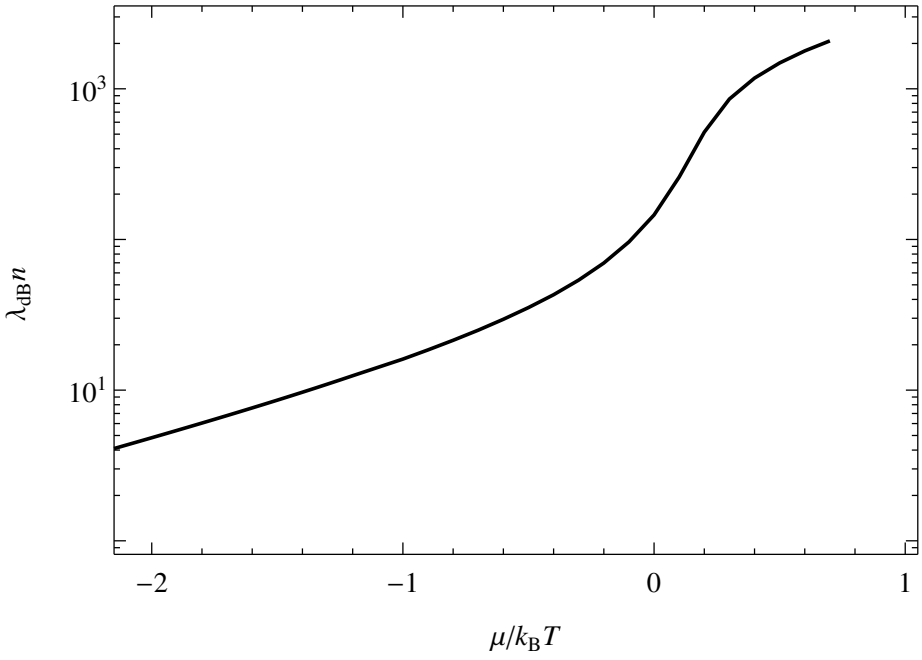


Figure 42: The dependence of the density on the chemical potential at a constant dimensionless temperature $t = 1000$.

Thus, the implementation of the LDA (3.6) for the case of a finite temperature has to be modified. The finite temperature LDA approximation should read:

$$\mu_{LDA}\left(n_1\left(z\right), T\right) + V_{ext}(z) = \mu_0, \tag{5.13}$$

where $\mu_0$ is a chemical potential in the trap center and it should be found from the normalization condition

$$\int_{-\infty}^{\infty} n(\mu_{LDA}(z), T)dz = N. \tag{5.14}$$

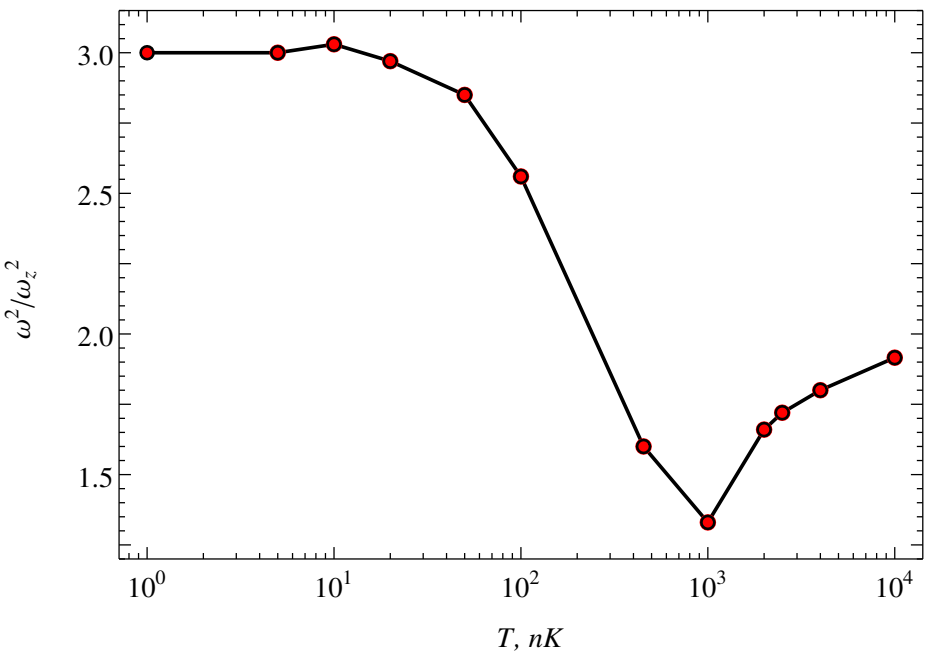


Figure 43: The dependence of the breathing mode frequency on temperature $T$ for a fixed interaction parameter $\Lambda = 65000$. The noise in the data is due to the noise in the numerical calculations.

This approach is at least applicable for the quasi-BEC and Tonks-Girardeau regimes.

The dependence of the breathing mode frequency on temperature $T$ for the interaction strength $\Lambda = 65000$ is presented in Fig. 43. In the zero-temperature limit it recovers the zero-temperature prediction (3.96). In the high-temperature regime the breathing oscillation frequency goes to the classical gas result (5.20).

## 5.5. Classical gas. Large negative chemical potentials

For finite temperatures Eqs. (5.10, 5.12) have solutions where the chemical potential is negative and the density is finite. In the regime with $\mu < 0$ and $|\mu| \gg T$, the gas should be quantum decoherent and can be approximated with the ideal Bose gas equation of state:

$$n(\mu, T) = \frac{1}{2\pi} \int_{-\infty}^{\infty} \frac{dk}{\exp\left(\frac{\frac{\hbar^2 k^2}{2m} - \mu}{k_B T}\right) \pm 1} = \sqrt{\frac{m k_B T}{2\pi\hbar^2}} \sum_{j=1}^{\infty} (\mp 1)^{j+1} \frac{\exp\left(\frac{j\mu}{k_B T}\right)}{j^{\frac{1}{2}}}. \qquad (5.15)$$

In Eq. (5.15) upper signs have to be used for fermions and lower for bosons correspondingly. The Yang-Yang solution reproduces this asymptotic behavior.

In very hot trapped systems for such parameters the chemical potential in the center is large and negative, so that we can neglect all terms except the first one. Thus for the classical gas in the LDA we obtain

$$n(z) = \sqrt{\frac{mk_BT}{2\pi\hbar^2}} \exp\left(\frac{\mu_0 - V_{ext}(z)}{k_BT}\right), \tag{5.16}$$

where $k_BT_Q = N\hbar\omega_z$ and $\mu_0 = k_BT \ln\left(\frac{T_Q}{T}\right)$ is fixed by the normalization condition. For the trapped system whose local equation of state is fully described by Eq.(5.15), the chemical potential $\mu_0 < -k_BT$ is needed. This condition is equivalent to $\ln(1 - e^{-1})T > T_Q$. The average radius of the system is

$$\langle z^2 \rangle = \frac{Nk_BT}{m\omega_z^2}. \tag{5.17}$$

The potential and interaction energies are:

$$E_{pot} = \frac{m\omega_z^2}{2} \int_{-\infty}^{\infty} z^2 n(z) dz = \frac{Nk_BT}{2}, \tag{5.18a}$$

$$E_{int} = g \int_{-\infty}^{\infty} n(z)^2 dz = \sqrt{\frac{\pi}{4}} \Lambda^{-\frac{1}{2}} k_BT_Q \sqrt{\frac{T_Q}{T}}. \tag{5.18b}$$

The potential and kinetic energies in Eqs. (5.18) can be considered as a consequence of the equipartition theorem. The scaling formula (1.41) gives the breathing mode frequency:

$$\omega^2 = \omega_z^2 \left(4 - \frac{1}{2} \frac{\sqrt{\pi}\Lambda^{-\frac{1}{2}}}{N} \left(\frac{T_Q}{T}\right)^{\frac{3}{2}}\right). \tag{5.19}$$

This formula can be applied only in the region of high temperatures. Thus, one can conclude that the breathing mode frequency for the classical gas is $2\omega_z$.

The sum rules for this regime give the following result:

$$\frac{\omega^2}{\omega_z^2} = 2. \tag{5.20}$$

The first order correction can be calculated taking into account the next term in equation (5.15). For free fermions the first order correction to the breathing mode frequency is

$$\frac{\omega^2}{\omega_z^2} \simeq 2 + \frac{3}{4} \frac{N\hbar\omega_z}{k_BT}, \tag{5.21}$$

and for free bosons:

$$\frac{\omega^2}{\omega_z^2} \simeq 2 - \frac{1}{4} \frac{N\hbar\omega_z}{k_BT}. \tag{5.22}$$

In general, if we take into account all the terms in Eq.(5.15), from the normalization condition we will obtain the following equation for the chemical potential:

$$\sum_{j=1}^{\infty} \frac{\exp\left(\frac{j\mu_0}{k_B T}\right)}{j} = \ln\left(\frac{1}{1-\exp\left(\frac{\mu_0}{k_B T}\right)}\right) = \frac{T_Q}{T}. \tag{5.23}$$

Thus, we have

$$\left.\frac{\partial \mu_0}{\partial k_B T_Q}\right|_T = \frac{1}{\exp\left(\frac{T_Q}{T}\right)-1}. \tag{5.24}$$

The average radius of the cloud is

$$\langle z^2\rangle = \frac{N k_B T}{m\omega_z^2} \frac{\sum_{j=1}^{\infty} \exp\left(\frac{j\mu_0}{T}\right)/j^2}{\sum_{j=1}^{\infty} \exp\left(\frac{j\mu_0}{T}\right)/j} = \frac{(k_B T)^2}{\hbar m \omega_z^3} \sum_{j=1}^{\infty} \exp\left(\frac{j\mu_0}{T}\right) j^{-2}. \tag{5.25}$$

The response of the system to a change in the trap frequency can be calculated as

$$\frac{\partial\langle z^2\rangle}{\partial \omega_z} = N\hbar \frac{\partial\langle z^2\rangle}{\partial k_B T_Q}. \tag{5.26}$$

We then obtain:

$$\frac{\partial\langle z^2\rangle}{\partial k_B T_Q} = -3\langle z^2\rangle (k_B T_Q)^{-1} + \frac{k_B T_Q}{\hbar m \omega_z^3} \frac{\partial \mu_0}{\partial k_B T_Q}. \tag{5.27}$$

Eq. (5.27) can be considered as a partial differential equation for the function $\langle z^2\rangle(T, T_Q)$. It has to be complemented with the condition $\langle z^2\rangle(T, T_Q = 0) = 0$. This condition says that if there are no particles, then the size of the system is zero. Thus, Eq. (5.27) has the following solution

$$\langle z^2\rangle = \frac{1}{m\omega_z^2} \frac{k_B^2 T^2}{\hbar\omega_z} \int_0^{\frac{T_Q}{T}} \frac{q}{\exp(q)-1} dq = \frac{N^3\hbar^2 T^2}{m k_B T_Q^3} \int_0^{\frac{T_Q}{T}} \frac{q}{\exp(q)-1} dq. \tag{5.28}$$

## 5.6. Tonks-Girargeau gas at a finite temperature

In the Tonks-Girargeau regime the Lieb-Liniger gas has a spectrum analogous to the free fermions spectrum. In this section we use the equation of state for free fermions with the local density approximation and the sum rule to calculate the breathing mode frequency.

At finite temperatures the Tonks-Girargeau gas is described by the Fermi-Dirac distribution function

$$\rho_n = \frac{1}{1+\exp\left(\frac{E_n-\mu}{k_B T}\right)} \tag{5.29}$$

From the normalization condition $\sum_n \rho_n = N$ in the thermodynamic limit $N \to \infty$,$L \to \infty$ and $N/L \to n$ we obtain the equation of state:

$$\int_{-\infty}^{\infty} \rho(k)dk = 2\pi n, \tag{5.30}$$

where

$$\rho(k) = \frac{1}{1 + \exp\left(\frac{\frac{\hbar^2 k^2}{2m} - \mu}{k_B T}\right)}, \tag{5.31}$$

is the continuous Fermi distribution function. The only characteristic scale in such a system is the de Broglie wavelength

$$\lambda_{dB} = \sqrt{\frac{2mk_B T}{\hbar^2}}. \tag{5.32}$$

After the integration we have

$$2\pi n \lambda_{dB} = \int_{-\infty}^{\infty} \frac{1}{1 + \exp\left(q^2 - \frac{\mu}{k_B T}\right)} dq. \tag{5.33}$$

The implementation of the LDA needs the calculation of the chemical potential in the center of the cloud. The related equation has the following form:

$$\int_{-\infty}^{\infty} \lambda_{dB} n \left(\frac{\mu_0}{k_B T} - x^2\right) dx = N \left(\frac{\lambda_{dB}}{a_z}\right)^2. \tag{5.34}$$

Equation (5.34) has the same form as Eq. (3.65), but with $a_{1D}$ changed to $\lambda_{dB}$, and it can be solved in the same way.

The breathing mode frequency for free fermions at a finite temperature is shown in Fig. 44. For such a system the breathing mode frequency depends on the parameter

$$\Lambda_Q = \frac{T_Q}{T}. \tag{5.35}$$

In the zero-temperature limit it recovers the result for the Tonks-Girargeau gas (3.78). In the limit of high temperatures the system enters the ideal Bose gas regime and its breathing mode frequency is given by Eq. (5.20).

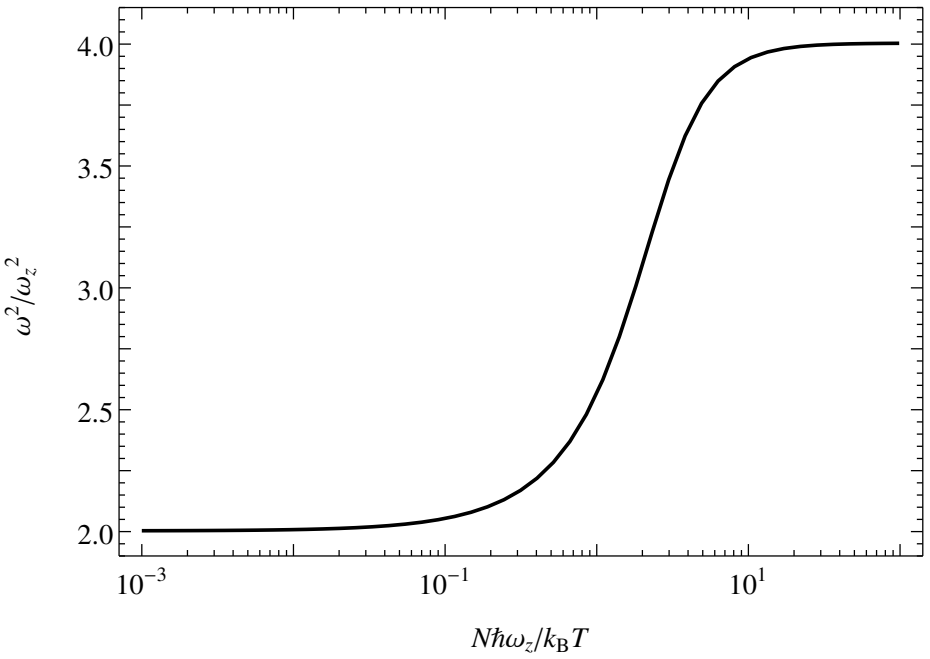


Figure 44: The dependence of the breathing mode frequency on the interaction parameter $\Lambda_Q = N\hbar\omega_z/k_BT$.

# 6. Conclusions

We have presented the study of breathing oscillations for a one-dimensional trapped interacting Bose gas. Oscillations are induced by the instantaneous change of the trapping frequency $\omega_z$.

We consider a 1D quantum Bose gas in a parabolic trap at zero temperature and explain, analytically and numerically, how the oscillation frequency depends on the number of particles, the interparticle interaction, and the trap strength. We have focused on the many-body spectral description, using the sum rule approximation. We identify the frequency as the energy difference between the ground state and a particular excited state for the repulsive interaction, and as the energy difference between the gas state and a particular excited state for the attractive interaction. We demonstrate the existence of three regimes, namely the Tonks-Girargeau regime, the Thomas-Fermi regime, and the Gaussian regime.

We describe a crossover from the Tonks-Girargeau to the Thomas-Fermi regime in terms of the local density approximation. For the description of the crossover from the Thomas-Fermi to the Gaussian regime we use the Hartree approximation. In both cases we demonstrate the regions of the parameters where the crossover happens. We perform extensive diffusion Monte Carlo simulations for a gas containing up to $N = 25$ particles. As the number of particles increases, predictions from the simulations converge to the ones from the Hartree and LDA in the corresponding regimes. This makes our results for the breathing mode frequency applicable for an arbitrary number of particles and for any value of the interaction strength. We complete our analysis with finite-$N$ perturbative results in the asymptotic regions. Our theory predicts the reentrant behavior of $\omega$ with increasing of the interaction strength and explains the recent experiment [14]. A detailed extension of the present theory to finite temperatures is still in progress.

# References


[1] L. Pitaevskii and S. Stringari, *Bose-Einstein Condensation*. Oxford: Oxford University Press, 2003.

[2] C. J. Pethick and H. Smith, *Bose-Einstein Condensation in Dilute Gases*. Cambridge: Cambridge University Press, 2008.

[3] M.-O. Mewes, M. R. Andrews, N. J. van Druten, D. M. Kurn, D. S. Durfee, C. G. Townsend, and W. Ketterle, "Collective Excitations of a Bose-Einstein Condensate in a Magnetic Trap," *Phys. Rev. Lett.*, vol. 77, pp. 988–991, Aug 1996.

[4] D. S. Jin, J. R. Ensher, M. R. Matthews, C. E. Wieman, and E. A. Cornell, "Collective Excitations of a Bose-Einstein Condensate in a Dilute Gas," *Phys. Rev. Lett.*, vol. 77, pp. 420–423, Jul 1996.

[5] F. Chevy, V. Bretin, P. Rosenbusch, K. W. Madison, and J. Dalibard, "Transverse Breathing Mode of an Elongated Bose-Einstein Condensate," *Phys. Rev. Lett.*, vol. 88, p. 250402, Jun 2002.

[6] J. Kinast, S. L. Hemmer, M. E. Gehm, A. Turlapov, and J. E. Thomas, "Evidence for Superfluidity in a Resonantly Interacting Fermi Gas," *Phys. Rev. Lett.*, vol. 92, p. 150402, Apr 2004.

[7] J. Kinast, A. Turlapov, and J. E. Thomas, "Damping of a Unitary Fermi Gas," *Phys. Rev. Lett.*, vol. 94, p. 170404, May 2005.

[8] A. Altmeyer, S. Riedl, C. Kohstall, M. J. Wright, R. Geursen, M. Bartenstein, C. Chin, J. H. Denschlag, and R. Grimm, "Precision Measurements of Collective Oscillations in the BEC-BCS Crossover," *Phys. Rev. Lett.*, vol. 98, p. 040401, Jan 2007.

[9] S. Riedl, E. R. Sánchez Guajardo, C. Kohstall, A. Altmeyer, M. J. Wright, J. H. Denschlag, R. Grimm, G. M. Bruun, and H. Smith, "Collective oscillations of a Fermi gas in the unitarity limit: Temperature effects and the role of pair correlations," *Phys. Rev. A*, vol. 78, p. 053609, Nov 2008.

[10] A. O. Gogolin, A. A. Nersesyan, and A. M. Tsvelik, *Bosonization and Strongly Correlated*

*Systems*. Cambridge: Cambridge University Press, 1999.

[11] T. Giamarchi, *Quantum Physics in One Dimension*. Oxford: Oxford University Press, 2004.

[12] M. Girardeau, "Relationship between Systems of Impenetrable Bosons and Fermions in One Dimension," *Journal of Mathematical Physics*, vol. 1, no. 6, 1960.

[13] H. Moritz, T. Stöferle, M. Köhl, and T. Esslinger, "Exciting Collective Oscillations in a Trapped 1D Gas," *Phys. Rev. Lett.*, vol. 91, p. 250402, Dec 2003.

[14] E. Haller, M. Gustavsson, M. J. Mark, J. G. Danzl, R. Hart, G. Pupillo, and H.-C. Nagerl, "Realization of an Excited, Strongly Correlated Quantum Gas Phase," *Science*, vol. 325, no. 5945, pp. 1224–1227, 2009.

[15] B. Fang, G. Carleo, A. Johnson, and I. Bouchoule, "Quench-Induced Breathing Mode of One-Dimensional Bose Gases," *Phys. Rev. Lett.*, vol. 113, p. 035301, Jul 2014.

[16] C. Menotti and S. Stringari, "Collective oscillations of a one-dimensional trapped Bose-Einstein gas," *Phys. Rev. A*, vol. 66, p. 043610, Oct 2002.

[17] R. Schmitz, S. Krönke, L. Cao, and P. Schmelcher, "Quantum breathing dynamics of ultracold bosons in one-dimensional harmonic traps: Unraveling the pathway from few- to many-body systems," *Phys. Rev. A*, vol. 88, p. 043601, Oct 2013.

[18] W. Tschischik, R. Moessner, and M. Haque, "Breathing mode in the Bose-Hubbard chain with a harmonic trapping potential," *Phys. Rev. A*, vol. 88, p. 063636, Dec 2013.

[19] E. Haller, R. Hart, M. J. Mark, J. G. Danzl, L. Reichsöllner, and H.-C. Nägerl, "Inducing Transport in a Dissipation-Free Lattice with Super Bloch Oscillations," *Phys. Rev. Lett.*, vol. 104, p. 200403, May 2010.

[20] E. Lipparini and S. Stringari, "Sum rules and giant resonances in nuclei," *Physics Reports*, vol. 175, no. 3в Ъ“4, pp. 103 – 261, 1989.

[21] S. Stringari, "Collective Excitations of a Trapped Bose-Condensed Gas," *Phys. Rev. Lett.*, vol. 77, pp. 2360–2363, Sep 1996.

[22] E. Haller, M. J. Mark, R. Hart, J. G. Danzl, L. Reichsöllner, V. Melezhik, P. Schmelcher, and H.-C. Nägerl, "Confinement-Induced Resonances in Low-Dimensional Quantum Systems," *Phys. Rev. Lett.*, vol. 104, p. 153203, Apr 2010.

[23] S. Chen, L. Guan, X. Yin, Y. Hao, and X.-W. Guan, "Transition from a Tonks-Girardeau gas to a super-Tonks-Girardeau gas as an exact many-body dynamics problem," *Phys. Rev. A*, vol. 81, p. 031609, Mar 2010.

[24] S. Giorgini, L. P. Pitaevskii, and S. Stringari, "Theory of ultracold atomic Fermi gases," *Rev. Mod. Phys.*, vol. 80, pp. 1215–1274, Oct 2008.

[25] K. Huang and C. N. Yang, "Quantum-Mechanical Many-Body Problem with Hard-Sphere Interaction," *Phys. Rev.*, vol. 105, pp. 767–775, Feb 1957.

[26] M. Olshanii, "Atomic Scattering in the Presence of an External Confinement and a Gas of Impenetrable Bosons," *Phys. Rev. Lett.*, vol. 81, pp. 938–941, Aug 1998.

[27] T. Bergeman, M. G. Moore, and M. Olshanii, "Atom-Atom Scattering under Cylindrical Harmonic Confinement: Numerical and Analytic Studies of the Confinement Induced Resonance," *Phys. Rev. Lett.*, vol. 91, p. 163201, Oct 2003.

[28] E. H. Lieb and W. Liniger, "Exact Analysis of an Interacting Bose Gas. I. The General Solution and the Ground State," *Phys. Rev.*, vol. 130, pp. 1605–1616, May 1963.

[29] E. H. Lieb, "Exact Analysis of an Interacting Bose Gas. II. The Excitation Spectrum," *Phys. Rev.*, vol. 130, pp. 1616–1624, May 1963.

[30] J. W. Abraham, K. Balzer, D. Hochstuhl, and M. Bonitz, "Quantum breathing mode of interacting particles in a one-dimensional harmonic trap," *Phys. Rev. B*, vol. 86, p. 125112, Sep 2012.

[31] J. W. Abraham and M. Bonitz, "Quantum Breathing Mode of Trapped Particles: From Nanoplasmas to Ultracold Gases," *Contributions to Plasma Physics*, vol. 54, no. 1, pp. 27–99, 2014.

[32] O. Bohigas, A. Lane, and J. Martorell, "Sum rules for nuclear collective excitations," *Physics Reports*, vol. 51, no. 5, pp. 267 – 316, 1979.

[33] T. Busch, B.-G. Englert, K. Rzażewski, and M. Wilkens, "Two Cold Atoms in a Harmonic Trap," *Foundations of Physics*, vol. 28, no. 4, pp. 549–559, 1998.

[34] S. H. Patil, "Harmonic oscillator with a $\delta$-function potential," *European Journal of Physics*, vol. 27, no. 4, p. 899, 2006.

[35] G. E. Astrakharchik, J. Boronat, J. Casulleras, and S. Giorgini, "Beyond the Tonks-Girardeau Gas: Strongly Correlated Regime in Quasi-One-Dimensional Bose Gases," *Phys. Rev. Lett.*, vol. 95, p. 190407, Nov 2005.

[36] E. Gross, "Structure of a quantized vortex in boson systems," *Il Nuovo Cimento (1955-1965)*, vol. 20, no. 3, pp. 454–477, 1961.

[37] L. Pitaevskii, "Vortex lines in an imperfect bose gas," *Sov. Phys. JETP*, vol. 13, no. 2, pp. 451–

454, 1961.

[38] T. Kaminaka and M. Wadati, "Higher order solutions of Lieb-Liniger integral equation," *Physics Letters A*, vol. 375, no. 24, pp. 2460 – 2464, 2011.

[39] M. Zvonarev, *Correlations in 1D boson and fermion systems: exact results*. PhD thesis, Copenhagen University, 2005.

[40] L. H. Thomas, "The calculation of atomic fields," *Mathematical Proceedings of the Cambridge Philosophical Society*, vol. 23, pp. 542–548, 1 1927.

[41] T. Cheon and T. Shigehara, "Fermion-Boson Duality of One-Dimensional Quantum Particles with Generalized Contact Interactions," *Phys. Rev. Lett.*, vol. 82, pp. 2536–2539, Mar 1999.

[42] F. N. C. Paraan and V. E. Korepin, "Perturbative correction to the ground-state properties of one-dimensional strongly interacting bosons in a harmonic trap," *Phys. Rev. A*, vol. 82, p. 065603, Dec 2010.

[43] Z. D. Zhang, G. E. Astrakharchik, D. C. Aveline, S. Choi, H. Perrin, T. H. Bergeman, and M. Olshanii, "Breakdown of scale invariance in the vicinity of the Tonks-Girardeau limit," *Phys. Rev. A*, vol. 89, p. 063616, Jun 2014.

[44] A. Minguzzi and D. M. Gangardt, "Exact Coherent States of a Harmonically Confined Tonks-Girardeau Gas," *Phys. Rev. Lett.*, vol. 94, p. 240404, Jun 2005.

[45] R. Pezer and H. Buljan, "Momentum Distribution Dynamics of a Tonks-Girardeau Gas: Bragg Reflections of a Quantum Many-Body Wave Packet," *Phys. Rev. Lett.*, vol. 98, p. 240403, Jun 2007.

[46] P. J. Forrester, N. E. Frankel, T. M. Garoni, and N. S. Witte, "Finite one-dimensional impenetrable Bose systems: Occupation numbers," *Phys. Rev. A*, vol. 67, p. 043607, Apr 2003.

[47] S. K. Adhikari, "Expansion of a Bose-Einstein condensate formed on a joint harmonic and one-dimensional optical-lattice potential," *Journal of Physics B: Atomic, Molecular and Optical Physics*, vol. 36, no. 19, p. 3951, 2003.

[48] J. W. Abraham, M. Bonitz, C. McDonald, G. Orlando, and T. Brabec, "Quantum breathing mode of trapped systems in one and two dimensions," *New Journal of Physics*, vol. 16, no. 1, p. 013001, 2014.

[49] A. I. Gudyma, G. E. Astrakharchik, and M. B. Zvonarev, "Reentrant behavior of the breathing-mode-oscillation frequency in a one-dimensional Bose gas," *Phys. Rev. A*, vol. 92, p. 021601, Aug 2015.

[50] W. Kohn, "Cyclotron Resonance and de Haas-van Alphen Oscillations of an Interacting Electron Gas," *Phys. Rev.*, vol. 123, pp. 1242–1244, Aug 1961.

[51] J. F. Dobson, "Harmonic-Potential Theorem: Implications for Approximate Many-Body Theories," *Phys. Rev. Lett.*, vol. 73, pp. 2244–2247, Oct 1994.

[52] D. S. Petrov, G. V. Shlyapnikov, and J. T. M. Walraven, "Regimes of Quantum Degeneracy in Trapped 1D Gases," *Phys. Rev. Lett.*, vol. 85, pp. 3745–3749, Oct 2000.

[53] V. Dunjko, V. Lorent, and M. Olshanii, "Bosons in Cigar-Shaped Traps: Thomas-Fermi Regime, Tonks-Girardeau Regime, and In Between," *Phys. Rev. Lett.*, vol. 86, pp. 5413–5416, Jun 2001.

[54] M. Panfil, J. De Nardis, and J.-S. Caux, "Metastable Criticality and the Super Tonks-Girardeau Gas," *Phys. Rev. Lett.*, vol. 110, p. 125302, Mar 2013.

[55] K. V. Kheruntsyan, D. M. Gangardt, P. D. Drummond, and G. V. Shlyapnikov, "Finite-temperature correlations and density profiles of an inhomogeneous interacting one-dimensional Bose gas," *Phys. Rev. A*, vol. 71, p. 053615, May 2005.

[56] K. V. Kheruntsyan, D. M. Gangardt, P. D. Drummond, and G. V. Shlyapnikov, "Pair correlations in a finite-temperature 1d bose gas," *Phys. Rev. Lett.*, vol. 91, p. 040403, Jul 2003.

[57] D. A. Steck, "Cesium D Line Data," *available online at http://steck.us/alkalidata*, (revision 2.1.4, 23 December 2010).

[58] A. Perelomov and Y. Zeldovich, *"Quantum Mechanics: Selected Topics"*. Singapur: World Scientific Publishing, 1998.

[59] I. Bouchoule, K. V. Kheruntsyan, and G. V. Shlyapnikov, "Interaction-induced crossover versus finite-size condensation in a weakly interacting trapped one-dimensional Bose gas," *Phys. Rev. A*, vol. 75, p. 031606, Mar 2007.

[60] C. N. Yang and C. P. Yang, "Thermodynamics of a One-Dimensional System of Bosons with Repulsive Delta-Function Interaction," *Journal of Mathematical Physics*, vol. 10, no. 7, 1969.